Sveriges geologiska undersökning

Ion probe dating of complex zircon in high-grade gneisses, southeast Sveconorwegian Province: constraints for metamorphism and deformation

Charlotte Möller, Jenny Andersson & Dick Claeson

Utförd inom programmet för
FoU

SGU-rapport
2005:35

Ion probe dating of complex zircon in high-grade gneisses, southeast Sveconorwegian Province: constraints for metamorphism and deformation

Results from research project 35055

December 2005

Charlotte Möller, Jenny Andersson & Dick Claeson
Geological Survey of Sweden

Contents

1. Summary

Nine selected localities in the polymetamorphic Eastern Segment and the Protogine Zone (southeast Sveconorwegian Province) have been investigated in order to define and date different phases of metamorphism and deformation. The mode of occurrence of secondary formed (metamorphic) zircon in the different rocks has been documented by detailed electron microscope imaging and different zircon domains have been dated by high-spatial resolution U-Pb-Th ion microprobe (NORDSIM) analysis.

In migmatitic gneisses, secondary zircon was found to have formed mainly in leucosome-rich parts of the rock. Most of the secondary zircon that formed in connection with partial melting occurs as recrystallisation rims or partial replacements of the igneous zircon grains, and commonly has a "ghost" texture that resembles a relict oscillatory zoning. The domains are dark in cathodoluminescence (CL) and dominantly bright in backscatter (BSE) images. All secondary zircon is characterised by low or very low Th/U ratios (<0.11 and commonly <0.03, values typical for metamorphic zircon) and high U contents (commonly 700-3000 ppm). The secondary zircon is clearly distinguished from the protolith zircon by its low Th/U signature. Igneous protolith zircon analysed in this study has considerably higher Th/U ratio (0.2-1.5, commonly >0.6).

Spot analyses of protolith zircon from migmatitic gneiss at three different localities in the Eastern Segment yielded weighted average $^{207}Pb/^{206}Pb$ ages in the range 1.70 –1.67 Ga. Secondary zircon formation associated with partial melting at the same three localities was dated at c. 1.44, 1.42 and 0.98 Ga, respectively. At one locality the age of leucosome sets an upper limit at 1.45 Ga for recumbent folding, subsequent dolerite intrusion and overprinting high-pressure granulite facies metamorphism. At a locality in the southwesternmost part of the Eastern Segment, leucosome formation in "Hallandia" gneiss was dated at 1.44 Ga. The age of 1.40 Ga for a folded granite dyke at the same locality sets an upper bracket for an upright phase of folding along SSW trending axes. At a third locality, leucosome that is synkinematic in relation to E-W trending regional fold structures was dated at 0.98 Ga. The 0.98 Ga age thus directly dates folding along E-W trending, subhorizontal axes.

In the investigated samples, U-Pb analytical data sets of pre-Sveconorwegian (>0.98 Ga) zircon spread considerably along the concordia (for protolith zircon between 1.74 and 1.63 Ga and for 1.44 Ga secondary zircon between 1.48 and 1.41 Ga). By contrast, the analyses of secondary zircon formed during Sveconorwegian migmatisation are tightly clustered at 0.98 Ga. This demonstrates that diffusion of U and Pb after 0.98 Ga has been negligible but that isotopic disturbance has been substantial in the pre-Sveconorwegian zircon domains.

Zircon from migmatitic and folded gneiss that occur as mega-xenoliths in ductilely deformed TIB-granite in the easternmost part of the Protogine Zone has been investigated. The zircons are complex, with 1.77 Ga igneous cores and two generations of secondary formed rims. Inner, BSE-bright rims were dated at c. 1.68 Ga and probably represents reworking and migmatisation during intrusion of the host granite. The interpretation of outer BSE-bright 1.41 Ga rims that occur as distinct overgrowths awaits further analytical work. It is tentatively suggested that the 1.41 Ga old overgrowths are related either to the regional ductile deforma-

tion that produced the NW-striking (old) foliation in the Protogine Zone and locally reached anatectic conditions, or to intrusions at c. 1.4 Ga in the area (or both).

Three different charnockite-like, greenish grey and pyroxene-bearing rocks in the southwestern part of the Eastern Segment have been investigated and compared to their assumed precursors. Rock samples from two localities have syenitoid bulk compositions and probable remnants of igneous pyroxene (clinopyroxene with orthopyroxene lamellae). These two rocks thus probably had high-temperature intrusive protoliths that were pyroxene-bearing prior to metamorphism. Protolith zircon from these two rocks yielded igneous emplacement ages at c. 1.70-1.67 Ga. They were thus coeval with the intrusions that were protoliths to the migmatitic gneisses of the Eastern Segment. One charnockite-like rock has been confirmed as a charnockitic variety of a K-feldspar-megacrystic, granitic precursor. The zircons in this rock are rounded igneous crystals with (on most grains) < 20 μm wide, backscatter-dark rims. Due to the small size of the rims they are difficult to analyse. One rim, wide enough to analyse, had low U concentration and a low Th/U ratio and gave a slightly discordant $^{207}Pb/^{206}Pb$ age at c. 0.9 Ga. This age suggests that the charnockitisation at this locality is Sveconorwegian in age.

2. Introduction

This report is an intermittent presentation (December 2005) of results from a three-year research project no. 35055, carried out at the Geological Survey of Sweden and running from 2004 to 2006. In addition to the present authors (Charlotte Möller, Jenny Andersson and Dick Claeson), Thomas Eliasson, Inger Lundqvist, Lena Lundqvist and Hugo Wikman, all presently or formerly coworkers at the Geological Survey of Sweden, have participated during the first project year (2004). Analytical work has been carried out during 2005 (Nordsim project number SE/2005/24). The present work will be supplemented in 2006 by ion probe analysis of additional samples. The combined results from selected localities will thereafter be presented in separate papers, co-authored by the project participants above, and submitted for publication in international scientific journals.

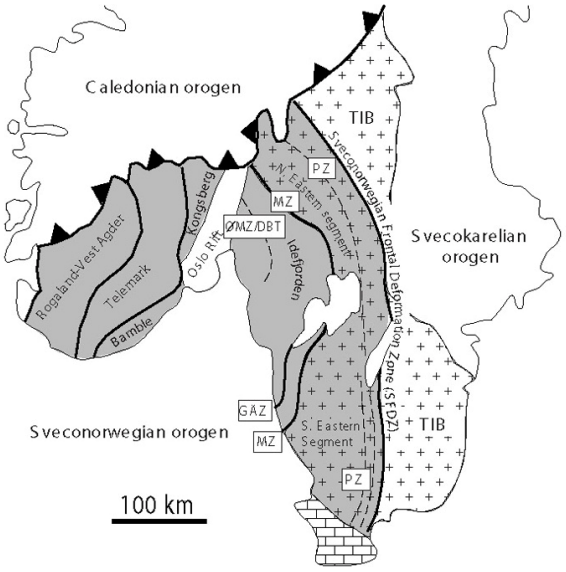

Figure 1. Sketch map of southern Sweden and Norway. The Sveconorwegian orogen is shown in shaded grey. Sveconorwegian deformation zones: PZ=Protogine Zone, MZ=Mylonite Zone; GÄZ=Göta Älv Zone; DBT=Dalsland Boundary Thrust; ØMZ=Ørje Mylonite Zone. TIB=Transscandinavian Igneous Belt. Location of the Sveconorwegian Frontal Deformation Zone north of Lake Vänern follows Stephens et al. (1996).

2.1 Objectives and scope

The aim of the research project has been twofold: 1) to obtain absolute U-Pb ages of zircon for different phases of metamorphism and deformation in the polymetamorphic, southeast Sveconorwegian Province (southwest Sweden) and 2) to investigate the mode of secondary zircon formation in a selection of metamorphic felsic igneous rocks. Although not a primary objective, protolith ages of the rocks have also been obtained. The results form a basis for geological interpretations pertinent to ongo-

ing bedrock mapping in southern Sweden by the Geological Survey of Sweden.

This report describes field relations and petrography of selected rocks at nine different localities, visited during 2004 and 2005, in the southern parts of the Eastern Segment and in the Protogine Zone (Fig. 1). It documents by backscatter electron (BSE) and cathodoluminescence (CL) images representative zircon morphologies from thirteen selected samples from these localities. The results from targeted ion probe analysis carried out in the spring 2005 are presented, comprising 118 individual spot analyses. Interpretations and conclusions are presented for each locality.

2.2 Geological setting

The Sveconorwegian Province forms a 500 kilometres wide mobile belt in the present day SW Baltic Shield. It is composed of several Proterozoic gneiss belts that are internally separated by roughly N-S-trending deformation zones (Fig. 1). The province is delimited to the east by the Sveconorwegian Frontal Deformation Zone (Wahlgren et al. 1994) east of which are c. 1.92-1.81 Ga rocks of the Svecokarelian orogen and generally undeformed rocks of the 1.81-1.66 Ga Transscandinavian Igneous Belt (Fig. 1). Age constraints of high-grade metamorphism across the Sveconorwegian Province points to a sequence of discrete compressional orogenic events that took place over a time period of more than 150 Ma, between approximately 1.13 and 0.96 Ga (Bingen et al. 2005, Andersson et al. 1999, 2002). A final compressional event at 0.97 Ga involved regional-scale metamorphism in the upper amphibolite to granulite facies in the southeasternmost part of the orogen. This event also included tectonic emplacement of eclogites and represents a tectonic scenario involving continental collisional orogenesis (Möller 1998,1999, Johansson et al. 2001).

The southern Eastern Segment forms a parautochthonous basement of the Sveconorwegian Province. It is composed of c. 1.73-1.66 Ga orthogneisses, largely migmatitic, that show geochemical similarities with largely undeformed coeval rocks of the Transscandinavian Igneous Belt (TIB) east of the Sveconorwegian Province. The orthogneisses of the Eastern Segment are separated from non-penetratively deformed and unveined rocks of the TIB by the Protogine Zone, a c. 25 km wide zone hosting numerous subvertical and discrete, N-S-trending deformation zones. To the west, the Eastern Segment is separated from allochthonous and overlying gneiss belts by the Mylonite Zone, a prominent and shallowly west-dipping deformation zone that represents a major lithological, metamorphic and structural terrane boundary (Andersson et al. 2002).

Pre-Sveconorwegian regional scale migmatisation in the southern Eastern Segment have been dated at about 1.44 Ga (Söderlund et al. 2002, Austin Hegardt et al. 2005). This event was succeeded at 1.40-1.38 Ga by intrusion of partly charnockitic granite and syenitoid rocks, and contemporaneous charnockitisation of country rock gneisses around felsic dyke intrusions at about 1.40 Ga (Hubbard 1975, Åhäll et al. 1997, Andersson et al. 1999, Johansson 1998, Rimsa et al. 2004). Estimates of metamorphic and tectonic conditions during the 1.44 and 1.40 Ga events are severely hampered due to overprinting by Sveconorwegian high-grade metamorphism and deformation. The Sveconorwegian metamorphism in the southern Eastern Segment reached upper amphibolite to high-pressure granulite conditions and P-T estimates obtained from metabasic rocks in the region yield temperatures between 680 and 770°C and corresponding pressures of 9-12 kbar (Johansson et al. 1991, Wang & Lindh 1996, Möller 1998, 1999, Söderlund et al. 2004). As a consequence, pre-Sveconorwegian minerals have recrystallised or re-equilibrated and early metamorphic min-

eral parageneses and mineral compositions are altered.

The youngest rocks in the southern Eastern Segment are high-angle discordant pegmatitic and granitic dykes dated at about 0.95 Ga (Möller & Söderlund 1997, Andersson et al. 1999). Structurally young metabasic dykes occur discordanct to veined gneissic fabrics in the country rocks but are themselves metamorphosed in the high-pressure granulite facies. The igneous emplacement age of these dykes is at present unknown.

2.3 Methodology

Age determination of a specific metamorphic or deformation event requires that (1) a mineral suitable for age determination is present and has crystallised, recrystallised or been through isotopic re-equilibration during the event of interest, and (2) the isotope system in the mineral used for age determination has remained closed to diffusion after the event of interest (i.e., the system has a closure temperature that is higher than temperature conditions succeeding the event). Few isotopic systems used today for age determination have closure temperatures high enough (> c. 650°C) to escape diffusion during cooling after high-grade metamorphism or re-heating during later events. Diffusion of U, Pb and Th in crystalline zircon is, however, known to be extremely slow at temperatures below 900 °C (Lee et al. 1997, Cherniak & Watson 2003). Unless zircon is recrystallised or resorbed and re-precipitated, its U-Pb-Th system therefore remains undisturbed after crystallisation even at elevated temperatures. The high closure temperature of zircon and the common occurrence of this mineral in crustal rocks make U-Pb analysis of zircon one of very few methods that are suitable for direct age determination of high-grade events.

During late Sveconorwegian orogenesis the southern part of the Eastern Segment was subjected to high-grade metamorphism at temperatures above 650°C (Möller 1998, and references therein). With the exception of the U-Pb system in zircon, all mineral isotope systems commonly used for age determination (such as for example the U-Pb system of titanite) have become completely reset (Johansson et al. 1991, Wang 1996, Connelly et al. 1996, Christoffel et al. 1999). The present project has exclusively used U-Pb analysis of zircon.

Due to the robustness of crystalline zircon to secondary alteration processes, age determination of metamorphic events using the U-Pb zircon system depends on that formation of secondary zircon has taken place during metamorphic recrystallisation of the rock. A complete resetting of the U-Pb isotopic clock essentially requires new crystallisation of zircon in the rock. Such new zircon growth may take place during partial melting, where zircon is partially dissolved by an aggressive fluid or melt and subsequently re-precipitated as a secondary phase as the melt crystallises (cf. Watson 1996). If partial melting has been extensive, such secondary zircon typically occurs as euhedral overgrowths around igneous zircon cores. The overgrowths may be discordant to the igneous zoning in the core and simple new zircon grains may form as well (cf. Andersson et al. 2002).

New growth of zircon may also take place during metamorphic recrystallisation connected to release of Zr (and Si) during metamorphic consumption or re-equilibration of zirconium-bearing igneous minerals, e.g. igneous pyroxene or ilmenite (cf. Fraser et al. 1997, Bingen et al. 2001, Moeller et al. 2002). This process is typically restricted to silica undersaturated, initially zircon-poor or zircon-free rocks (basic igneous rocks) in which Zr was incorporated in igneous mineral phases other than zircon. This type of secondary zircon typically occurs as U-poor, simple, unzoned or weakly zoned, commonly oblate and small grains, sometimes

forming microscopic strings of pearls along relict grain boundaries of pre-existing Zr-bearing igneous minerals (Bingen et al. 2001, Söderlund et al. 2004). In felsic igneous rocks, where zircon has become stable early in the magmatic crystallisation process, almost all Zr has been incorporated into igneous zircon. Remobilisation of Zr in these rocks therefore requires breakdown of highly robust crystalline zircon.

Despite the low diffusive rate of U-Pb-Th in zircon, in situ recrystallisation has been described from high-grade metamorphic rocks (Hoskin & Black 2000, Söderlund et al. 2002, Hoskin & Schaltegger 2003). The in situ recrystallised zircon typically occurs as domains that are CL-dark and BSE-bright and have a diffuse transitional, often concordant, textural relation to the protolith zircon. It commonly also exhibits a relict igneous zoning ("ghost zoning", Hoskin & Black 2000, Söderlund et al. 2002, Hoskin & Schaltegger 2003). The mechanism behind in situ recrystallisation fronts in zircon is at present poorly known.

Since secondary zircon can form by different mechanisms, successful dating of a specific metamorphic event relies not only on the ability to identify the secondary formed zircon phase (i.e., to distinguish between igneous and metamorphic zircon). Discrimination between different types and textural generations of secondary formed zircon is essential for the interpretation of which process acted during formation of the analysed zircon phase, and thereby for the connection between the zircon age and a geological event. In this study we combine documentation of the structural and lithological field relations of sampled rocks with petrography and high-spatial resolution zircon spot analysis guided by detailed BSE and CL imaging.

The aim of the present project has been to sample localities where secondary zircon can be expected to have formed and where the process is significant in a regional geological context. The four first localities described below (chapters 4-7) are examples of well-exposed relationships between partial melts and deformation structures. The three last localities (chapters 8-10) represent transitions between granitic and charnockite-like rocks.

3. Analytical methods

3.1 Preparatory work

Clean zircon mineral separates were obtained from grinding about one kg of rock sample in a swing mill to a fine powder with a size <200 μm mesh (90%). The rock powder was mixed with water and mild detergent (to avoid surface tension) and thereafter loaded in small portions on a full size Wilfley panning table. The magnetic minerals were removed from the obtained heavy mineral separate by a hand magnet. About 100-200 zircon crystals from each sample were hand picked and mounted on double faced tape before “moulded” in epoxy. After polishing the zircon mounts were ready for analysis.

3.2 Electron microscopy

Backscatter electron (BSE) and cathodoluminescence (CL) images have been used to locate texturally different types of zircon domains. BSE- and CL-images have been retrieved by standard electron microscopy at the Department of Geology, Lund University, and the Museum of Natural History in Stockholm, respectively.

3.3 Ion probe analysis

High-spatial resolution secondary ion masspectrometer analysis was made using a Cameca IMS 1270 at the Nordsim facility at the Swedish Museum of Natural History in Stockholm. Detailed descriptions of the analytical procedures for these analyses are given in Whitehouse et al. (1997, 1999). For sample/analysis OX-1/01a-09a and HB-1/01-12a, data were obtained in automatic chain analysis mode. Tables of analytical data are given in the Appendix. In the text, all statistical errors are referred to in a 95 percent confidence interval. Data plots were made using software Isoplot 3.00 (Ludwig 2003).

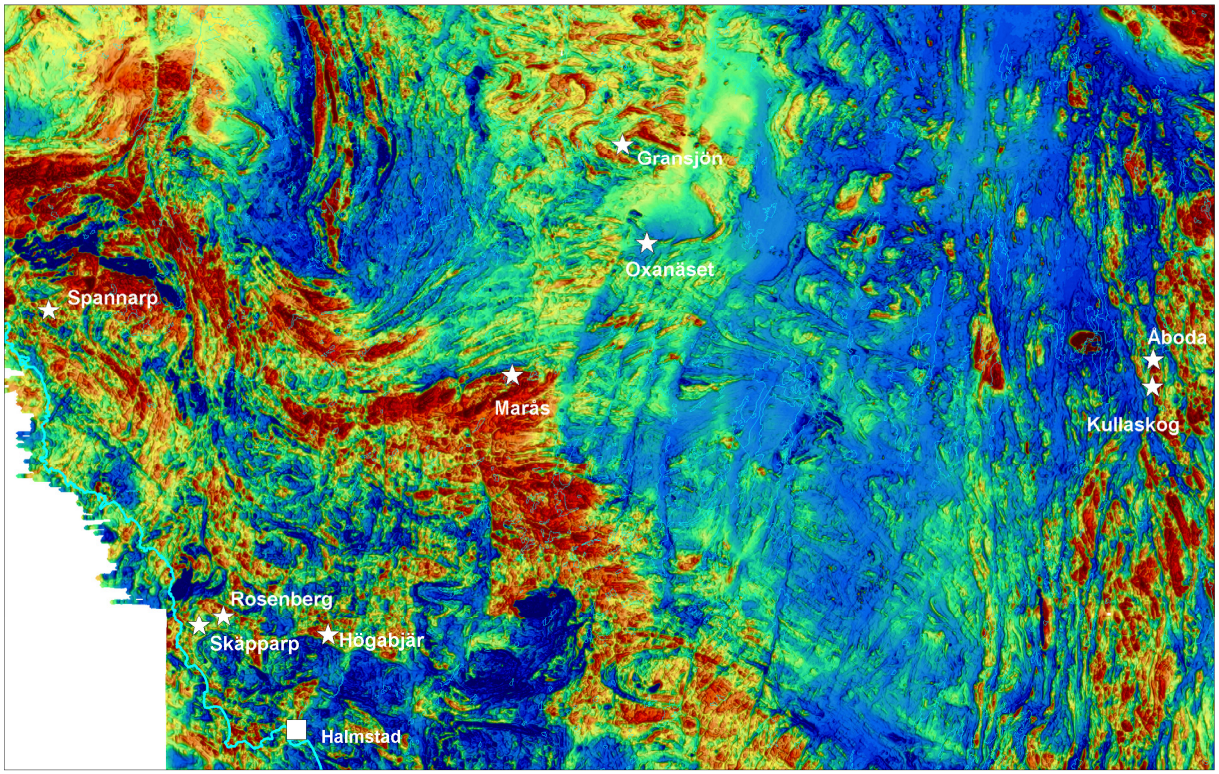

Figure 2. Magnetic anomaly map of a part of the southern Eastern Segment and the Protogine Zone. Red areas are magnetic highs and blue magnetic lows. The Protogine Zone shows up by distinct, north-south trending structures in the right hand part of the figure, whereas the Eastern Segment has a strongly banded and folded pattern. White stars mark investigated localities. Scale: 1 cm = 9 km. Part of the airborne magnetic map (total field) over SW Sweden. Data source: Geological Survey of Sweden, data compiled by Ildiko Antal.

4 Oxanäset: Late Sveconorwegian migmatisation and synchronous folding

4.1 Field relations and petrography

Regional context

Regional-scale, E-W-trending fold structures form a conspicuous structural pattern in the south and central Eastern Segment. The folds are upright to moderately overturned, have subhorizontal fold axes and wavelengths of c. 4-15 km. The fold structures form a spectacular pattern also on magnetic anomaly maps (Figs. 2 & 3A). Mapping in the region has shown that the migmatitic gneisses have been tightly folded along E-W-trending horizontal axes and garnet amphibolite layers have been stretched and boudinaged along the same E-W direction. An older fold phase has been identified as outcrop-scale, tight to isoclinal intrafolial

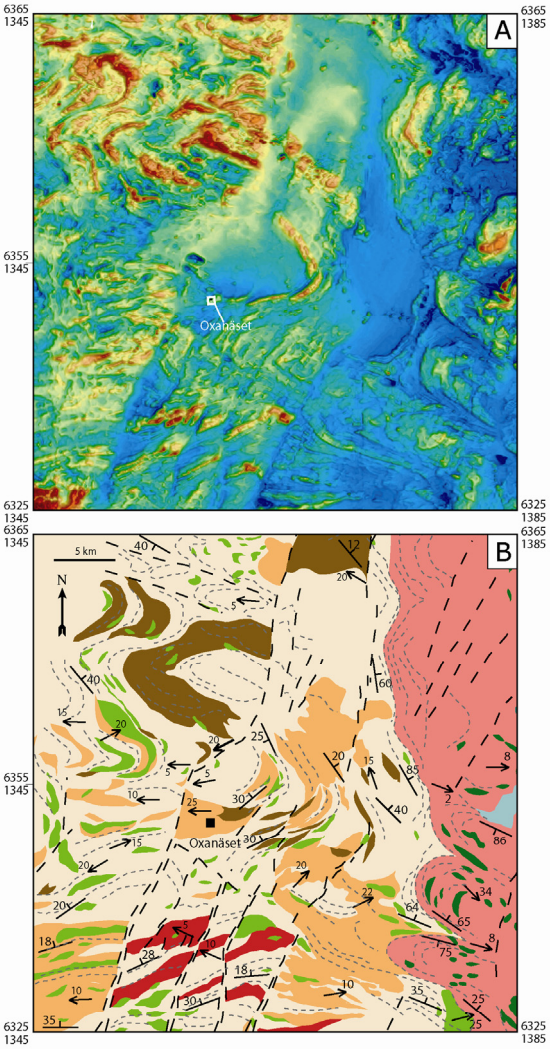

Eastern Segment, upper tecctonostratigraphic level

Light red granitic gneiss (meta-TIB with protolith age 1.67 Ga). Not migmatised.

Well preserved gabbro and metagabbro, locally garnet amphibolite (protolith age 1.57 Ga)

Garnet amphibolite locally with preserved igneous texture (meta-gabbro/dolerite, protolith ages 1.73-0.92 Ga). Not migmatised.

Eastern Segment, lower tectonostratigraphic level

Grey to red, granodioritic-granitic migmatite gneiss (protolith ages 1.73-1.66 Ga)

Grey and reddish grey quartz-monzonitic to quartzmonzodioritic (tonalitic-) gneiss, partly migmatised (protolith ages 1.73-1.66 Ga)

Greyish red and red granitic gneiss, partly migmatised (protolith ages 1.73-1.66 Ga)

Granitic to quartzmonzonitic augen gneiss, partly migmatised, partly well preserved K-feldspar megacrystic rock (protolith age: 1.39 Ga)

Garnet amphibolite, commonly migmatitic, and mafic high-pressure granulite, locally with partly preserved igneous texture (protolith ages 1.73-0.92 Ga)

Trend lines of regional gneissic layering and foliation

Fractures and faults

Gneissic foliation with dip

20 Lineation with plunge

20 Gneissic foliation with dip

Figure 3. A) Airborne magnetic map (total field). **B)** Geological map of the Oxanäset area, southcentral Eastern Segment. Simplified from the preliminary map of Jönköping county (in scale 1:250 000) . Data source: Geological Survey of Sweden.

folds, in places rootless. In the area south and west of Oxanäset small-scale folds are commonly south-vergent with subhorizontal E-W-trending fold axes (Fig. 4A). Another conspicuous structural feature characteristic of the high-grade rocks in the region is strongly developed stretching lineations defined by strung-out mineral aggregates, partial melts or amphibolite bands. The lineations are subhorizontal (undulating), roughly E-W striking and subparallel to the fold axes of the regional and outcrop scale E-W folds. In general, the linear fabric is more strongly developed than the planar and locally a planar fabric is lacking.

Locality
A quarry at Oxanäset (Swedish national grid (SNG): 6341958/1359701, Figs. 3A, B) exposes migmatite gneiss typical for the high-grade metamorphic, southern Eastern Segment. It is a light greyish red to reddish grey, fine- to medium-grained rock of predominantly granitic composition. Remnants of a coarser-grained, relict igneous protolith fabric are locally recognisable. The granitic gneiss at Oxanäset is penetratively migmatised. The veining varies in intensity from discrete to penetrative stromatic layering (Fig. 4B). The Oxanäset locality is located in the southern limb of a regional scale upright synform that has a slightly west-plunging axis and a fold wavelength of about 15 km, a fold structure that is easily distinguished on the magnetic anomaly map (Fig. 3A). In the region, granitic gneisses generally have higher contents of magnetite and thereby higher magnetic susceptibility than gneisses of tonalitic and granodioritic composition. The structure exemplifies that the magnetic anomaly map can be useful in tracing gneisses of granitic composition (cf. Figs. 3A, B). At outcrop scale, the migmatite gneiss has been tightly folded along gently west-plunging fold axes (Fig. 4A). The axial planes to these folds are gently north-dipping (Fig. 4A). The Oxanäset migmatite gneiss is intercalated with cm- to dm-wide bands and lenses of amphibolite (Fig. 4C) and with thick, up to 10 metres wide, boudins of compositionally layered garnet amphibolite (Fig. 4D). Vein material has been injected into the boudin necks.

At least three structural generations of veins can be recognised at Oxanäset. The oldest ones are penetrative, mm- to cm-wide, fine- to medium-grained granitic veins that define a stromatic layering concordant with the gneissic layering and which is folded at outcrop scale (pre-kinematic leucosome, Figs. 4A, B). A structurally younger generation of leucosome occurs as more than cm-wide, locally pegmatoid, veins that commonly are concordant to the gneissic layering, folded, but in places crosscut the fold structures (syn- to post-kinematic leucosome Figs. 4E-G). These veins locally host porphyroblasts of magnetite or hornblende (Fig. 4H). Both types of veins are bordered by melanosome and are interpreted to have formed from in situ partial melting of the granite gneiss protolith. A third type of leucosome is diffuse medium-grained anatectic leucocratic segregations that crosscut or just blur the folded veined gneissic structures (Figs. 4A, H). The leucosome that occurs in both folded and semi-discordant relations to the folds demonstrates that migmatisation took place synchronously with folding along E-W axes.

Three different samples were selected within the migmatite gneiss at the Oxanäs locality: gneiss mesosome (OX-1), migmatitic gneiss with pre-kinematic leucosome (OX-2), and syn- to post-kinematic leucosome (OX-3).

Gneiss mesosome (sample OX-1)
Sample OX-1 was selected from a fine- to medium-grained, strongly foliated granitic gneiss (Fig. 5A) without distinct leucosome segregations. Thin section shows that the rock consists dominantly of quartz, microcline and plagioclase (locally myrmekite) with granoblastic or

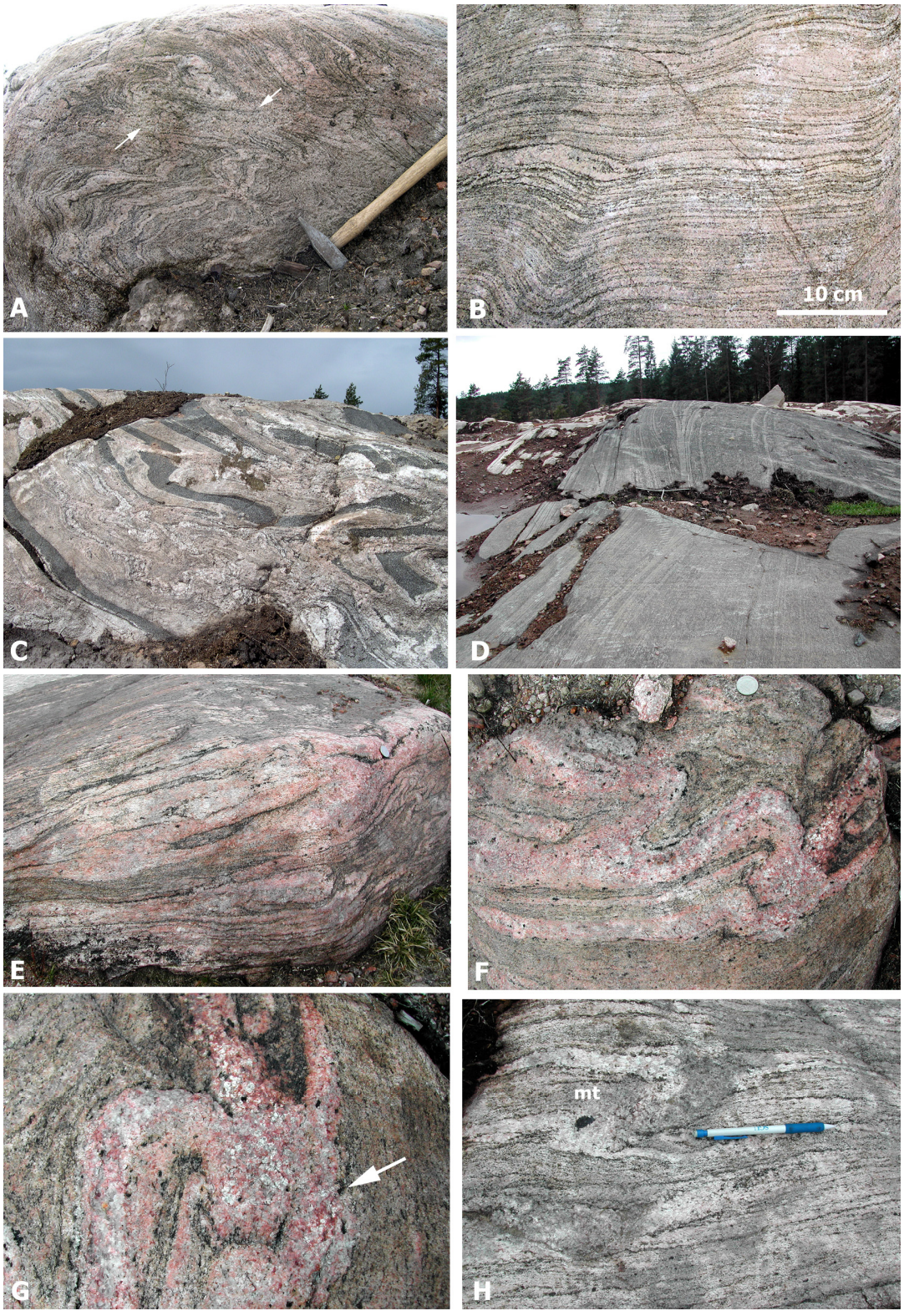

Figure 4. Oxanäset granitic gneiss, southcentral Eastern Segment. **A)** Migmatite gneiss, folded along gently west-plunging fold axis and gently north-dipping axial plane. North is towards the right. Arrows denote an anatectic segregate obscuring deformation textures. **B)** Stromatic layering in granitic gneiss. **C)** Disrupted and folded amphibolite bands in migmatite gneiss. **D)** Compositional layering in a concordant, c. 10 metres wide garnet amphibolite layer, boudinaged in E-W direction. **E)** Syn-kinematic, deformed and concordant pegmatitic material in folded migmatite gneiss, c.f. (G, H). North is towards the viewer. Coin (25 mm) for scale. **Continued on next page.**

smoothly sutured grain boundaries. Oriented grains of olive green biotite and titanite define the gneissosity. Titanite is abundant. Accessory minerals are opaque minerals, subhedral garnet, apatite, zircon, and single grains of flourite. Orange-coloured hematite occurs along grain boundaries.

Migmatitic gneiss with pre-kinematic leucosome (sample OX-2)
Sample OX-2 was selected from a reddish grey gneiss with fine-grained, greyish mesosome and distinct, light reddish, about 0.3-15 mm wide, folded leucosome of granitic composition (pre-kinematic leucosome, Fig. 5B). The rock is composed of quartz, microcline, plagioclase and small amounts of muscovite. Dark mineral phases are biotite (partly altered to chlorite), garnet, titanite, and opaque minerals. Accessory minerals are zircon, apatite, calcite, and strongly altered allanite. Muscovite occurs in small amounts in the leucocratic segregates where quartz may form up to 2-3 mm large grains.

Syn- to post-kinematic leucosome (sample OX-3)
Sample OX-3 was selected from an intensely migmatised, reddish grey, fine- to medium-grained gneiss with up to 10 cm wide, coarse-grained syn- to post-kinematic pegmatitic leucosome veins that are both folded and locally discordant to the folded veined gneiss structures (Figs. 4E-G, 5C). The texture is uneven-grained, with coarse-grained quartz, microcline, plagioclase and opaque minerals and fine-grained titanite and biotite. Accessory minerals are apatite, zircon and allanite. Aggregates of titanite contain small rounded zircon grains about 5 µm in diameter.

4.2 Zircon analysis: electron microscopy and analytical results

Thirty-seven spot-analyses were obtained from the three samples (OX1, OX2 and OX3) from Oxanäset. These are shown in Terra Wasserburg diagram (Figs. 6A, C, E). Thirty-two of the analyses define two distinct clusters at about 1.67 Ga (n=18, protolith age) and 0.98 Ga (n=14, migmatisation age). Five analyses spread along the concordia between 1.44 and 1.07 Ga. In the Th/U vs. U diagram (Figs. 6B, D, F). 1.67 Ga zircon is distinguished by its high Th/U ratio (> 0.69). The 0.98 Ga zircons have low Th/U ratios (<0.02) as have the remaining five analyses that spread between 1.44 and 1.07 Ga (0.01-0.07).

Gneiss mesosome (sample OX-1)
Zircon grains in sample OX-1 are approximately 100-200 µm in size, typically short prismatic (length to width ratios between 1.5 and 2) and anhedral with rounded terminations. Euhedral morphologies are rare and only found among small clear <50 µm grains. Most crystals are colourless but commonly contain cracks and inclusions, sometimes abundant. Reddish hematite staining occurs, especially along cracks. Images of internal textures typically show CL-bright and BSE-dark oscillatory zoned core domains, surrounded by a more or less anhedral and thin, commonly about 5-15 µm wide, CL-dark and BSE-bright rim (Fig. 7). These rims are, however, too thin to analyse with the spot size used during analysis.

Eight concordant spot analyses from igneous oscillatory zoned CL-bright and BSE-dark, domains yield a concordia age of 1668±11 Ma (MSWD=0.01, probability of fit=0.94; Fig. 6A). This age is identical to a weighted average $^{207}Pb/^{206}Pb$ age of 1667±15 Ma for the same eight

Figure 4 continued. F) Syn-kinematic, folded leucosome partly cross-cutting a stromatic layering. Coin (25 mm) for scale. **G)** Close-up of the cross-cutting relation in (F). **H)** Magnetite blastesis in leucosome.

Figure 5. Samples from Oxanäset granitic gneiss selected for zircon geochronological work. Coin (20 mm) for scale. **A)** Strongly foliated gneiss mesosome, sample OX-1. **B)** Migmatite gneiss with pre-kinematic leucosome, sample OX-2. **C)** Syn- to post-kinematic pegmatitic leucosome, sample OX-3.

analyses (MSWD=0.89, probability of fit=0.51). Th/U ratios are 0.76-0.94 and U concentrations are 61-105 ppm (Fig. 6).

Migmatitic gneiss with pre-kinematic leucosome (sample OX-2)

The zircon morphology is similar to that of sample OX-1 except for the occurrence of larger, slightly turbid and clouded greyish grains. CL-bright and BSE-dark cores with igneous oscillatory zoning dominate. The core domains are typically surrounded by 5-30 µm wide, CL-dark and BSE-bright rims. Most rims are anhedral but some grains have sub- to euhedral outer CL-dark and BSE-bright rims (Fig. 7, analysis n1753-03a). CL-dark and BSE-bright zircon is, however, also found in the interior parts of some grains. These CL-dark and BSE-bright internal domains in places show a faint relict igneous oscillatory zoning although blurred (Fig. 7, analysis n1753-08a), probably by overprinting diffusion.

Nine spot analyses were obtained from zircon in sample OX-2 (Fig. 6C). Three concordant analyses in core domains (two oscillatory-zoned CL-bright and BSE-dark and one CL-dark and BSE-bright) yield a concordia age of 1688±26 Ma (Fig. 6C, MSWD=1.08, probability of fit=0.30) or a weighted average $^{207}Pb/^{206}Pb$ age of 1692±45 Ma (MSWD=2.4, probability of fit=0.51). These ages are within errors identical with ages for protolith zircon obtained in the gneiss mesosome (sample OX-1, described above). The three core domains all have high Th/U ratios (> 0.75) similar to the protolith zircon in sample OX-1 (Fig. 6D). The U content is, however, higher (c. 500-900 ppm) in two of the analysed core domains.

One analysis, slightly discordant (0.7% at 2σ level), of an unzoned, CL-dark and BSE-bright zircon gave a $^{207}Pb/^{206}Pb$ age of about 970±14 Ma (Fig. 7; analysis n1753-02a). This age is identical to the age of migmatisation obtained in other parts of the southern Eastern Segment (Andersson et al. 1999, 2002). This analytical point also yields the highest U and lowest Th content obtained among the analyses from OX-2 (2774 ppm U, Th/U<0.01).

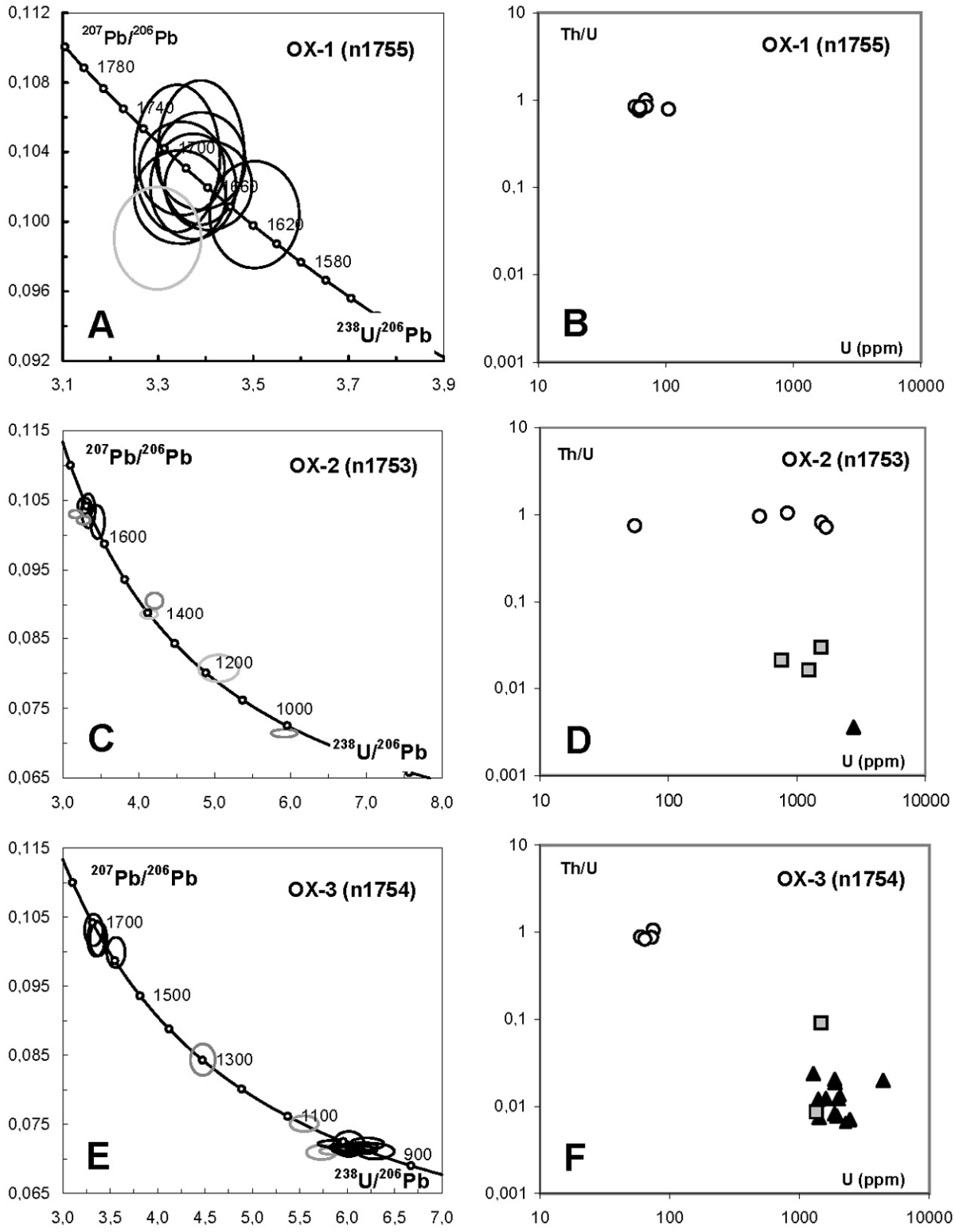

Figure 6. Inverse concordia (Terra-Wasserburg) and Th/U vs. U diagrams of ion microprobe zircon U-Pb-Th data from the Oxanäset granitic gneiss. Black error ellipses denote data used for age calculation. Symbols in the Th/U vs. U diagram; open circles = 1.7 Ga igneous core domains, grey squares = mix between two different types of zircon domains, black triangles = Sveconorwegian secondary formed (metamorphic) domain. **A, B)** Strongly foliated gneiss mesosome, sample OX-1. **C, D)** Migmatitic gneiss with pre-kinematic leucosome, sample OX-2. **E, F)** Syn- to post-kinematic pegmatitic leucosome, sample OX-3.

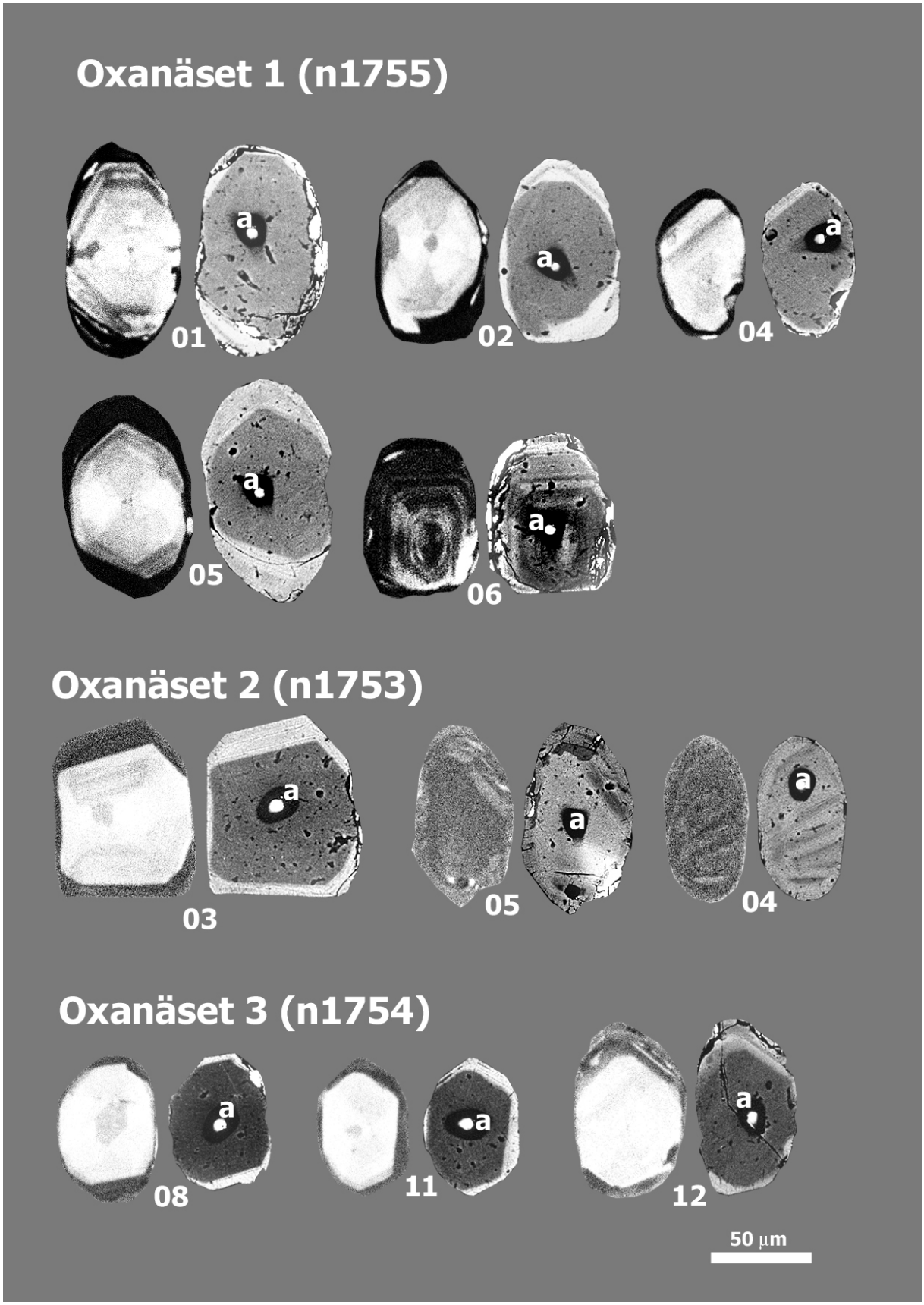

Figure 7. CL- and BSE-images of zircon from the three samples from Oxanäset granitic gneiss (OX-1, OX-2 and OX-3) used for U-Pb ion microprobe analyses. Individual crystals are shown both as CL-image (left) and BSE-image (right). Numbers refer to grain number in the Appendix. **Continued on the next page.**

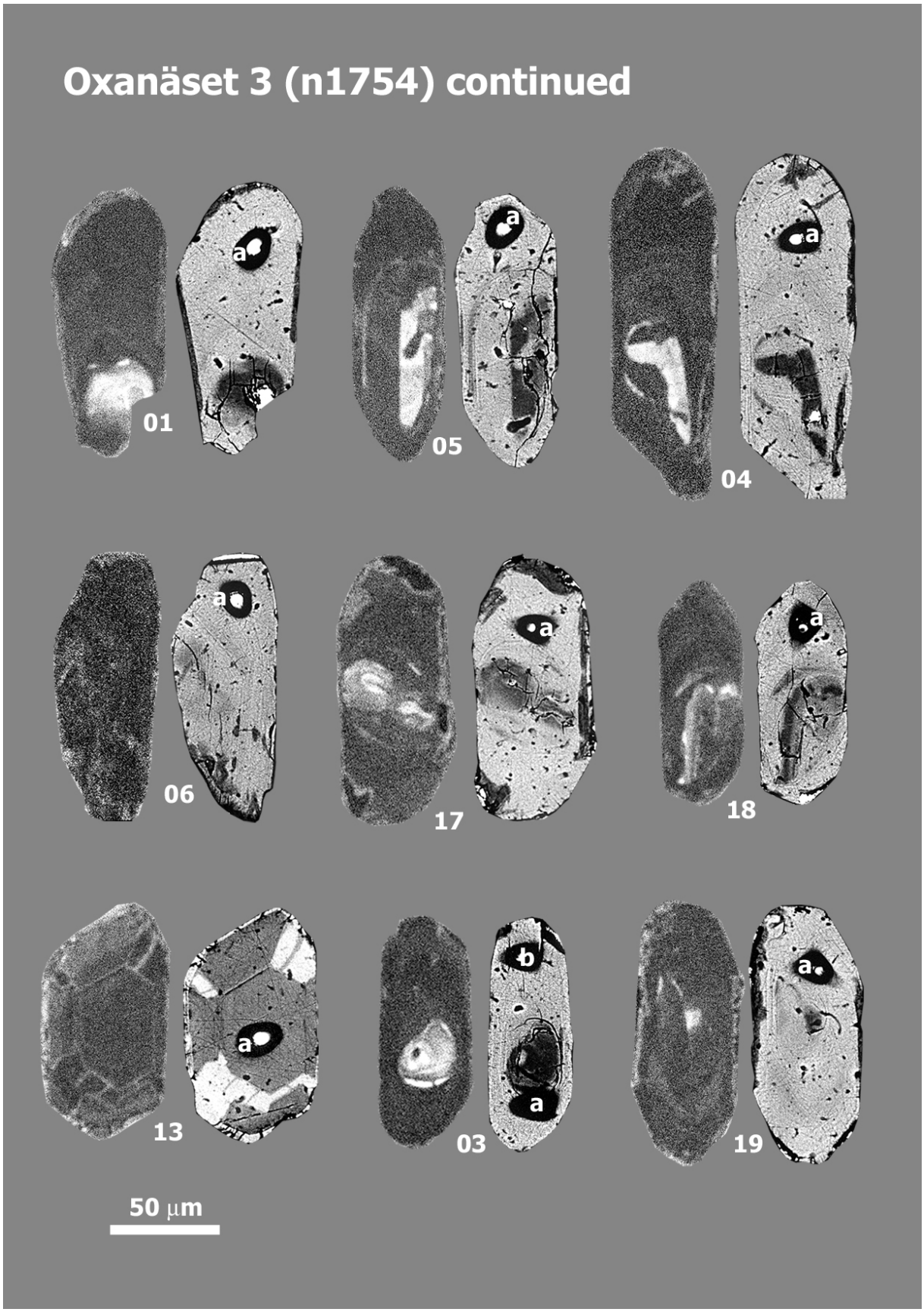

Figure 7 continued. Analysed spots occur as black areas in the BSE-images. Letter in black spot area refers to identity of analysed spot in the Appendix.

Two analyses in CL-bright and BSE-dark unzoned core domains and one analysis in CL-bright and BSE-dark rim (not distinct overgrowth) yield $^{207}Pb/^{206}Pb$ ages between 1.44-1.21 Ga. They have U concentrations between 760-1543 ppm and Th/U ratios at 0.03-0.02, values that are between the values obtained for the 1.67 Ga old protolith zircon and the young 0.97 Ga zircon in the sample.

Syn- to post-kinematic leucosome (sample OX-3)
The zircon morphology is similar to that of OX-2, but some grains also have euhedral crystal faces. CL-bright and BSE-dark core domains, in places with igneous oscillatory zoning, occur in some grains, but the area of CL-dark and BSE-bright domains is significantly larger and the domains more homogenous than in OX1 and 2 (Fig. 7). The majority of the CL-dark and BSE-bright domains are large and unzoned rims that surround small irregular CL-bright and BSE-dark remnant cores of igneous protolith zircon (Fig. 7). In some grains "ghost structures" of igneous oscillatory zoning may be recognised in the secondary altered CL-dark and BSE-bright domains (e.g., grain 06, 04 and 19 in Fig. 7). These CL-bright and BSE-dark domains are similar to secondary zircon domains that form by diffusion after igneous crystallisation (in situ recrystallisation, cf. Hoskin & Black 2000). Some grains also have an outer unzoned rim without relict igneous zoning that appears as an overgrowth of newly crystallised zircon. This type of newly crystallised zircon is abundant and voluminous in sample OX-3.

Nineteen spot analyses of zircon (two of them discordant) were obtained from the OX-3 sample (Fig. 6E). Four analyses in CL-bright and BSE-dark core domains with broad igneous zoning bands (Fig. 7) yielded $^{207}Pb/^{206}Pb$ ages between 1.68 and 1.62 Ga that are identical with ages obtained in protolith zircon in sample OX-1 and 2. These domains also have low U concentrations (<75 ppm U) and high Th/U ratios (>0.79, Fig. 6E).

Eleven concordant analyses from secondary CL-dark and BSE-bright domains, including both unzoned homogenous rim domains and domains with remnants of an igneous oscillatory zoning, yielded a weighted average $^{207}Pb/^{206}Pb$ age of 976±7 Ma (MSWD=1.7, probability of fit=0.08). These domains are also high in U (>1250 ppm) and have low Th/U ratios (<0.02).

Two analyses in CL-dark and BSE-bright domains surrounding igneous protolith zircon core domains yielded $^{207}Pb/^{206}Pb$ ages of 1072±12 and 1301±21 Ma (analyses n1754-03a and 19a, respectively) and likely include material from both igneous protolith zircon and partly or completely reset domains.

4.3 Summary and interpretation

All three samples have CL-bright and BSE-dark oscillatory zoned zircon core domains characterised by high Th/U ratios (>0.69) and relatively low U contents (<105 ppm U, except for a few analyses in sample OX-2). This type of zircon is interpreted as igneous protolith zircon. The analyses of igneous zircon in the gneiss mesosome (sample OX-1) dates the igneous emplacement of the Oxanäset granite gneiss at 1668±11 Ma (concordant age, n=8, MSWD=0.01, Probability of concordance=0.94). The Oxanäset gneiss protolith is thus coeval with 1.73-1.66 Ga gneiss protoliths in the southcentral Eastern Segment (Connelly et al. 1996, Christoffel et al. 1999, Söderlund et al. 2002, Andersson et al. 2002, in press, Johansson et al. in press).

Comparison of the zircon populations in the three different samples demonstrates that the same type of zircon can be found in all three samples. The three principal zircon types are: (1) CL-bright and BSE-dark oscillatory zoned igneous protolith zircon cores with low U concentrations and high Th/U ratios (Figs. 6B, D, F), (2) CL-dark and BSE-bright secondary zircon domains with relict igneous oscillatory zoning and, (3) unzoned homogenous CL-dark and BSE-bright secondary formed outer rims and overgrowths without remnants of relict zoning. The two types of secondary formed zircon are both high in U and have corresponding low Th/U ratios (Fig. 6). The proportion of the different types of zircon, however, varies widely between the three samples. Protolith zircon dominates in the mesosome (OX-1) where secondary formed zircon is sparse and only occurs as thin <5μm rims. Secondary formed zircon is more common in the migmatite gneiss (OX-2), but still not abundant. In contrast, zircon in the dm-wide leucosome vein (OX-3) is dominated by secondary formed domains. The correlation between the amounts of leucosome and secondary zircon demonstrates that formation of secondary zircon is related to migmatisation of the gneiss protolith. The formation of this secondary zircon and the timing for migmatisation is set at 976±7 Ma (weighted average $^{207}Pb/^{206}Pb$ age of secondary formed zircon in OX-3). This age of migmatisation at Oxanäset is identical with 0.98-0.96 Ma ages of migmatisation and metamorphism in the upper amphibolite and high-pressure granulite facies metamorphism in other parts of the southern Eastern Segment (Wang 1996, Cornell et al. 1997, Söderlund et al. 2002, Andersson et al. 1999, 2002). It is also within error identical to the age of 972±14 Ma for eclogite metamorphism (Johansson et al. 2001) recorded from tectonically emplaced eclogite remnants occurring 30-50 km west of Oxanäset. The 976±7 Ma age of syn-kinematic leucosome at Oxanäset dates directly the regional folding along E-W axes in the southern Eastern Segment.

Five of the zircon analyses from OX-2 and OX-3 give ages that fall between the 1.67 and 0.98 Ma generations of igneous and migmatite zircon at Oxanäset. These analyses spread along the concordia between 1.44 and 1.07 Ma and can either represent ages of pre-Sveconorwegian secondary zircon or artefacts produced by mixed volumes of 1.67 Ga protolith zircon and domains completely or partly reset at 0.98 Ga. At several other localities in the south-central ES, secondary zircon formation caused by metamorphism and partial melting at c. 1.44 and 1.40 Ga has been identified (Christoffel et al. 1999, Söderlund et al. 2002, Rimsa et al. 2004, this report chapter 5 and 6). If any of these generations of secondary zircon are present in the Oxanäset zircon populations, they are clearly subordinate.

5. Gransjön: 1.42 Ga migmatisation and age brackets for recumbent folding and mafic dyke intrusion

5.1 Field relations and petrography

Regional context

In the area west of Gislaved and Hestra (Fig. 8) the magnetic anomaly map shows a spectacular fold pattern characterised by gently plunging, E-W trending axes and upright geometry. Outcrop-scale folds with subhorizontal fold axes and axial planes appear structurally early in relation to the map-scale folds. These recumbent folds have been documented at several localities in the area around Gislaved but their age is unknown.

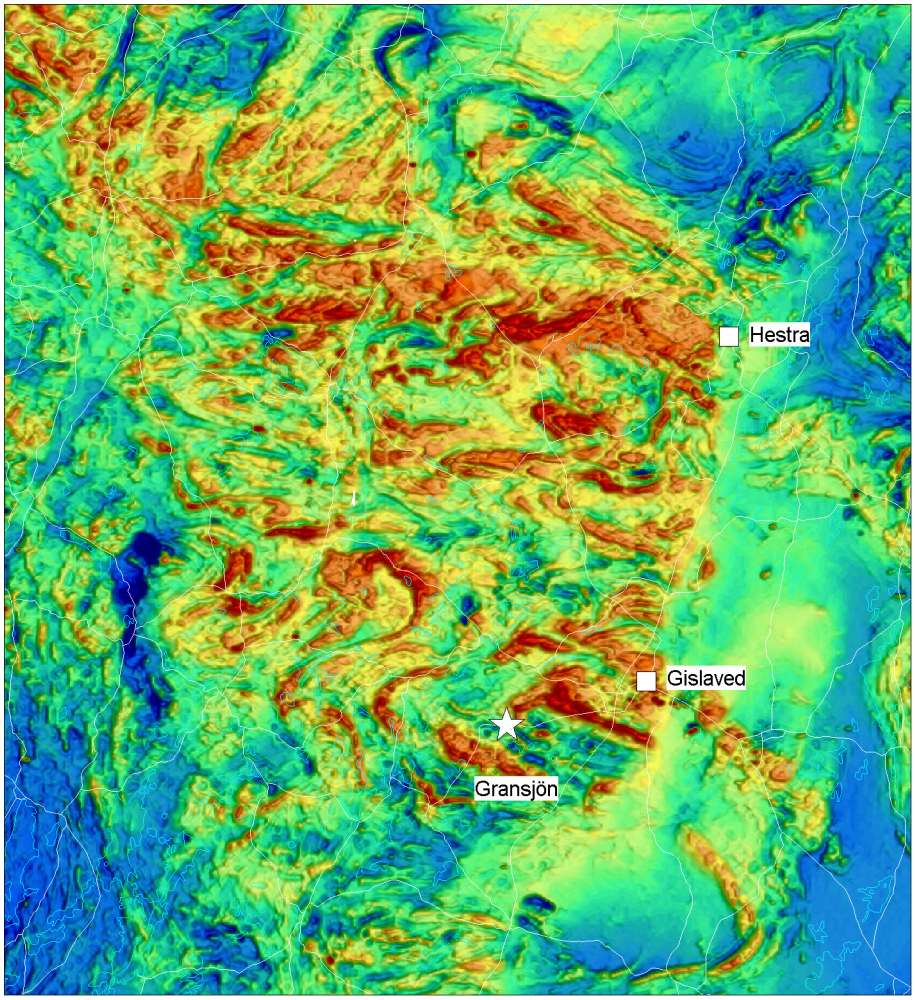

Figure 8. Close-up of the magnetic anomaly map in Fig. 2 illustrating the large-scale E-W trending folds in the area west of Gislaved and Hestra and the location of the road cut at Gransjön (marked by a white star). Scale: 3 cm = 10 km. Roads are outlined by very thin, white lines.

At several localities throughout the southern part of the Eastern Segment, ductile and migmatitic structures are crosscut by high-grade metamorphic dolerite. The intrusion of these dolerites reflects a regional, extensional event but the age of this event is unknown, mainly because age determination of primary igneous minerals has been regarded difficult due to Sveconorwegian high-grade metamorphic recrystallisation. One of these young metadolerites cut a recumbent fold structure in the area west of Gislaved.

Zircon from leucosome in migmatitic and folded gneiss, cut at a high angle by metadolerite, has been investigated and dated in the purpose of 1) defining an approximate age of migmatisation and 2) setting an upper age bracket for recumbent folding and subsequent mafic dyke intrusion.

Locality

Grey gneiss is well exposed along a road cut at Gransjön, c. 3 km west of Gislaved (SNG: 6353415/1356884). It is partly migmatitic and most veins are concordant with the gneissosity that is folded along subhorizontal axial planes (Fig. 9A). The structures are crosscut at a high angle by a moderately west-dipping mafic dyke, c. 2 metres wide (Figs. 9B, C). The mafic dyke is fine-grained and has a high-pressure granulite facies assemblage (cf. thin section description below).

Figure 9. Photographs of the locality at Gransjön. **A)** Fold structure in grey gneiss with light reddish leucosome at Gransjön. The height of the outcrop is c. 4 metres. **B)** West-dipping metadolerite (dark), crosscutting migmatitic, grey gneiss at Gransjön. The height of the outcrop is c. 5 metres. **C)** Metadolerite crosscutting the leucosome and the gneissic foliation in the host gneiss. In the upper left part of the picture is metadolerite with a sharp contact to the host rock. The lower part of the photo shows a thin apophysis cross-cutting the folded leucosome and the gneissic foliation in the host gneiss. In the upper left part of the picture is metadolerite with a sharp contact to the host rock. The lower part of the photo shows a thin apophysis cross-cutting the folded gneissic foliation. Coin (25 mm) for scale.

Samples

The dated sample was taken from grey gneiss with light reddish leucosome veins situated next to thin apophyses of the metadolerite. The gneiss matrix and leucosome are foliated, folded and cut at a high angle by the apophyses (Fig. 9B). After crushing, pieces of leucosome with subordinate volumes of mesosome were picked out for zircon separation.

The grey gneiss is fine-grained with a foliation defined by alternating dark and light mineral domains. Main minerals are feldspars, including antiperthite, quartz, olive-green hornblende, and brown biotite (Fig. 10A). Grains are uneven in size and grain boundaries are irregularly shaped, locally sutured (Fig. 10B). Accessory minerals are titanite, anhedral garnet, opaque minerals, apatite, allanite (altered), and zircon.

The mafic dyke is very fine-grained and has a high-pressure granulite facies assemblage rich in clinopyroxene, plagioclase and garnet, with lesser amounts of biotite, quartz and opaque minerals (Fig. 10C). Grain boundaries are granoblastic or smoothly irregular. A foliation (very subtle in hand specimen) is defined by elongated light and dark mineral domains and by the orientation of biotite grains. Larger (0.3-0.5 mm) grains of clinopyroxene have a dusty appearance due to numerous small opaque inclusions and are probably chemically modified remnants of primary igneous clinopyroxene.

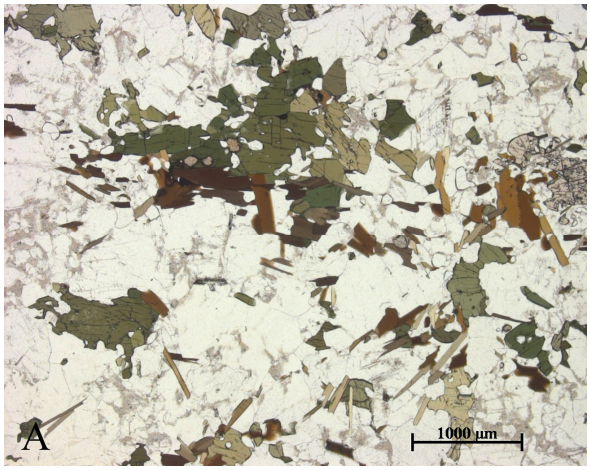

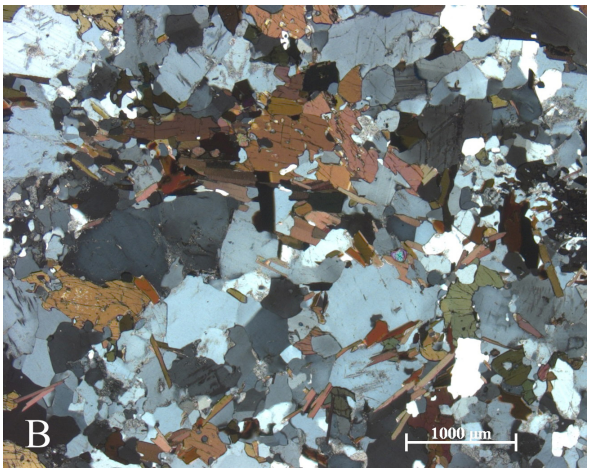

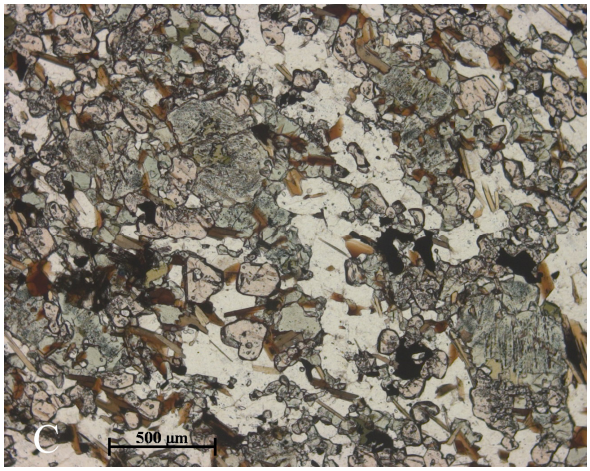

Figure 10. Photomicrographs of rocks from the Gransjön locality. **A)** Grey gneiss in plane light, illustrating the dark mineral assemblage. Hornblende is pleochroic in olive green shades, biotite is pleochroic in brown, a single garnet grain is strongly anhedral (light reddish, high relief in the right part of the picture) and titanite occurs as small brownish inclusions in hornblende (central to upper left part of the photo). **B)** Grey gneiss (in A) under crossed polars, illustrating the granoblastic and irregular grain shapes of feldspars and quartz (white to dark grey shades). **C)** Metadolerite, plane light, with a fine-grained, granoblastic, high-pressure granulite facies assemblage. Clinopyroxene is light green, garnet light reddish (high relief), plagioclase is colourless (low relief). Small, oriented biotite grains define the foliation. Slightly larger grains of clinopyroxene have a dusty appearance caused by tiny opaque inclusions and are most likely remnants of primary igneous clinopyroxene.

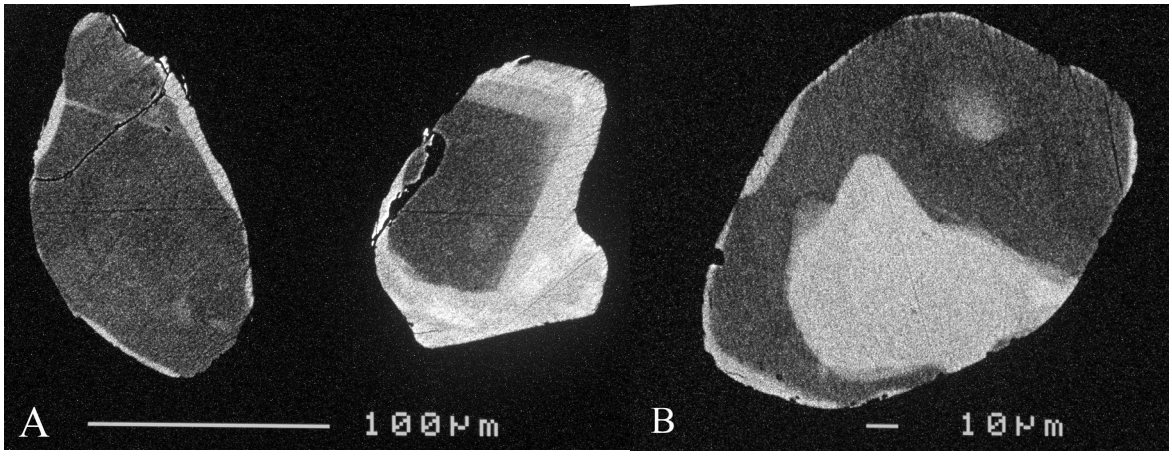

Figure 11. BSE-images of zircon grains from the leucosome in grey gneiss at Gransjön. **A)** Two typical zircon grains with rounded shapes, BSE-dark igneous cores and up to 40 µm wide BSE-light, secondary rims. Spot analysis of the dark domain in the grain on the left yielded a $^{207}Pb/^{206}Pb$ age of 1688±20 Ma (analysis n1750-01c). The light rim on the grain at the right yielded $^{207}Pb/^{206}Pb$ age of 1431±21 Ma (analysis n1760-02a). **B)** Rounded zircon crystal with secondary BSE-light domain yielding a $^{207}Pb/^{206}Pb$ age of 1446±8 Ma (analysis n1760-09a).

5.2 Zircon analysis: electron microscopy and analytical results

Zircon grains are oval or facetted with rounded edges and tips. A few grains have irregular morphology. In BSE-images most zircon grains have a dark, homogeneous interior and a distinct, light, up to 40 µm thick rim (Figs. 11A, B). A few grains were found with oscillatory zoning or BSE-light interiors.

Four analyses were made from zircon interiors and five from rims. The concordia diagram (Fig. 12A) illustrates that the rims are c. 1.4 Ga and distinctly younger than the igneous zircon (weighted average $^{207}Pb/^{206}Pb$ age =1415±36, MSWD=9.5). The analyses of igneous zircon form a crude discordia with an upper intercept at c. 1.7 Ga (1697 +96/-37 Ma, MSWD=0.54, LI= 934 + 330/-230). In the U vs. Th/U plot the analyses form two distinct groups where the interiors have a typically igneous character with low U contents (38-204 ppm) and high Th/U ratios (0.75-1.15) whereas the rims are higher in U (233-542 ppm) and have low Th/U ratios (0.03-0.05).

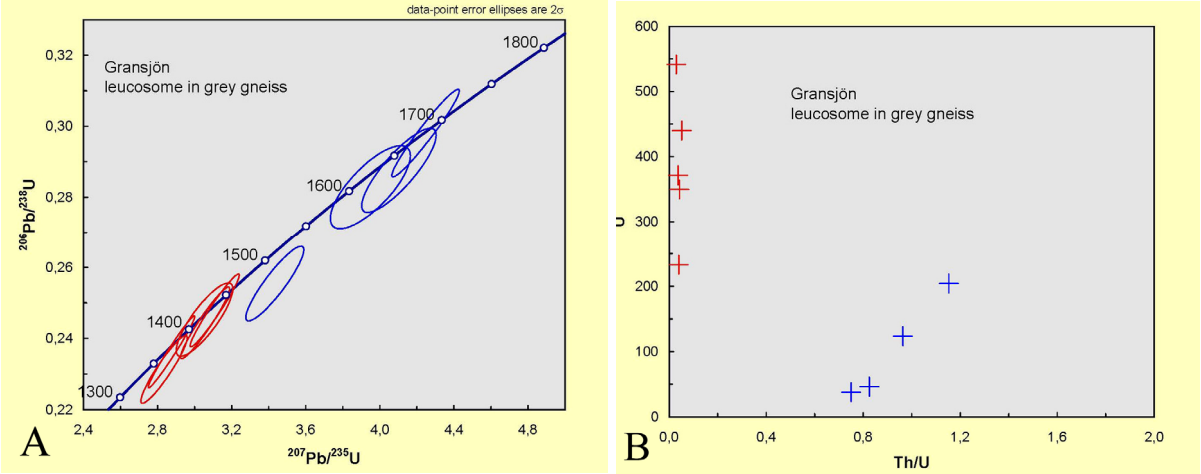

Figure 12. Analytical data from zircon in the Gransjön leucosome. **A)** U-Pb concordia diagram showing zircon analyses of igneous BSE-dark (blue) and secondary (red) domains. Error ellipses are plotted at 2σ level.
B) U vs. Th/U plot, illustrating the chemical difference between igneous, BSE-dark (blue) and secondary BSE-light (red) zircon.

5.3 Summary and interpretation

Zircon from the leucosome records a protolith age of c. 1.7 Ga for the grey gneiss at Gransjön. It thus belongs to the 1.73-1.66 Ga old generation of intrusions that dominate the bedrock in the Eastern Segment (cf. Oxanäset, 4.3 above). The migmatisation took place prior to the Sveconorwegian orogeny, at 1.40-1.45 Ga, and can be compared to similar ages obtained from southwestern parts of the Eastern Segment (Söderlund et al. 2002).

The age for migmatisation also sets an upper age limit at 1.45 Ga for the recumbent folding and for the dolerite intrusion. It is posssible that the dolerite belongs to one of the generations known from the Protogine Zone just east of the Eastern Segment dated at 1.40, 1.20 and 0.95 Ga (Johansson & Johansson 1990, Lundqvist 1996, Söderlund et al. 2005). The high-pressure granulite facies metamorphism sets a lower age bracket for recumbent folding and for the dolerite intrusion at c. 0.95 Ga (cf. Möller & Söderlund 1997, Möller 1998, Wang 1996, Andersson et al. 1999, Johansson et al. 2001, Söderlund et al. 2002). The present data thus set restrictions for the tectonic scenario. Two models appear feasible:

1) Migmatisation and folding along subhorizontal axial planes are both the results of orogenic processes at 1.40-1.45 Ga. Dyke intrusion took place thereafter, possibly at 1.4, 1.2 or 0.95 Ga (dolerite generations occurring in the Protogine Zone). The Sveconorwegian orogeny resulted in a high-grade metamorphic overprint but the bedrock domain (areal extent unknown) escaped significant deformational overprint.

2) A thermomagmatic or an orogenic event at 1.40-1.45 Ga resulted in migmatisation. Folding along subhorizontal axial planes took place during the Sveconorwegian orogeny, at c. 0.98-0.96 Ga. Dyke intrusion and high-pressure granulite facies metamorphism are both expressions of orogenic collapse at c. 0.95 Ga, prior to uplift and cooling of the Eastern Segment.

6 Högabjär: Migmatitisation and fold structures in "Hallandia" gneiss

6.1 Field relations and petrography

Regional context
The southern part of the Eastern Segment has undergone regional Sveconorwegian high-pressure granulite facies metamorphism, migmatisation and deformation but also experienced an older migmatisation event at c. 1.44 Ga (Söderlund et al. 2001). The character of this event is relatively poorly defined and distinction between Sveconorwegian and 1.44 Ga

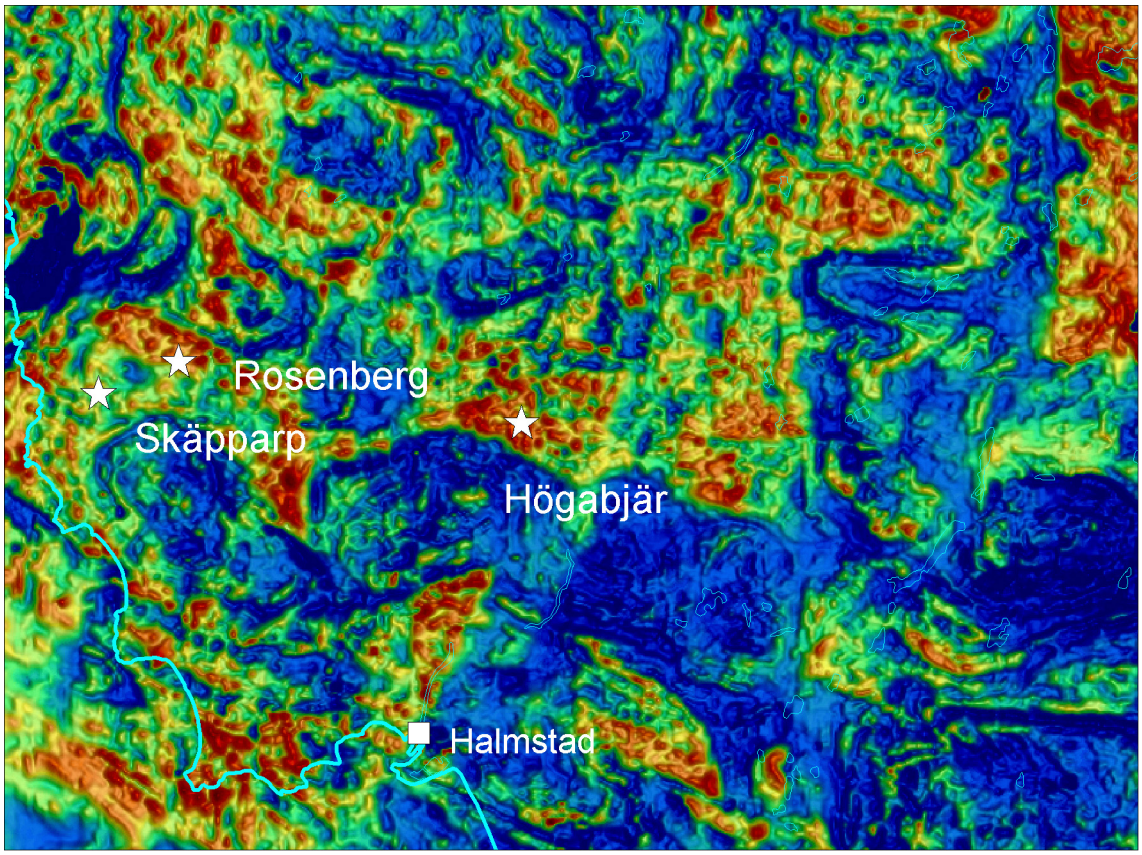

Figure 13. Magnetic anomaly map of the area north of Halmstad (close-up of Fig. 2) showing the locations of Högabjär, Skäpparp and Rosenberg. Scale: 3 cm = 8 km. A light blue line outlines the coastline.

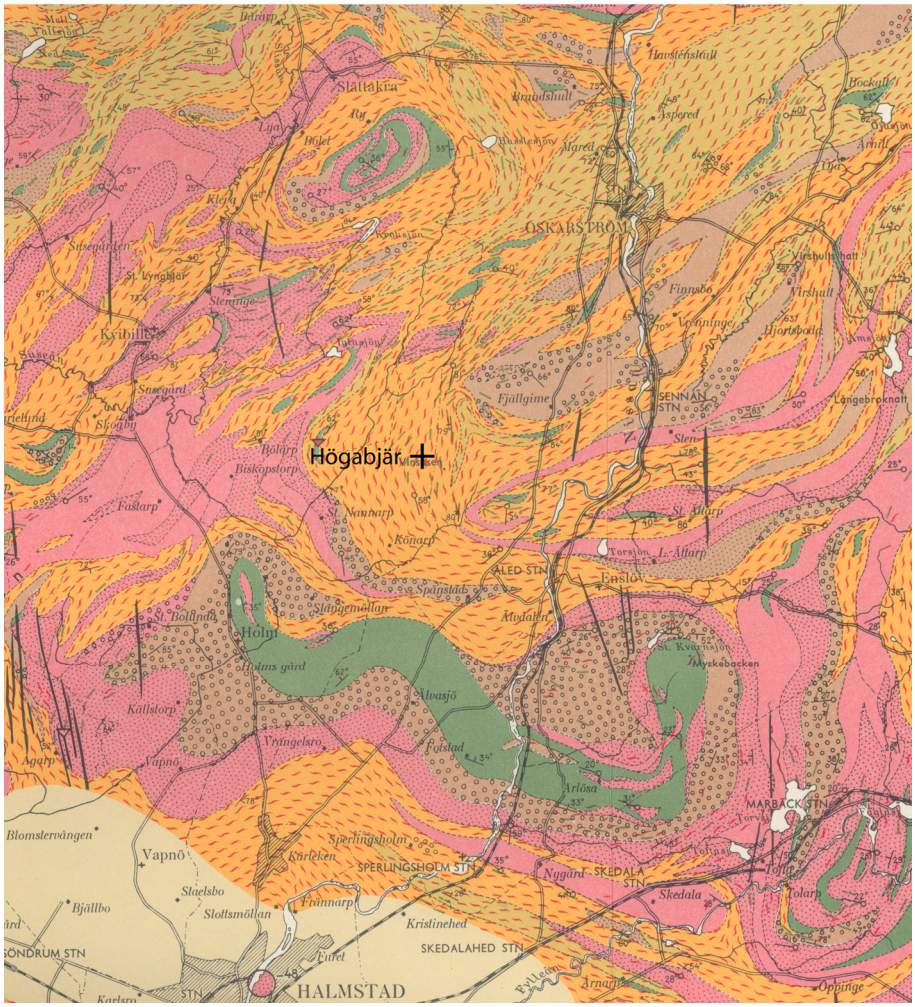

Figure 14. Detail of the geologic map by Larsson (1956) of the area north of Halmstad, illustrating the fold interference patterns and the location of Högabjär. Different varieties of gneiss are shown in pink, brown and orange colours (pink and brown are granitic compositions). Metabasites, mainly garnet amphibolite, are shown in green. Black streaks mark occurrences of metadolerite. Circles mark augen texture, red and wavy lenses mark migmatitic structure. Scale: 1 cm = 1.5 km.

structures and metamorphic features is difficult. A migmatitic gneiss, representative for large parts of the southwest Eastern Segment and quarried and marketed under the name “"Hallandia"”, has been investigated in the aim of defining characteristic migmatite and fold structures in the region.

Locality

A quarry at Högabjär (SNG: 6296485/1322810), 10 kilometres north of Halmstad (Figs. 13 & 14), exposes three dimensional structural relations typical for "Hallandia" gneiss.

The "Hallandia" gneiss is reddish grey, fine- to medium-grained and has medium-grained, greyish-red, granitic leucosome that make up c. 20-30% of the rock volume (Figs. 15A, B). The leucosome veins are generally up to 5 cm thick but locally decimetre-wide leucosome occurs. Melanosome is lacking. The veins are oriented subparallel to one another and define a gneissic layering with an overall attitude around 200/70 WNW (strikes are given in 0-360°/ dips in 0-90°).

Red, medium- to coarse-grained granitic dykes, up to 0.5 m wide, have intruded the migmatised gneiss and occur with low- to high-angle discordant relations to the gneissic layering (Figs. 15B, C). The granitic dykes are oriented roughly 150/60 W, but both dykes and migmatite gneiss have been folded together (Figs. 15B, C, D) and the original structural geometry at the time of dyke intrusion has thus been severely modified.

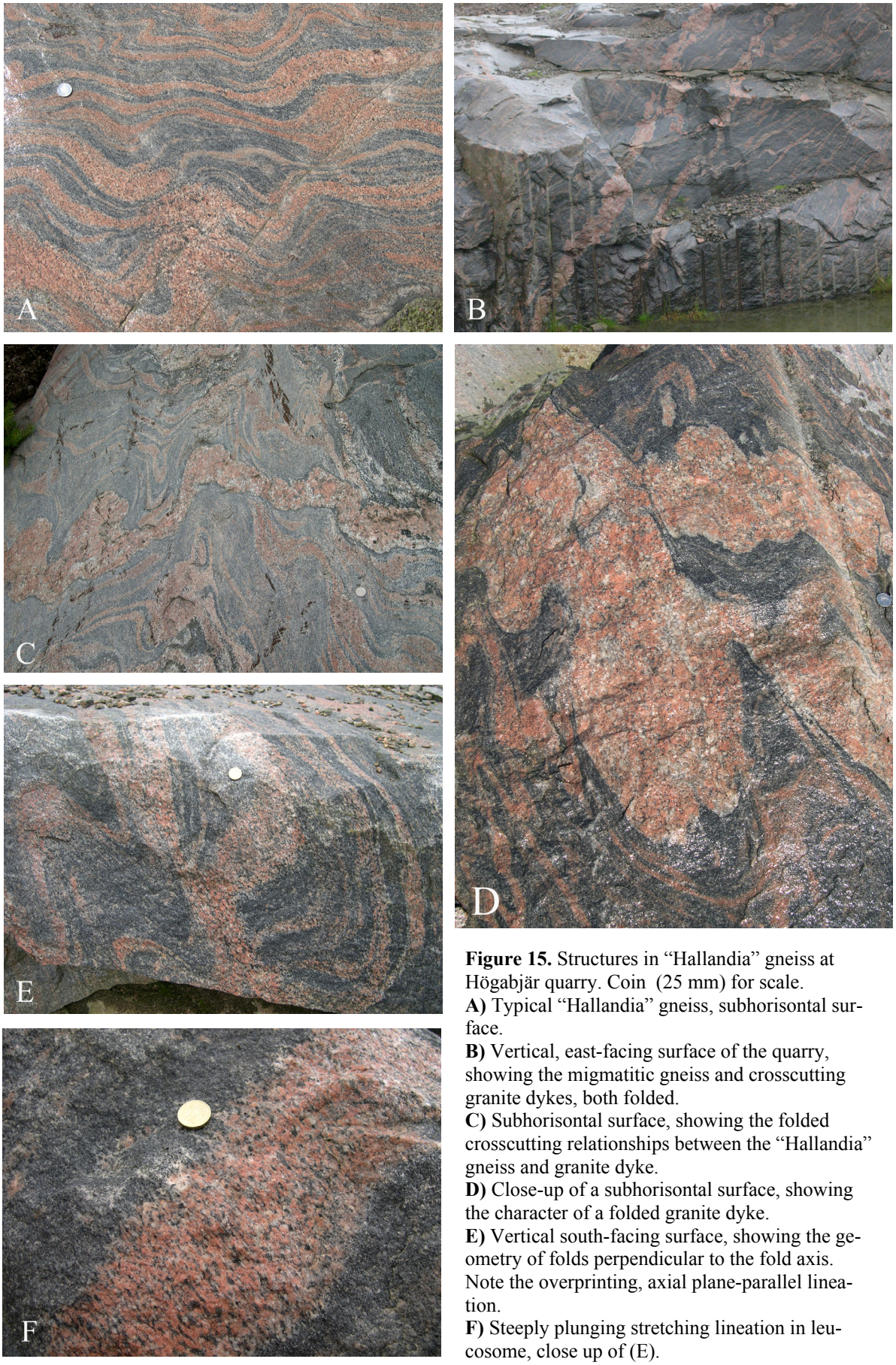

Figure 15. Structures in "Hallandia" gneiss at Högabjär quarry. Coin (25 mm) for scale.
A) Typical "Hallandia" gneiss, subhorisontal surface.
B) Vertical, east-facing surface of the quarry, showing the migmatitic gneiss and crosscutting granite dykes, both folded.
C) Subhorisontal surface, showing the folded crosscutting relationships between the "Hallandia" gneiss and granite dyke.
D) Close-up of a subhorisontal surface, showing the character of a folded granite dyke.
E) Vertical south-facing surface, showing the geometry of folds perpendicular to the fold axis. Note the overprinting, axial plane-parallel lineation.
F) Steeply plunging stretching lineation in leucosome, close up of (E).

Figure 16. Post-deformational granitic dykes at Högabjär. Coin (25 mm) for scale. **A)** Crosscutting, pinkish granite-pegmatite dyke, vertical E-W trending surface. **B)** Thin, crosscutting granite-pegmatite dyke (arrow) exposed on a subhorisontal surface.

The structures appear complex on horizontal surfaces and the leucosome pods highly irregular (Figs. 15A, C). The structural relations are best exposed on south- and north-facing vertical surfaces, which are roughly perpendicular to the axial surface of outcrop-scale folds (Fig. 15E). The folds are tight, upright to slightly overturned, with axial surfaces oriented around 30/60 ESE. In places leucosome material appears to have developed along the axial-planar fold limbs (Fig. 15E). Fold axes plunge c. 200/30 SSW (trends are given in 0-360°/plunges in 0-90°).

A linear deformation fabric, oriented parallel with the axial-plane of the folds, has developed in medium- and coarse-grained rock domains, i.e., leucosome and folded granitic dykes (Figs. 15 E, F). It is pronounced in the axial planar leucosome domain (Fig. 15F). The fabric is a stretching lineation and is defined by elongated and recrystallised mineral aggregates. The stretching lineation is, however, not parallel to the fold axis, but oriented c. 120/70 SE.

Late, crosscutting dykes occur at a few places. Two occurrences of undeformed granite dykes, 4-20 cm wide, are fine- to coarse-grained, pinkish and have an isotropic mineral fabric. The dykes are oriented around 165/75 W and crosscut the folded structures of the host rock (Figs. 16A, B). A mafic dyke oriented 350/50 E, in the southern part of the quarry (SNG: 6295980/1322840) crosscuts the same structures. It is very fine-grained and has a high-grade, granulite facies metamorphic assemblage (hornblende, clinopyroxene (possibly also orthopyroxene), plagioclase, and opaque minerals).

Five samples have been selected for zircon geochronology:

HB 1= reddish grey gneiss mesosome (i.e., gneiss material excluding leucosome). The mesosome has a grey, fine-grained matrix and diffuse, red microdomains of granitic composition. It consists mainly of quartz, antiperthitic plagioclase and microperthitic K-feldspar (Fig. 17A). The grain size is variable and grain boundaries show transitions between granoblastic and sutured texture. Small amounts of olive-green hornblende, anhedral to granoblastic garnet and biotite are present (Fig. 17B). Accessories are opaque minerals, apatite, zircon, and allanite.

HB 2 = leucosome. The leucosome is greyish red, medium-grained, granitic in composition and has a linear fabric. It consists of quartz, plagioclase (partly antiperthitic) and microperthitic K-feldspar, in places with week cross-hatched twinning. Grain size is variable and grain boundaries are granoblastic or smoothly irregular (Fig. 17B). Minor amounts of myrmekite are present. Small amounts of olive-green hornblende, biotite (in part altered to low-grade sheet silicates) and opaque minerals occur together with accessory apatite, garnet, zircon, and allanite (Fig. 17C).

HB 3 = folded granitic dyke (cf. Figs. 15C, D). The granite is red and had originally medium or coarse quartz and feldspar grains that have been stretched and recrystallised to form a strong linear fabric. Quartz occurs as coarse ribbons and lenses, while feldspar form elongated aggregates of perthitic microcline and plagioclase (sericitised) with granoblastic texture and variable grain size (Fig. 18A). Locally, myrmekite occurs along grain boundaries. Small amounts of opaque minerals, biotite (altered to chlorite) and accessory garnet grains occur.

HB4 = crosscutting, undeformed granitic dyke (Fig. 16A). The undeformed granite is pink, fine- to coarse-grained and has an isotropic fabric. It consists of microcline, plagioclase and quartz with lesser amounts of hornblende, biotite, euhedral titanite, and zircon (Fig.18B).

HB6 = 4 cm wide, crosscutting and undeformed granitic pegmatite dyke (Fig. 16B). Although only 4 cm wide, this dyke can be followed for c. 100 metres. It is coarsely medium-grained, isotropic, pegmatite-looking and consists of grey quartz, red K-feldspar and white plagioclase.

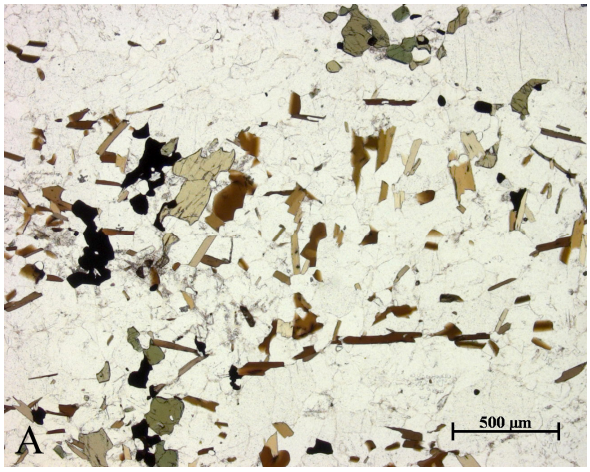

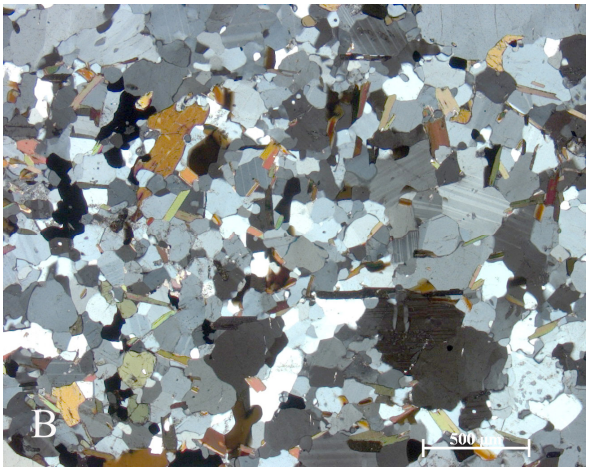

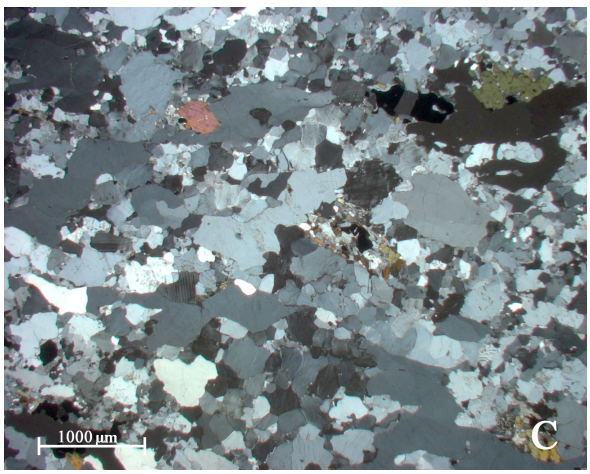

Figure 17. Photomicrographs of "Hallandia" gneiss.
A) Gneiss mesosome (gneiss excluding leucosome, sample HB1) in plane light, illustrating the dark mineral assemblage. Hornblende is pleochroic in olive-green and beige shades, biotite is pleochroic brown and opaque minerals are black.
B) Gneiss mesosome in (A) under crossed polars, illustrating the nearly granoblastic texture of feldspars and quartz.
C) Leucosome (sample HB2) under crossed polars, illustrating the uneven grain size and the smoothly irregular grain boundaries. Note the elongated quartz domains.

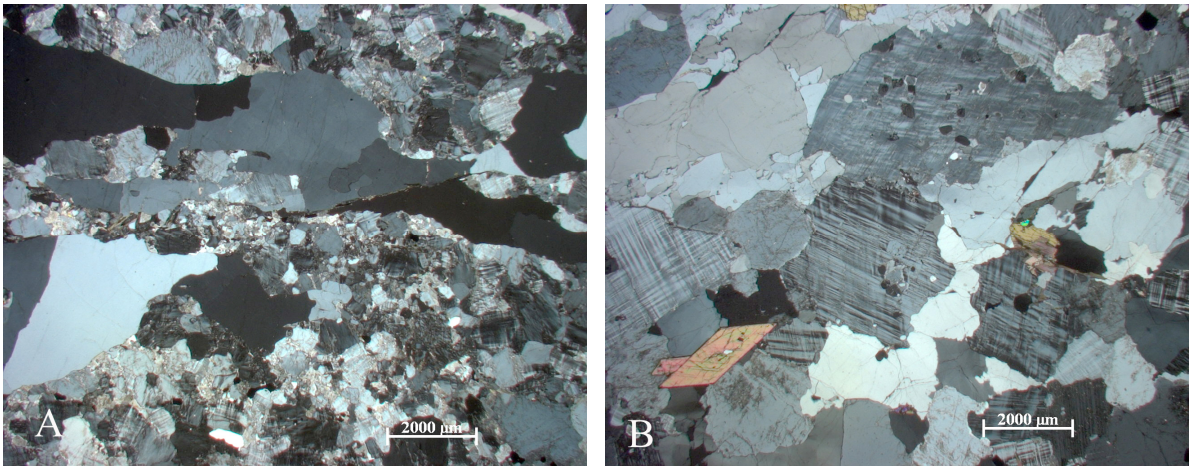

Figure 18. Photomicrographs (crossed polars) of granite-pegmatite dykes at Högabjär. **A)** Folded granite dyke (sample HB3), with coarse, elongated and lens-shaped quartz domains. **B)** Undeformed, crosscutting granite dyke (sample HB4), with isotropic fabric. A grain of euhedral titanite (high relief, diamond-shaped grain with high birefringence) is shown in the lower left part of the photo.

6.2 Zircon analysis: electron microscopy and analytical results

Age data obtained hitherto include samples HB1, HB2 and HB3. Zircon separates from samples HB4 and HB6 have been mounted but await analysis during 2006. Forty-one analyses were made on zircon from gneiss mesosome and leucosome (HB1 and HB2) at Högabjär and fifteen additional analyses from the sample of crosscutting and folded granitic dyke (HB3). All data are shown in the concordia diagrams (Figs. 19A, B).

Gneiss mesosome (HB1) and leucosome (HB2)

The zircon crystals in the *mesosome (HB1)* are subprismatic to oval and rounded with length to width ratios between 1.5 and 4 (Fig. 20A). The crystals have rounded edges and tips and euhedral shapes are rare. Most crystals have well-developed oscillatory, igneous zoning (Fig. 20B), although the cores of some crystals are unzoned (dark or bright in CL). Many grains have a 5-15 µm wide, CL-dark and BSE-bright rim that is too thin to analyse. Twelve analyses were aimed at igneous domains. Eight of these (05a-12a) resulted in concordant data with $^{207}Pb/^{206}Pb$ ages ranging between 1632±8 and 1721±14 Ma. During analysis of spots 01a-08a, a hang-up of the automatic analysis routine caused a displacement of each spot location by c. 25 µm. One of these displaced analyses (02a) gave a significantly younger age (discordant $^{207}Pb/^{206}Pb$ age of 1484 ±28 Ma), caused by mixing between igneous and secondary domains. The four first analyses (01a-04a) resulted in discordant data, possibly caused by the displacement of the spot across the grain boundary of zircon into epoxy.

The zircon morphology and CL- and BSE-character in *leucosome (HB2)* is essentially similar to that of mesosome (HB1). Most grains from the leucosome, however, have well-developed CL-dark and BSE-bright rims, up to 100 µm wide (Fig. 21A). The rim-core contacts are generally not distinct and the rims have a structure that resembles a relict oscillatory zoning (Figs. 21B, C, D). A few CL-dark and almost entirely BSE-bright grains lack remnants of igneous protolith zircon domains (Fig. 21E). Seven analyses of igneous, oscillatory zoned or CL-bright cores yielded concordant $^{207}Pb/^{206}Pb$ ages between 1615±22 and 1741±25 Ma. Two analyses (08b, 27a), targeted at igneous domains, resulted in significantly lower ages (1577±58 and 1572±21 Ma) and represent mixes of igneous and secondary zircon. Nineteen analyses of secondary rims resulted in $^{207}Pb/^{206}Pb$ ages ranging from 1482 ± 18

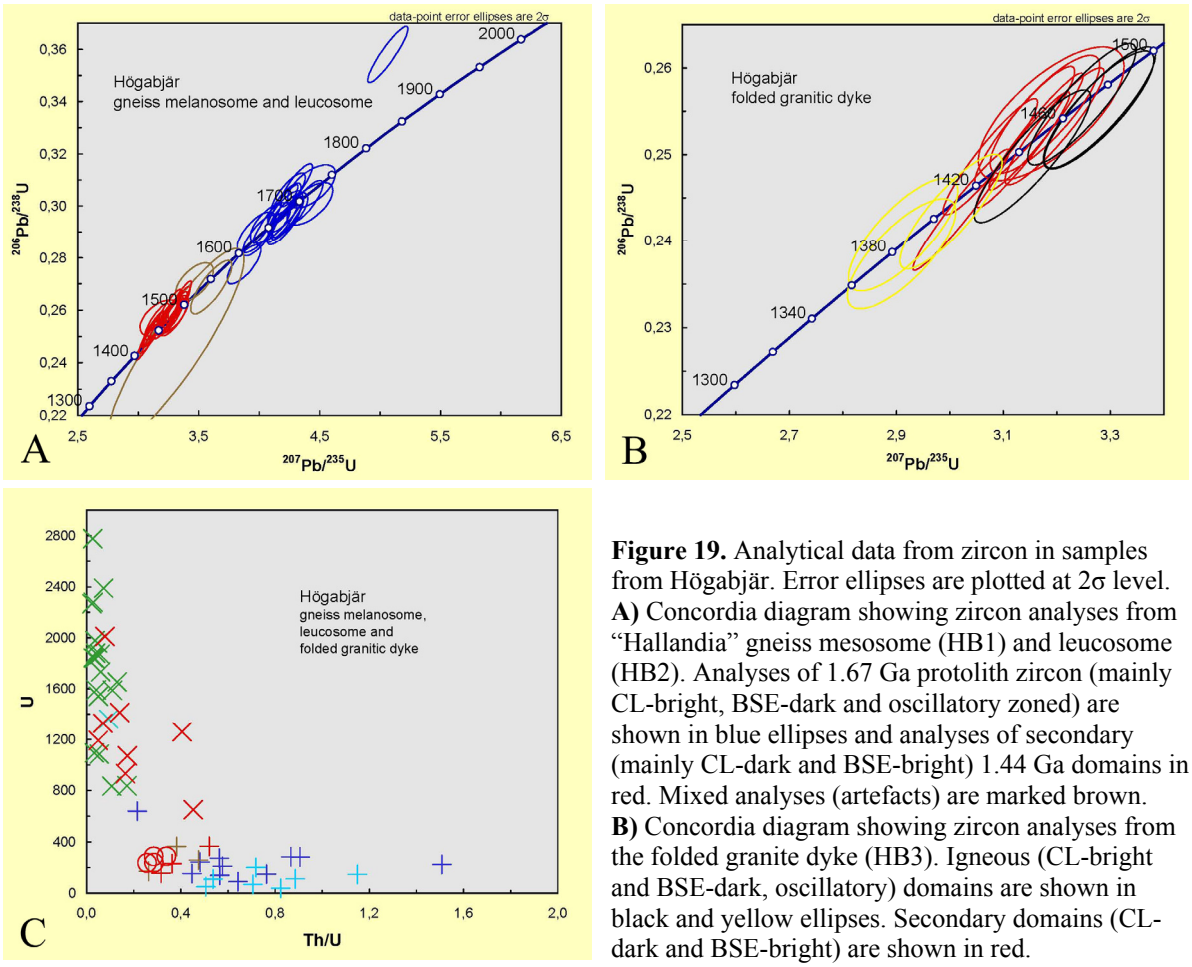

Figure 19. Analytical data from zircon in samples from Högabjär. Error ellipses are plotted at 2σ level. **A)** Concordia diagram showing zircon analyses from "Hallandia" gneiss mesosome (HB1) and leucosome (HB2). Analyses of 1.67 Ga protolith zircon (mainly CL-bright, BSE-dark and oscillatory zoned) are shown in blue ellipses and analyses of secondary (mainly CL-dark and BSE-bright) 1.44 Ga domains in red. Mixed analyses (artefacts) are marked brown. **B)** Concordia diagram showing zircon analyses from the folded granite dyke (HB3). Igneous (CL-bright and BSE-dark, oscillatory) domains are shown in black and yellow ellipses. Secondary domains (CL-dark and BSE-bright) are shown in red. **C)** U vs. Th/U plot, illustrating the chemistry of zircon populations in samples from Högabjär. (+) denotes CL-bright, BSE-dark and oscillatory protolith zircon from mesosome (HB1, dark blue, 1.67 Ga), leucosome (HB2, light blue, 1.67 Ga), mixed domains (HB1 and HB2, brown, artefacts) and folded granite dyke (HB3, red, 1.40 Ga). (X) denotes CL-dark, commonly BSE-bright secondary domains from leucosome (HB2, green 1.44 Ga; HB2, light blue, 1.65 Ga, one analysis), and deformed granite dyke (HB3, red, 1.44 Ga). Red circles denote igneous xenocrysts (CL-bright, BSE-dark and oscillatory igneous zircon, 1.48 Ga) in HB3.

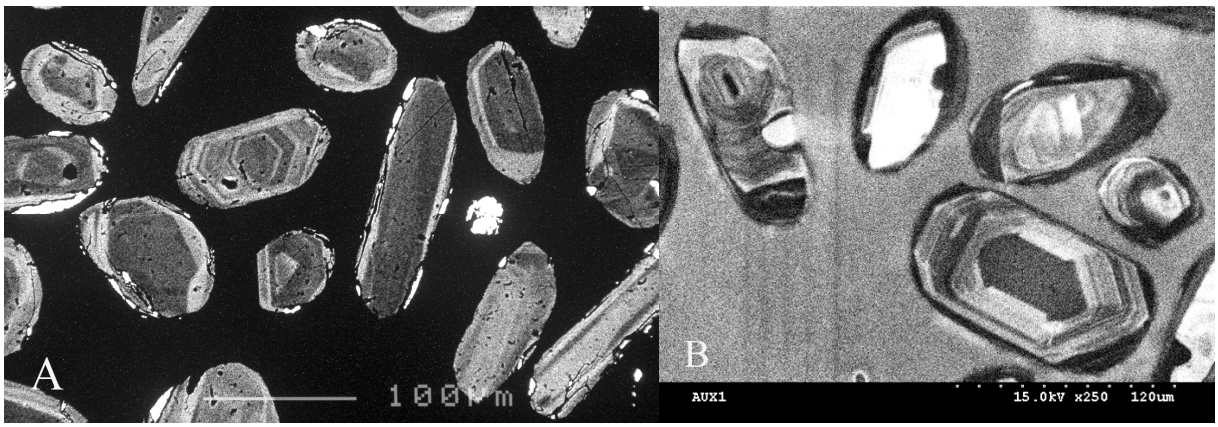

Figure 20. Zircon crystals in the mesosome (HB1) of "Hallandia" gneiss.
A) BSE-image (overview) showing the dominance of igneous domains. Very bright spots are remnants of gold coating.
B) CL-image showing the oscillatory zoning and dominantly CL-bright character of the zircons. Analyses n1759-11a and 12a were taken in oscillatory domains of the two large grains on the right (yielding $^{207}Pb/^{206}Pb$ ages 1721±14 and 1698±12 Ma, respectively).

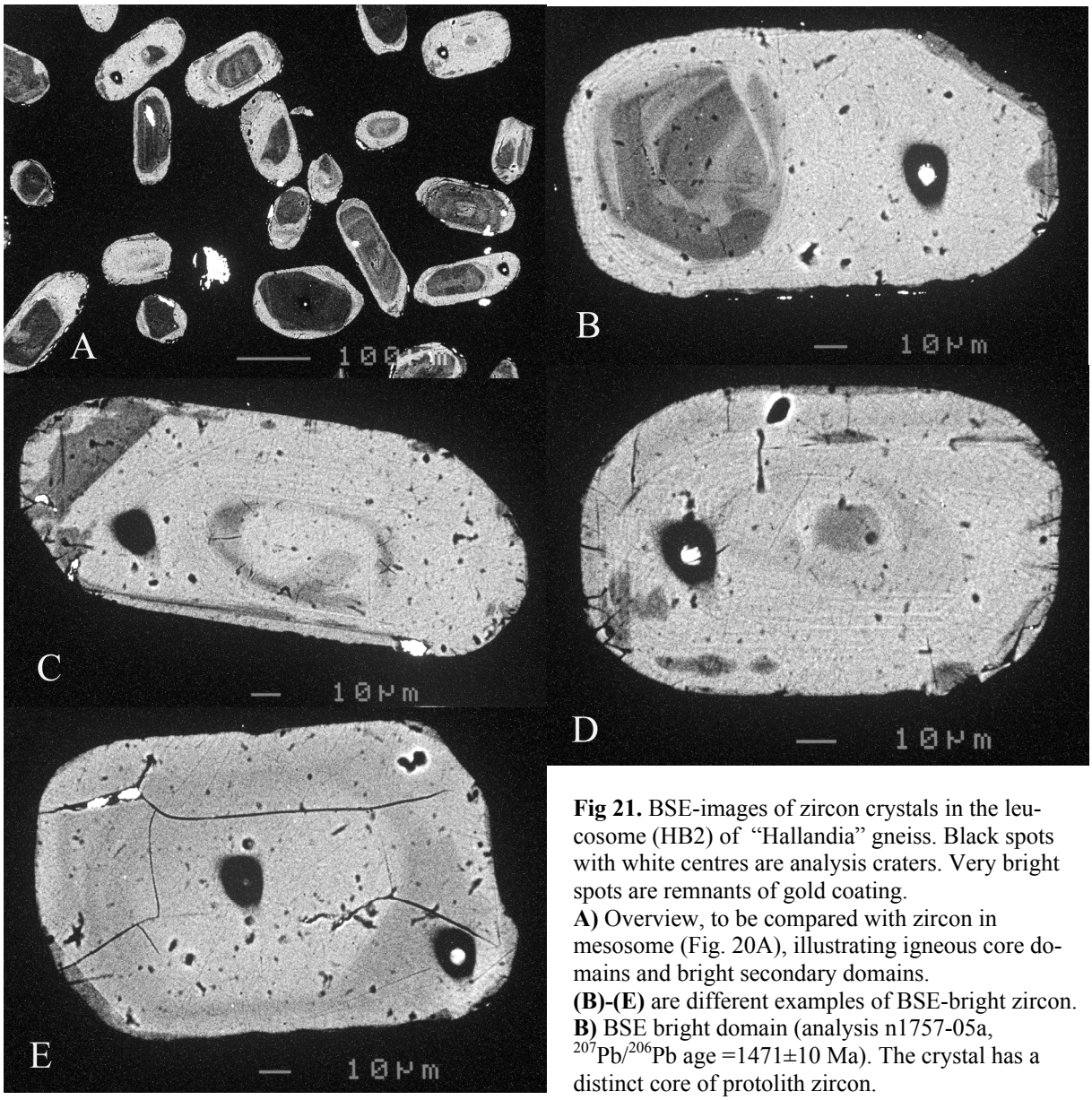

Fig 21. BSE-images of zircon crystals in the leucosome (HB2) of "Hallandia" gneiss. Black spots with white centres are analysis craters. Very bright spots are remnants of gold coating.
A) Overview, to be compared with zircon in mesosome (Fig. 20A), illustrating igneous core domains and bright secondary domains.
(B)-(E) are different examples of BSE-bright zircon.
B) BSE bright domain (analysis n1757-05a, $^{207}Pb/^{206}Pb$ age =1471±10 Ma). The crystal has a distinct core of protolith zircon.
C) Oscillatory "ghost" zoning in BSE bright domain (analysis n1757-22a, $^{207}Pb/^{206}Pb$ age =1458±12 Ma). The crystal has a discernible core of protolith zircon. **D)** Almost entirely BSE-bright crystal with oscillatory "ghost" zoning and barely visible core remnant (analysis n1757-19a, $^{207}Pb/^{206}Pb$ age =1471±13 Ma). **E)** Crystal consisting of entirely secondary zircon (almost entirely BSE-bright) and lacking oscillatory-looking zoning (analyses n1757-13a and b, $^{207}Pb/^{206}Pb$ ages =1431±5 and 1422±8 Ma).

to 1411±8 Ma (Fig. 19a). The secondary zircon in HB2 is rich in U (835-2777 ppm) and has low Th/U ratios (0.02-0.11, Fig. 19C). One single analysis of a BSE-bright, 20 µm wide rim (n1757-23a), with high U content (1361 ppm) and low Th/U ratio (0.09), yielded an age of 1650±9 Ma.

Thirty-three of the ages obtained from gneiss mesosome (HB1) and leucosome (HB2) are concordant and have been used for calculation of weighted average $^{207}Pb/^{206}Pb$ ages. Three analyses of mixed zircon domains have been discarded and another five analyses that are discordant have also been excluded from calculation. Fifteen concordant analyses of typical igneous domains resulted in a weighted average $^{207}Pb/^{206}Pb$ age of 1671±19 Ma

(MSWD=5.8) and dates the protolith of the "Hallandia" gneiss. In the U vs. Th/U diagram (Fig. 19C), 1.67 Ga zircon is characterised by values that are common for igneous zircon. One exception is a single analysis of a U-rich rim (n1757-23a, U=1361 ppm, Th/U=0.09) that still yielded a $^{207}Pb/^{206}Pb$ age within error identical to the protolith age. The leucosome (HB2) contains abundant secondary zircon that does not form characteristic overgrowths but rather recrystallised domains or replacement of primary zircon with diffuse transitional contacts to igneous core domains. Seventeen concordant analyses yield a weighted average $^{207}Pb/^{206}Pb$ age of 1.44 Ga (1444±11 Ma, MSWD=4.9) that dates the migmatisation. The secondary domains are distinctly different from the igneous zircon, i.e., rich in U and low Th/U ratios (Fig. 19C, with the exception of the single analysis mentioned above).

Folded granitic dyke (HB3)

Zircon crystals in the folded granitic dyke (HB3) are subprismatic to oval with rounded terminations. Igneous zircon domains with oscillatory zoning are present (Fig. 22A) as well as domains that appear similar to the secondary-formed domains in sample HB2 (Fig. 22B). The latter domains are CL-dark and most of them BSE-bright. Seven analyses of igneous zircon domains (from four crystals) and eight analyses of CL-dark and BSE-bright zircon (from eight crystals) were made.

Two generations of igneous zircon, dated at c. 1.48 (n=4, two grains) and 1.40 Ga (n=3, two grains), were identified (Fig. 19B). Both are low in U (236-287 and 157-365 ppm respectively) and have moderate Th/U ratios (0.26-0.34 and 0.32-0.52, respectively, Fig. 19C). The youngest, 1.40 Ga, generation gives an approximate age for the intrusion of the dyke. The 1.48 Ga igneous zircon grains are interpreted as xenocrysts. Eight analyses of BSE-bright domains yield a spread along the concordia from 1.41 to1.48 Ga, with an average at 1.43 Ga

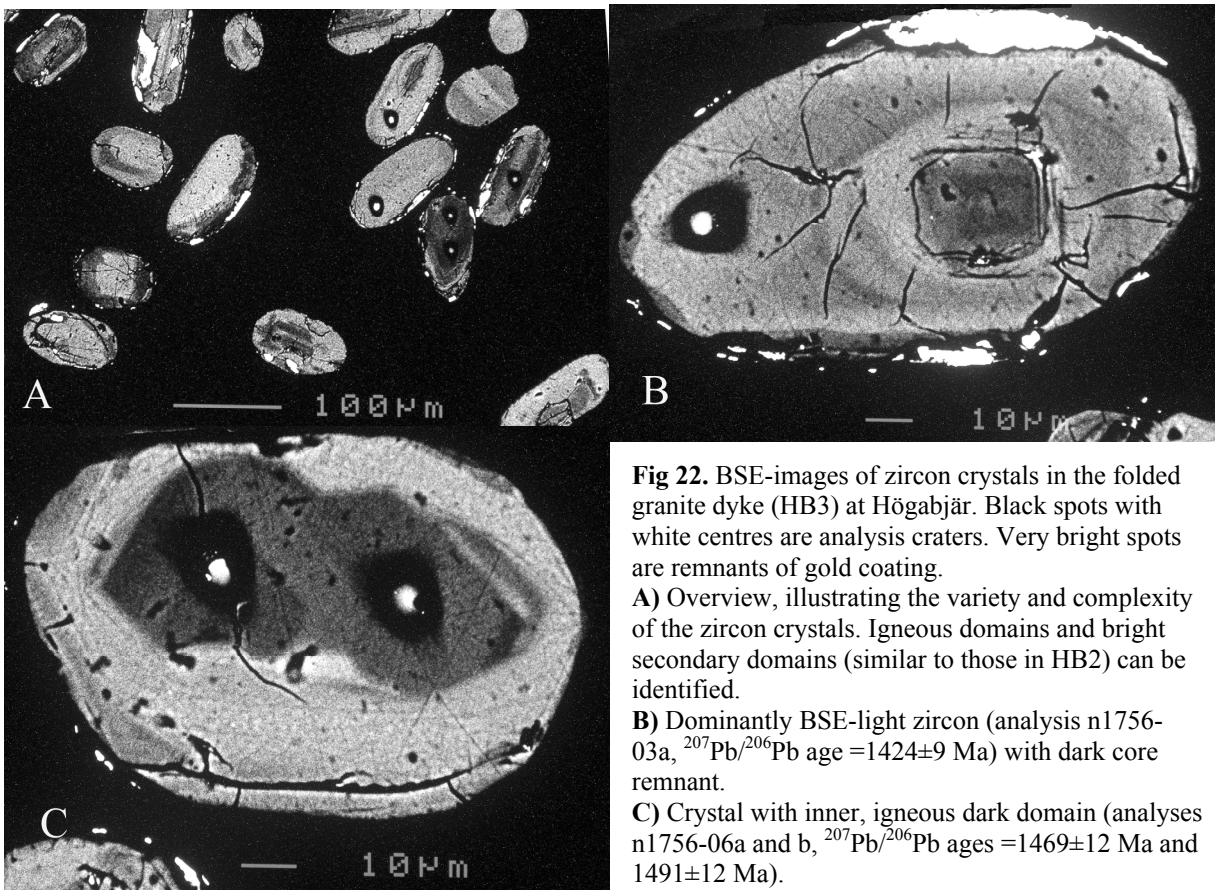

Fig 22. BSE-images of zircon crystals in the folded granite dyke (HB3) at Högabjär. Black spots with white centres are analysis craters. Very bright spots are remnants of gold coating.
A) Overview, illustrating the variety and complexity of the zircon crystals. Igneous domains and bright secondary domains (similar to those in HB2) can be identified.
B) Dominantly BSE-light zircon (analysis n1756-03a, $^{207}Pb/^{206}Pb$ age =1424±9 Ma) with dark core remnant.
C) Crystal with inner, igneous dark domain (analyses n1756-06a and b, $^{207}Pb/^{206}Pb$ ages =1469±12 Ma and 1491±12 Ma).

(Fig. 19B, weighted average $^{207}Pb/^{206}Pb$ age = 1434±12 Ma, MSWD=3.3). This zircon has very low to moderate Th/U ratios (0.03-0.45) and moderate to very high contents of U (651-2777 ppm, cf. Fig. 19C and the Appendix). The zircon grains with U-rich, 1.43 Ga domains are also interpreted as xenocrysts. One of the igneous zircon grains dated at 1.48 Ga (Fig. 22C) has a distinct, BSE-bright rim that probably is secondary.

6.3 Summary and interpretation

Igneous zircon in "Hallandia" gneiss (mesosome and leucosome) dates igneous emplacement of the protolith at c. 1.67 Ga. The gneiss is thus coeval with the 1.73-1.66 Ga intrusions that dominate in the Eastern Segment, similar to the orthogneisses dated at Oxanäset and Gransjön above (see chapter 4 and 5). There is a clear textural and chemical difference between zircon in the mesosome and the leucosome, with abundant U-rich replacements in the latter. This demonstrates that the U-rich, secondary zircon replacements formed during migmatisation. The 1.44 Ga secondary zircon thus directly dates the pre-Sveconorwegian migmatisation.

The deformed and folded granite dyke was dated at c. 1.40 Ga. The age sets an upper bracket for the tight folding along SSW-plunging axes and for the development of the steeply ESE-plunging linear fabric. Coeval granite-pegmatite dykes are known from three other localities, NW of Halmstad (Söderlund 1996, Christoffel et al. 1999, Rimsa et al. 2004), where the one investigated by Söderlund (1996; Glassvik locality) has been tightly folded along a subvertical fold axis.

The geological map from 1956 of the Halmstad area (Fig. 14) shows fold patterns that typically results from superposed phases of folding (or non-coaxial folding). Dome and basin structures are present, which result from two upright phases of folding with roughly perpendicular axes. The map pattern suggests that (roughly) WNW-ESE trending upright folds have been refolded along (roughly) NNE-SSW trending axes. The final interpretation regarding the formation of the fold pattern and the relative ages of the different phases of folding has to await results from ongoing mapping in the area. It is, however, tentatively suggested that deformation during the Sveconorwegian orogeny resulted in two or more distinctly different phases of folding. The undulating plunges of regionally occurring Sveconorwegian, E-W to WNW-ESE trending and subhorizontal fold axes and associated lineations (cf. Oxanäset, chapter 4) suggest that these Sveconorwegian folds were refolded. Refolding may have formed in connection with deformation during uplift of the Eastern Segment (after 0.97 Ga, cf. Johansson et al. in press).

The SSW-trending folds in the Halmstad area may, however, have an older origin. This is suggested by field relations observed at several localities along the coast of southwest Sweden, where upright SSW-trending folds and leucosome or pegmatoid material oriented along axial planes, similar to those at Högabjär (cf. Fig. 15E), have been overprinted by a strong, ESE-plunging stretching lineation. At Högabjär, the same kind of linear fabric overprints 1.44 Ga old leucosome, 1.40 Ga old granite dyke, and axial plane-parallel vein. If the persistent stretching lineation is linked to the regional WNE-ESE oriented folds this phase of folding should be younger than the NNE-SSW oriented. In any case, the age of the granite dyke is clear evidence that the SSW-trending folds and the stretching lineation are both young structures, 1.40 Ga or younger.

7. Kullaskog – Åboda: Migmatitic mega-xenoliths and ductilely deformed granites in the eastern part of the Protogine Zone

7.1 Field relations and petrography

Regional context
At several localities along the Protogine Zone, gneiss of unknown origin occurs as xenoliths, ranging in size from metre-long inclusions to several square kilometres. The gneiss is migmatitic and commonly has a folded ductile foliation, whereas the host TIB-granitoid has a homogeneous, ductile, NW-striking foliation that locally has been openly folded along steep axes. Both rock types are transected by late Sveconorwegian, discrete, N-S-striking subvertical shear zones that are characteristic of the Protogine Zone. The metamorphic events that caused migmatisation of the gneiss and the ductile, comparatively homogeneous, foliation in the TIB-granite reflect regional, thermal or magmatic activities that are structurally older than the late Sveconorwegian shear zones.

In addition to ductile foliation, some granitic rocks in the easternmost part of the Protogine Zone show strong recrystallisation, possibly with incipient partial melting. This metamorphic event is clearly higher-grade than the late Sveconorwegian metamorphism that is associated with the N-S trending shear zones. In the easternmost part of the Protogine Zone (c. 20 km east of the Eastern Segment) the Sveconorwegian shear zones are characterised by greenschist facies metamorphism.

Currently, virtually nothing is known about the thermal event (s) that caused the medium- to high-grade structures in the Protogine Zone. It is unclear whether the c. 1.44 Ga old thermotectonic activity recorded in the southern Eastern Segment (cf. Högabjär chapter 6, and references therein) also affected rocks within the Protogine Zone and east thereof. Neither is it known whether or not 1.45 Ga magmatism took place in the area. U-Pb TIMS dating of zircon has yielded protolith ages of 1.80-1.70 Ga for granitoids in the eastern part of the Protogine Zone, and most granitic rocks have been mapped as deformed TIB rocks (Wikman 2000 and references therein). A possible equivalent to the 1.45 Ga Karlshamn granite (in Blekinge) was identified by Wikman (2000). The rock has a conspicuous texture with tabular K-feldspar megacrysts up to 50 mm long. Age determination has, however, not yet been carried out.

Locality Kullaskog
The relations between gneiss xenoliths and their host rocks are well exposed at Kullaskog, (9 km NNW of Alvesta; Fig. 2). Fine-grained, grey migmatitic gneiss with light reddish, folded veins occurs as a xenolith in a TIB-granitoid. The veins and the foliation of the gneiss are clearly cut by the TIB-rock (Fig. 23A; SNG: 6325542/1418098). Fresh outcrops on a hill nearby (SNG: 6325263/1418166) show the structural relations between a xenolith and a granitic host rock. The host granite has developed a ductile foliation that is parallel with the axial plane of the folds in the xenolith (Fig. 23B). This relation suggests that the ductile, homogeneous and generally NW-striking foliation in the host granitoids and the folding of the foliation in the gneiss xenolith developed during the same event. At the same locality, the

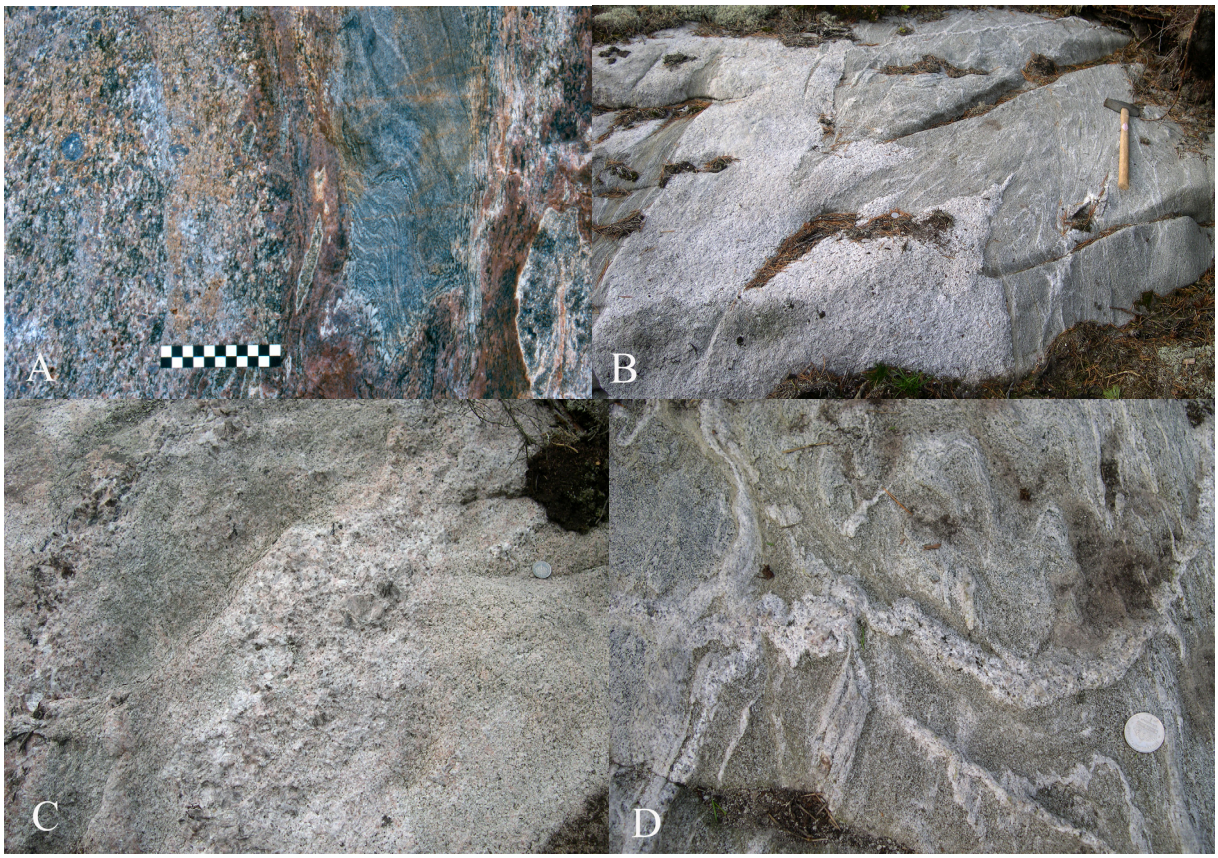

Figure 23. Lithological and structural relations at Kullaskog. **A)** Foliated, K-feldspar megacryst-bearing TIB-granitoid enclosing a xenolith of fine-grained gneiss. Scale is 10 cm. Photograph by H. Wikman. **B)** Folded, migmatitic grey gneiss xenolith enclosed in granite. The ductile foliation in the granite is parallel with the axial plane of the fold in the gneiss xenolith. Hammer (50 cm) for scale. **C)** Granite, locally grading into pegmatite. Coin (25 mm) for scale. **D)** Folded veinlets (apophyses) of medium-grained granite that crosscut migmatitic, older and finer-grained veins in the gneiss xenolith. Close up of xenolith in (B). Coin (25 mm) for scale.

host granite has locally sent cm-wide apophyses into the grey gneiss (Fig. 23D). Locally the host granite grades into pegmatite (Fig. 23C).

Samples from Kullaskog

A fine-grained, grey migmatitic and foliated gneiss with light reddish veins (Fig. 23B, sample *Kull*) at Kullaskog was sampled by H. Wikman (SNG: 6325262/1418163, 900 m SSE of Kullaskog), in order to determine the protolith age of the gneiss and the age of migmatisation.

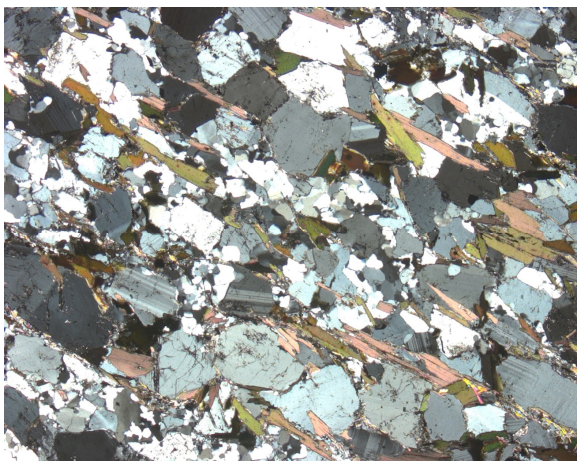

In thin-section (Fig. 24), the fine-grained, grey gneiss (sample *Kull*) shows thin biotite-rich bands with a preferred orientation of the biotite grains (foliation in 3D). Some biotite

Figure 24. Photomicrograph (crossed polars) of fine-grained, grey gneiss (sample Kull). The rock has a distinct orientation of biotite grains. Quartz has uneven grain size due to recrystallisation. Width of image is 5.5 mm.

grains are oriented at a high angle to the bands. The quartz shows, to some extent, the same orientation in small domains. The quartz has undulous extinction, shows sign of recrystallisation and is suturated. The feldspars show grain boundary migration and recrystallisation. Plagioclase is to a minor degree sausseritised or sericitised and myrmekite is present. K-feldspar shows cross-hatched twinning and microperthite. There are two types of biotite (possibly two generations), where one is associated with the opaque minerals and slightly darker brown. Both show only lesser degrees of alteration to chlorite. Ilmenite and magnetite dominate among the opaque minerals, no sulphide was detected. Euhedral apatites are abundant. A few grains of white mica (muscovite), zircon and monazite occur. One small aggregate of needle-shaped epidote is present. A point count of the thin-section suggests a rhyolitic or granitic composition. The overall impression is that the rock is an orthogneiss, possibly of volcanic origin.

As a second step, sampling of host granitoids was carried out during October 2005. The objective is to obtain ages of intrusion and, if possible, metamorphism of the host granitoids. Ion probe analysis of these additional samples will be carried out during 2006.
Kull 2: A foliated (310/subvertical), K-feldspar megacryst-bearing TIB-granitoid enclosing a xenolith of the fine-grained, grey gneiss (Fig. 23A, SNG: 6325542/1418098)
Kull 4: Granite, which in places grades into pegmatite (Fig. 23C, SNG: 6325263 /1418166).

Locality Åboda
A K-feldspar megacryst-bearing granitoid, with up to 50 mm tabular megacrysts (Fig. 25A, B), at Åboda (Fig. 2; 10 km NNW of Alvesta) prompted Wikman (2000) to place an area of 1.45 Ga granitoid on the map 5E Växjö NV. Its age has, however, never been determined nor has any 1.45 Ga rocks been found in this part of the TIB. The rock has co-magmatic mafic enclaves (Fig. 25C). The granite is affected by weak, ductile deformation (Fig. 25B) and is locally transected by discrete, low-grade shear zones related to Protogine Zone deformation (Fig. 25D). Granitic gneiss, mapped as TIB-granite (Wikman 2000), in the same area shows strong recrystallisation, possibly with incipient anatexis (Figs. 25E, F). Pegmatitic dykes crosscut the deformation fabric in the granitic gneiss (Fig. 25E).

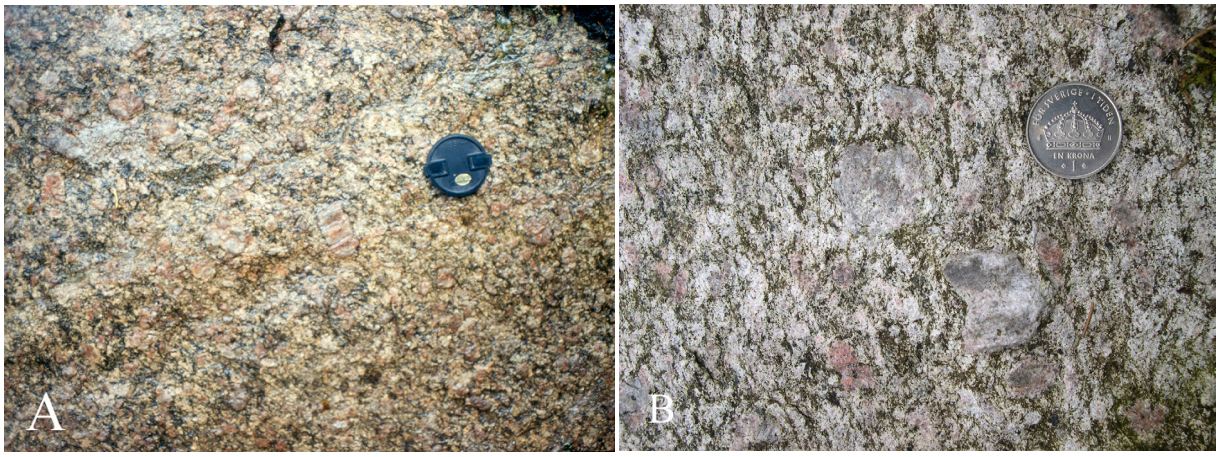

Figure 25. Rocks and structural relations at Åboda. Coin (25 mm) for scale in pictures (B)-(F). **A)** Well-preserved, K-feldspar megacryst-bearing granitoid (suggested to be 1.45 Ga), with up to 50 mm long tabular megacrysts. Lens cap (50 mm) for scale. **B)** Weak deformation fabric in K-feldspar megacryst-bearing granitoid. **Continued on next page.**

Figure 25 continued. C) Mafic enclave in K-feldspar megacryst-bearing granitoid. **D)** Thin, discrete shear zone (arrows, S=335°/subvertical) typical of the Protogine Zone deformation in the area, transecting the K-feldspar megacryst-bearing granitoid. **E)** Granitic gneiss that is strongly deformed (L>S fabric) and recrystallised. A pegmatite dyke (left and upper part of the photo) and a 2 cm wide apohysis of pegmatite cuts the structure . **F)** Deformed and strongly recrystallised granitic gneiss, possibly with incipient anatectic features.

Samples from Åboda

Two samples from Åboda will be analysed during 2006:

Åboda 1: K-feldspar megacryst-bearing metagranitoid (possible 1.45 Ga intrusion, Fig. 25A,B, SNG: 6328390/1418300, 1 km south of Åboda).

Åboda 3: Granitic gneiss, strongly deformed and recrystallised, possibly affected by incipient anatexis (Fig. 25F, SNG: 6329087/1418680).

7.2 Zircon analysis: electron microscopy and analytical results

Ten analyses were made on zircon from veined and folded gneiss (*Kull)* at Kullaskog. The data are shown in the concordia diagram and the U vs. U/Th plot (Figs. 26A, B). The zircon crystals are subprismatic with length to width ratios around 2, both euhedral and rounded shapes are present. BSE- and CL-images reveal that many crystals have two or three texturally different types of domains.

Primary igneous zircon is preserved as cores. The cores are CL-bright and BSE-dark and many of them show oscillatory zoning (Fig. 27A). Three concordant analyses from cores yielded a concordia age of 1770±12 Ma (MSWD=0.13, Fig. 26A, C). This zircon is characterised by low U contents (158-275 ppm) and high Th/U ratios (0.81-0.99 and forms a dis-

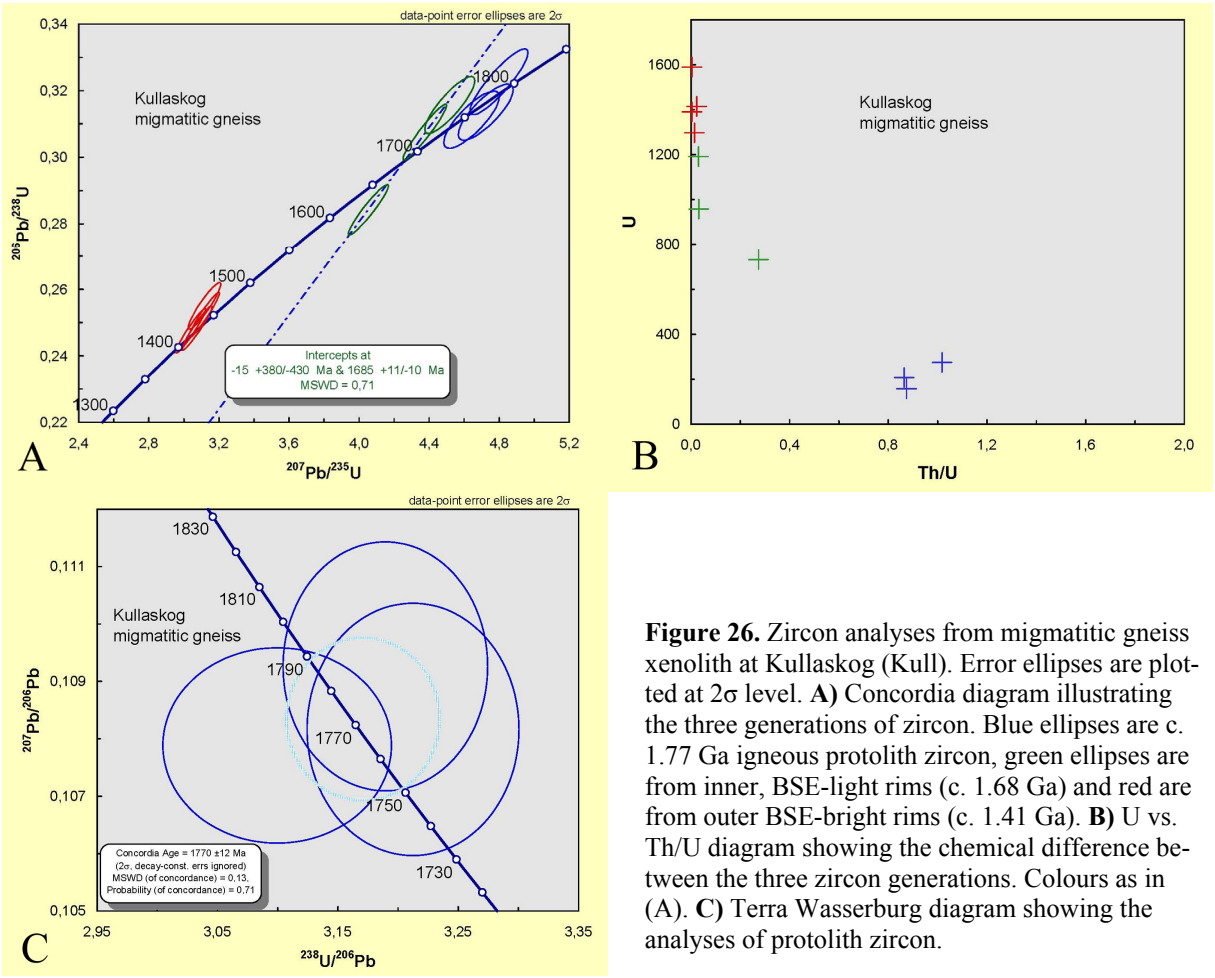

Figure 26. Zircon analyses from migmatitic gneiss xenolith at Kullaskog (Kull). Error ellipses are plotted at 2σ level. **A)** Concordia diagram illustrating the three generations of zircon. Blue ellipses are c. 1.77 Ga igneous protolith zircon, green ellipses are from inner, BSE-light rims (c. 1.68 Ga) and red are from outer BSE-bright rims (c. 1.41 Ga). **B)** U vs. Th/U diagram showing the chemical difference between the three zircon generations. Colours as in (A). **C)** Terra Wasserburg diagram showing the analyses of protolith zircon.

tinct cluster in the U vs. U/Th diagram (Fig. 26B).

Two generations of CL-dark and BSE-bright zircon occur as overgrowths or reworked rims around igneous protolith zircon (Figs. 27B, C). The *outer rims* appear as distinct overgrowths with a sharp boundary to the inner domains. Four spots in outer rims yielded one discordant and three concordant analyses. The concordant analyses gave a weighted average $^{207}Pb/^{206}Pb$ age of 1414±21 Ma (MSWD=0.79), and the discordant analysis 1397±9 Ma. The overgrowths are high in U (1297-1589 ppm) and have distinctly low Th/U ratios (0.00-0.01, Fig. 26B).

Inner rims have less distinct boundaries to the igneous cores (Figs. 27D, E). They are slightly less BSE-bright than the outer rims, and are characterised by relatively high U contents (733-1191 Ma, lower than the outer rims) and low Th/U ratios (0.03-0.27, Fig. 26B). Three analyses of inner rims yielded discordant ages resulting in an upper intercept at 1685 +11/-10 Ma (MSWD=0.71, lower intercept at –15 +380/-430 Ma).

7.3 Summary and interpretation

The gneiss protolith formed at c. 1.77 Ga and is thus coeval with relatively early stages of TIB magmatism. The inner BSE-bright rim (first secondary zircon growth), dated at c. 1.68 Ga, probably reflects reworking and migmatisation during entrapment into the host granite magma. The interpretation of the outer 1.41 Ga old rim, which is a BSE-bright, distinct overgrowth, has to await further analysis. It is suggested that it is related either to regional, duc-

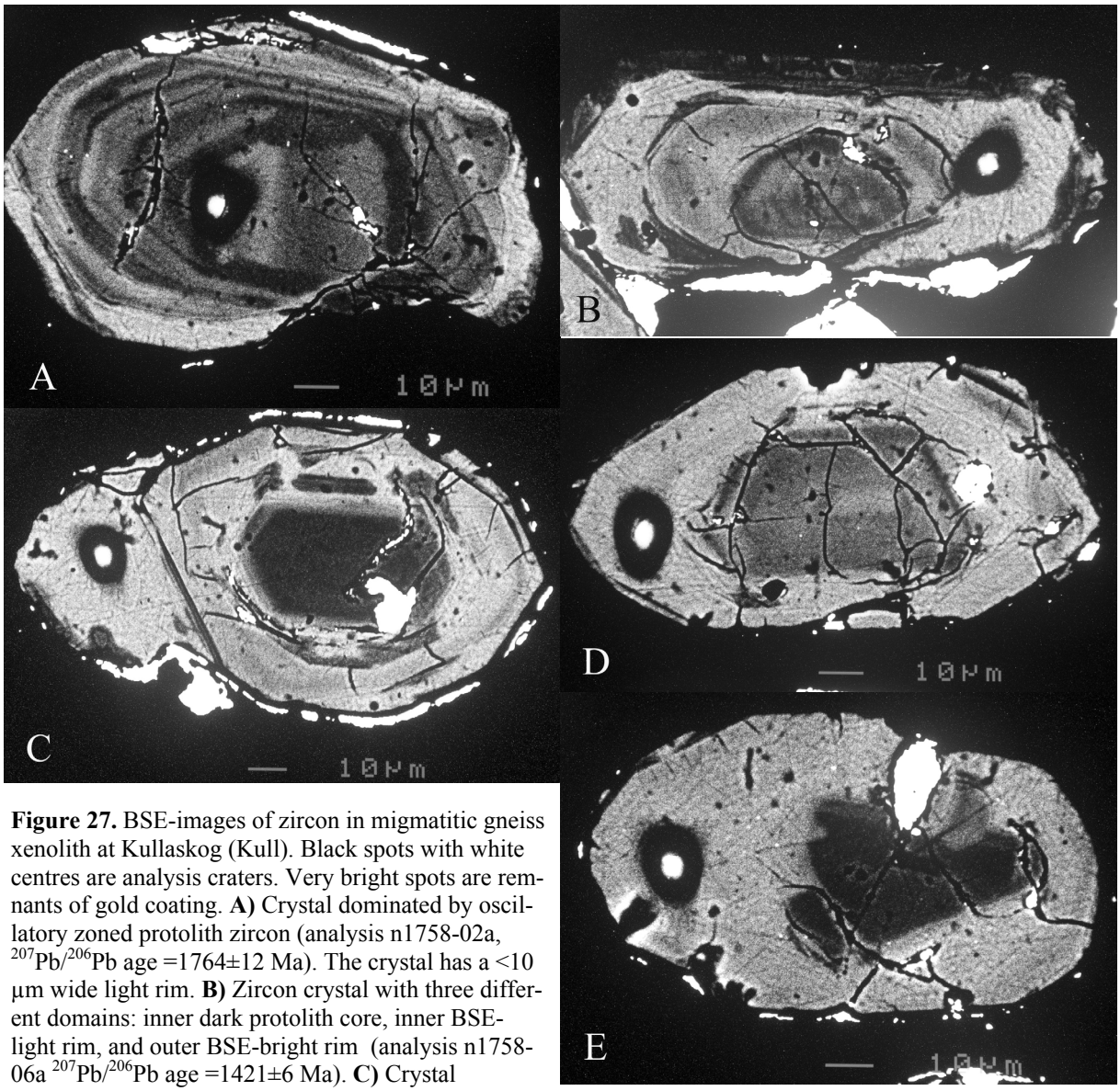

Figure 27. BSE-images of zircon in migmatitic gneiss xenolith at Kullaskog (Kull). Black spots with white centres are analysis craters. Very bright spots are remnants of gold coating. **A)** Crystal dominated by oscillatory zoned protolith zircon (analysis n1758-02a, $^{207}Pb/^{206}Pb$ age =1764±12 Ma). The crystal has a <10 µm wide light rim. **B)** Zircon crystal with three different domains: inner dark protolith core, inner BSE-light rim, and outer BSE-bright rim (analysis n1758-06a $^{207}Pb/^{206}Pb$ age =1421±6 Ma). **C)** Crystal with three different domains: inner dark protolith core, inner BSE-light rim, and outer BSE-bright rim (analysis n1758-05a $^{207}Pb/^{206}Pb$ age =1405±6 Ma). **D)** Crystal with a BSE-dark core and a BSE-light rim yielding a $^{207}Pb/^{206}Pb$ age of 1687±7 Ma (n1758-03a). **E)** Zircon crystal with a BSE-dark core and a BSE-light rim yielding a $^{207}Pb/^{206}Pb$ age of 1682±6 Ma (n1758-07a).

tile deformation that produced the (generally) NW-striking foliation in the area, or to 1.40-1.45 Ga magmatism in the area, or both.

Sveconorwegian zircon has not been found in the studied material. This is in agreement with a c. 20 kilometres distance to the Eastern Segment, which during the Sveconorwegian orogeny was reworked under amphibolite and high-pressure granulite facies metamorphism. Yet, there has apparently been at least two thermal events, recorded in the grey gneiss as zircon reworking or growth at about 1.68 and 1.41 Ga. If these findings are of regional significance in the Protogine Zone or elsewhere are still to be established.

8. Spannarp: Apparent transition from granite to charnockite

8.1 Field relations and petrography

Regional context
Charnockite and charnockite-like, greenish-grey (brownish weathering) and pyroxene-bearing rocks are relatively common in the southern Eastern Segment. Many of them occur as a few metres wide patches with gradual transition to the host granite (cf. Johansson 1998, Rimsa et al. 2004, Harlov et al. in press, Lundqvist in press). A locality at Spannarp was sampled across a gradual transition between granite and charnockite in order to compare the zircon morphology in granite and charnockite and, if possible, date the charnockitisation.

Locality
Transitions, gradual over c. 2 metres, between granite and charnockite are exposed just north of the railway, c. 2 kilometres northwest of Spannarp (Fig. 2; 6 km southeast of Varberg).

The *granite* at Spannarp is fine- to medium-grained, greyish red (Fig. 28A, SNG: 6334135/1290520), and has a faint mineral fabric defined by grey quartz domains. The granite was sampled 2-3 m away from charnockite. The rock has an uneven grain size with irregularly shaped larger grains of quartz and perthitic K-feldspar, both with undulous extinction, and granoblastic (recrystallised) smaller grains, mainly K-feldspar (partly microperthitic, partly with cross-hatched twinning) and some quartz (Fig. 28B). The rock is leuco-

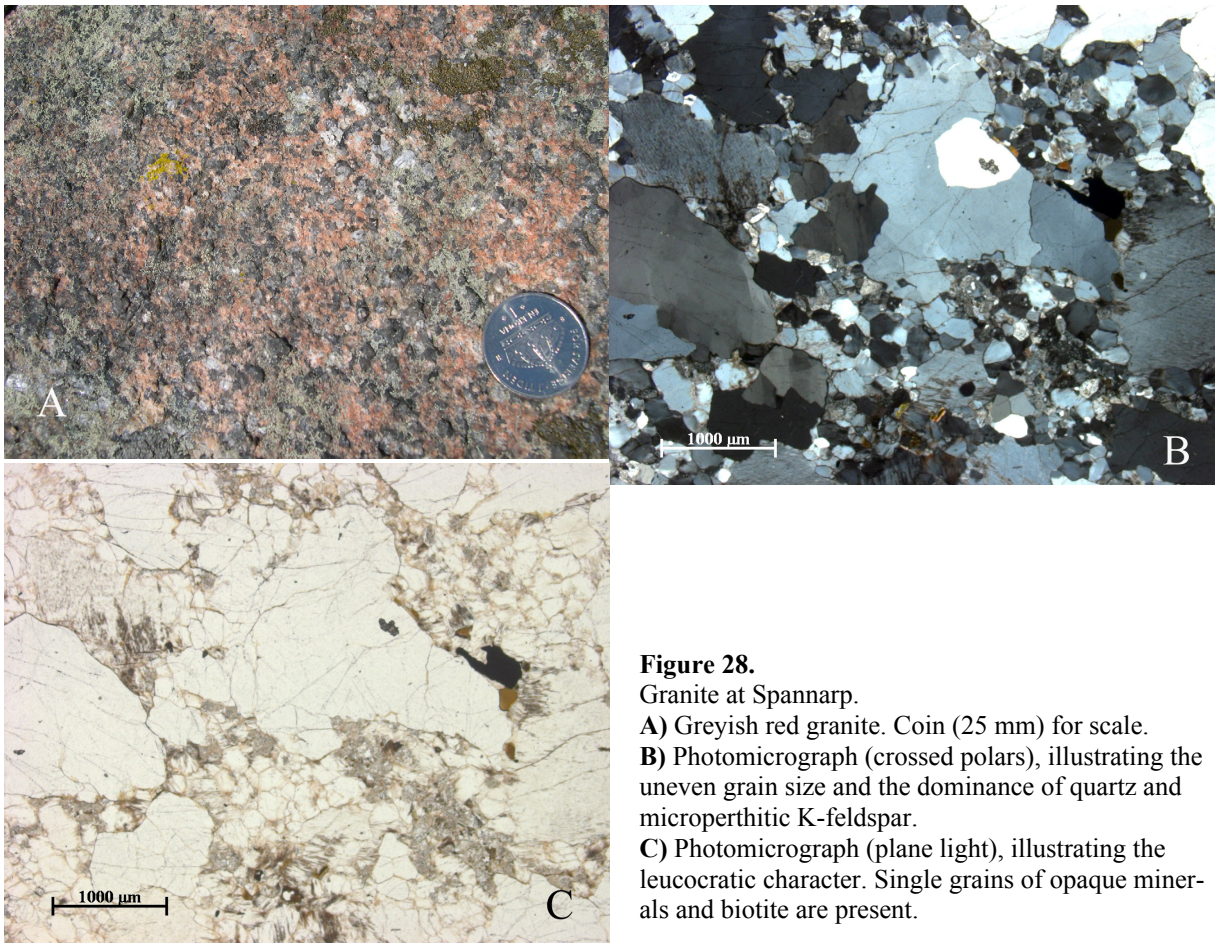

Figure 28.
Granite at Spannarp.
A) Greyish red granite. Coin (25 mm) for scale.
B) Photomicrograph (crossed polars), illustrating the uneven grain size and the dominance of quartz and microperthitic K-feldspar.
C) Photomicrograph (plane light), illustrating the leucocratic character. Single grains of opaque minerals and biotite are present.

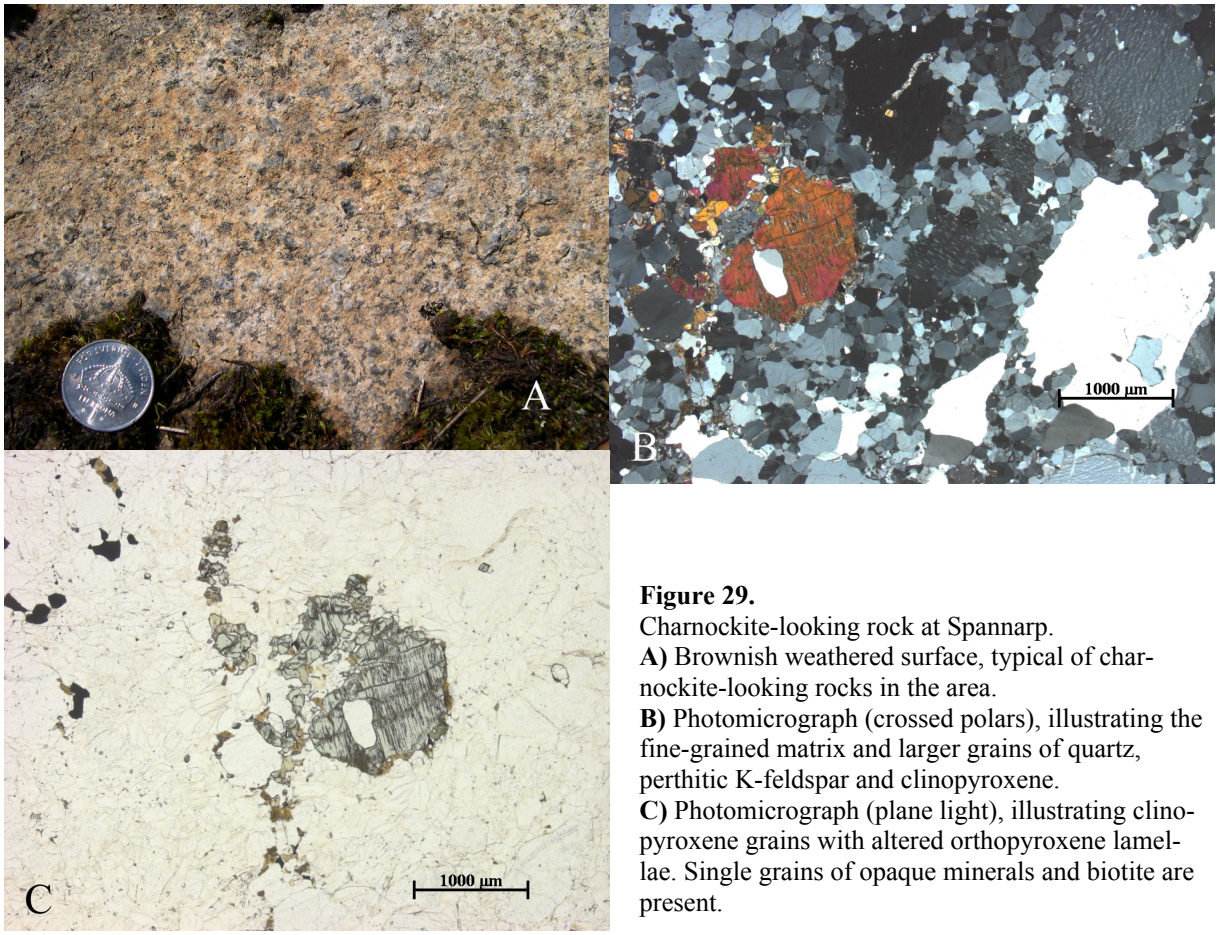

Figure 29.
Charnockite-looking rock at Spannarp.
A) Brownish weathered surface, typical of charnockite-looking rocks in the area.
B) Photomicrograph (crossed polars), illustrating the fine-grained matrix and larger grains of quartz, perthitic K-feldspar and clinopyroxene.
C) Photomicrograph (plane light), illustrating clinopyroxene grains with altered orthopyroxene lamellae. Single grains of opaque minerals and biotite are present.

cratic and has very small amounts of plagioclase. Biotite and opaque minerals occur as single, small grains. Fractures and grain boundaries are impregnated with very fine-grained, brownish and opaque minerals, probably iron oxides or hydroxides (Fig. 28C).

The *charnockite* is fine- to medium-grained, greenish grey (Fig. 29A), and has a weakly developed foliation defined by dark minerals. A sample was taken immediately north of the railway (SNG: 6333993/1290463). The grain size is uneven with irregularly shaped larger (1 mm) grains of quartz, perthitic K-feldspar (both with undulous extinction) and clinopyroxene, and granoblastic (recrystallised) smaller grains of K-feldspar (perthitic and microperthitic), quartz and some plagioclase (Fig. 29B). Dark aggregates, up to 8 mm long, are composed of small grains of opaque minerals, biotite, hornblende, clinopyroxene, and altered orthopyroxene, together with some feldspar and quartz. Apatite and zircon are present as accessory minerals. The larger grains of clinopyroxene have lamellae of altered orthopyroxene and are probably remnants of primary igneous clinopyroxene (Fig. 29B, C).

8.2 Zircon analysis: electron microscopy and analytical results

Zircon in *the granite* occurs as rounded prismatic and small oval grains. In BSE-images the zircons are texturally complex. Domains with oscillatory zoning are present but large parts of the zircon grains are both fractured and altered to complex alternating domains with BSE-dark and BSE-light zircon (Figs. 30A-C).

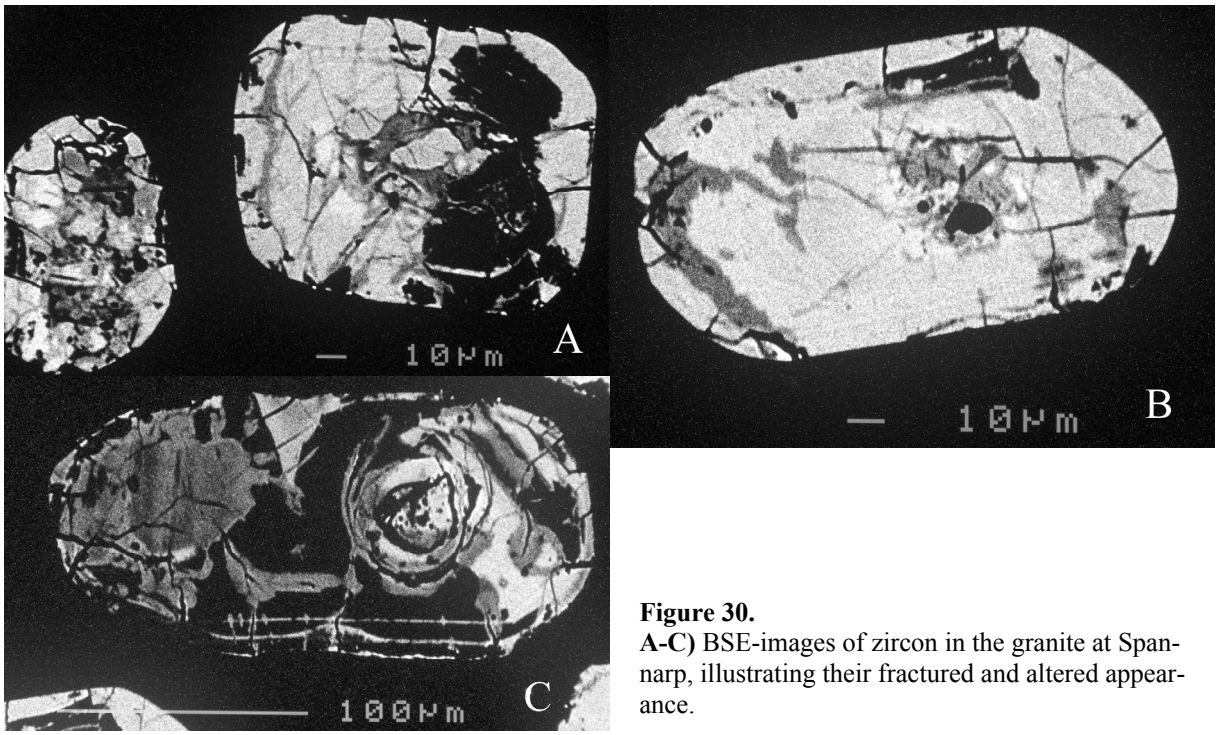

Figure 30.
A-C) BSE-images of zircon in the granite at Spannarp, illustrating their fractured and altered appearance.

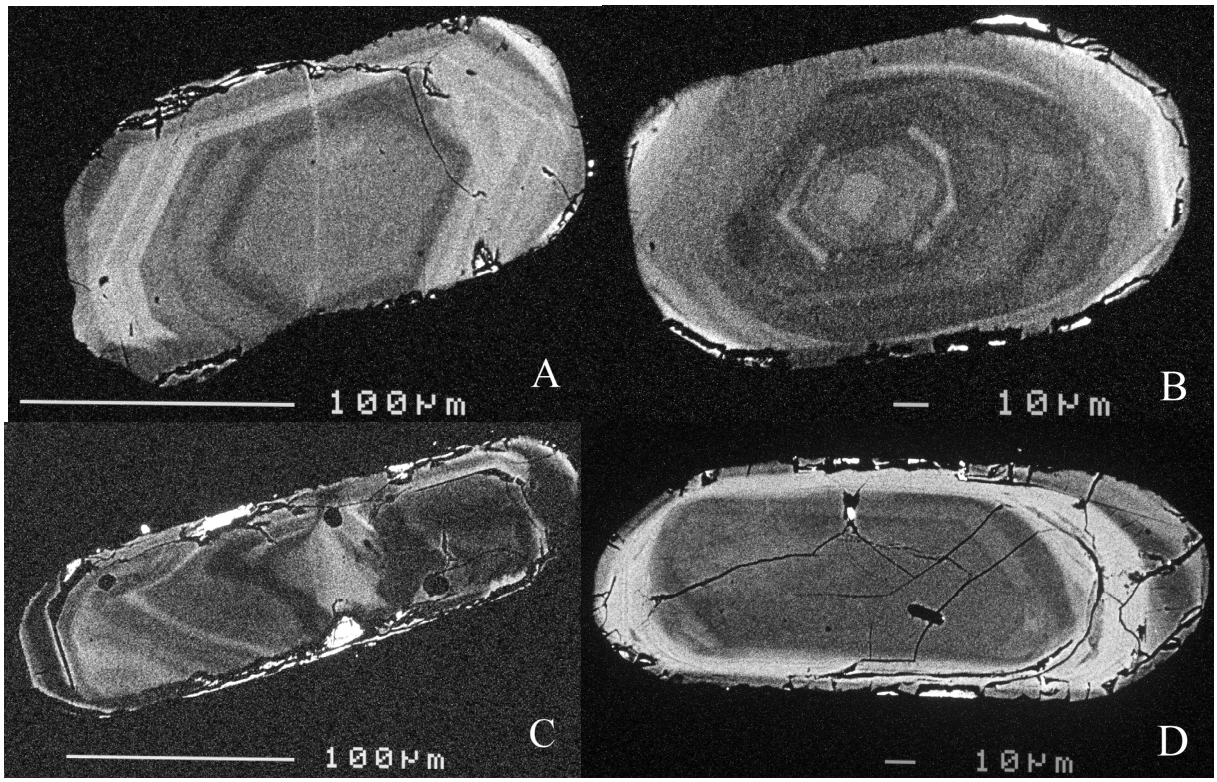

Figure 31. BSE-images of zircon from the charnockite-looking rock at Spannarp. Very bright spots, mainly along grain margins, are remnants of gold coating. **A, B)** Crystals with well-preserved, igneous oscillatory zoning. **C)** Igneous crystal with <20 µm wide BSE-dark, probably secondary, rim. **D)** BSE-bright, inner rim that possibly is secondary.

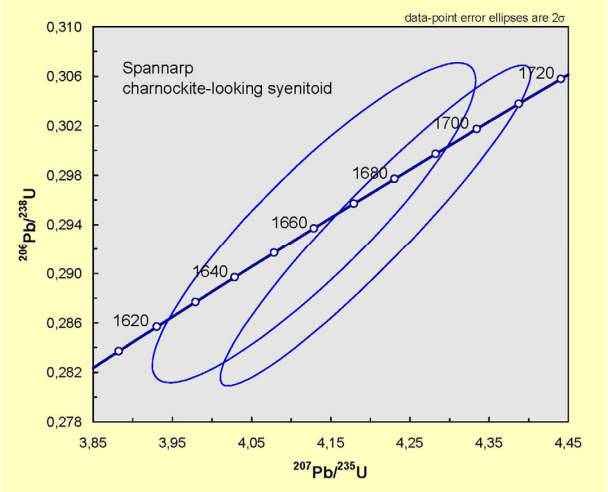

Figure 32. Concordia diagram with analyses of igneous protolith zircon in the charnockite-looking rock at Spannarp. Error ellipses are plotted at 2σ level.

Zircon in *the charnockite* includes prismatic and needle-shaped grains with rounded tips and edges, and small short prismatic, rounded grains. In BSE-images the crystals have an igneous character, commonly with oscillatory zoning (Fig. 31A, B). Some grains have BSE-light or BSE-dark rims that resemble secondary overgrowths (Fig. 31C) or replacements with transitional boundaries (Fig. 31D). The rims are however very thin, locally reaching 20 µm.

Two analyses were made in oscillatory zoned igneous zircon domains in crystals from the charnockite. Both yielded concordant $^{207}Pb/^{206}Pb$ ages at c. 1.7 Ga (Fig. 32).

8.3 Summary and interpretation

Comparison of thin sections from the granite and the charnockite-like rock suggests that their bulk chemical compositions are different, the granite being leucocratic and very poor in plagioclase. This difference in composition implies that the transition does not represent progressive charnockitisation within one and the same rock. The clinopyroxene in the charnockitic rock contains orthopyroxene lamellae, a texture that suggests that the pyroxenes are remnants of primary igneous minerals and that the igneous precursor was pyroxene-bearing.

BSE-images demonstrate significant differences in the zircon populations with fracturing and complex BSE-bright alteration in zircon from the leucocratic granite. This is most likely magmatic, U-rich alteration of a kind commonly encountered in high-silica, leucocratic granites. Igneous zircon in the charnockite is, on the contrary, without significant alteration. Potential secondary zircon in the charnockite occurs as less than 20 µm wide rims that were regarded too thin for analysis. Two spots in igneous zircon yielded a protolith age of c. 1.7 Ga, which shows that the charnockite protolith belongs to the dominant, 1.73-1.66 Ga old generation of intrusions in the Eastern Segment.

9. Skäpparp and Rosenberg: Granitic and charnockitic augen gneiss

9.1 Field relations and petrography

Regional context

Granitic augen gneiss occurs in large parts of the southern Eastern Segment. Its protolith age has been determined at 1.67 Ga (Andersson et al. in press). In the Steninge area, 15 kilometres northwest of Halmstad (Figs. 13 & 33), augen gneiss is locally charnockitic. At some of these localities the charnockitisation appears spatially associated with metabasic rocks. Granitic and charnockitic varieties of the augen gneiss were sampled at two localities in order to compare their zircon populations and, if possible, determine the age of charnockitisation.

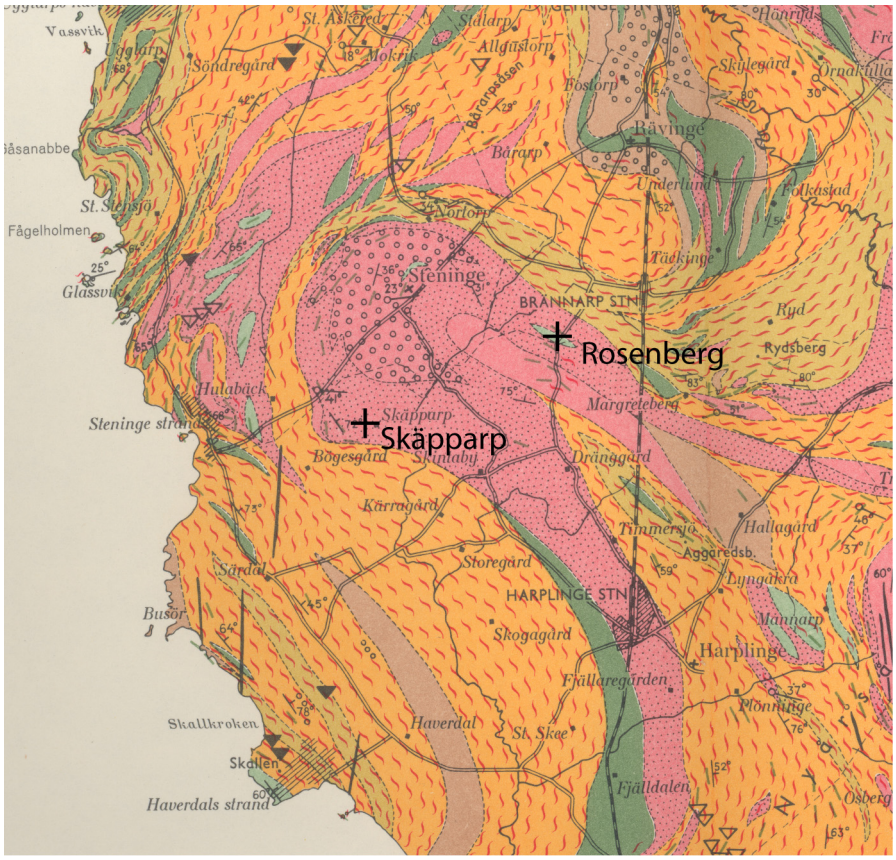

Figure 33. Detail of the geologic map by Larsson (1956) of the area around Steninge. Locations of Skäpparp and Rosenberg are marked with (+). Different varieties of gneiss are shown in pink, brown and orange colours (pink and brown are granitic compositions). Light green is charnockite. Metabasites, mainly garnet amphibolite, are shown in dark green. Black streaks mark occurrences of metadolerite. Circles mark augen texture, red and wavy lenses mark migmatitic structure. Scale: 1 cm = 1 km.

Localities

Granitic augen gneiss

Fresh granitic augen gneiss was sampled at an abandoned quarry at Skäpparp (SNG: 6297540/1307890). The rock has originally been K-feldspar porphyritic, but the K-feldspar megacrysts have recrystallised into 1-3 cm long lens-shaped aggregates of polycrystalline, fine-grained, red microcline (cf. Fig. 34). Locally, remnants of primary, grey orthoclase are present in these aggregates. The rock has a pronounced LS-fabric with a distinct lineation (L=113/22) and a weaker foliation (S=113/90), defined by polycrystalline and elongated K-feldspar augen and elongated aggregates of grey quartz, white plagioclase and dark minerals. In thin section, the K-feldspar porphyroclasts show Carlsbad twinning, microperthitic texture and are strained. The matrix is recrystallised with granoblastic or smoothly irregular grain boundaries (Fig. 35A). K-feldspar aggregates consist of fine-grained, granoblastic microcline with cross-hatched twinning. Locally myrmekite is present, most abundant close to the grain boundaries of orthoclase porphyroclasts. Quartz-domains are elongated and uneven-grained and plagio-

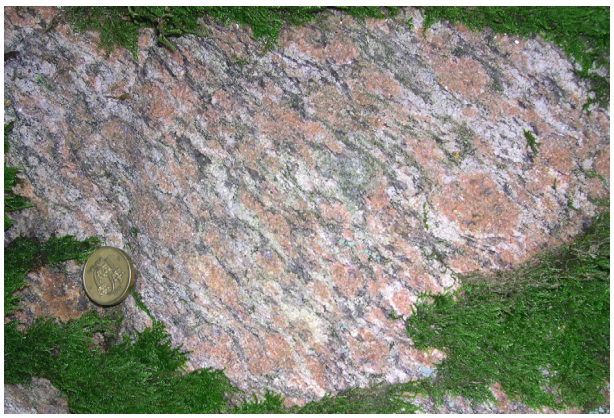

Figure 34. Granitic augen gneiss in the Steninge area. Former K-feldspar megacrysts have been recrystallised and deformed and form light reddish K-feldspar augens up to 3 cm long. Note the small remnants of grey orthoclase within the augens. Grey quartz domains are strongly elongated, as are domains of white plagioclase. Locality at Skipås (6299145/1306504). Coin (20 mm) for scale.

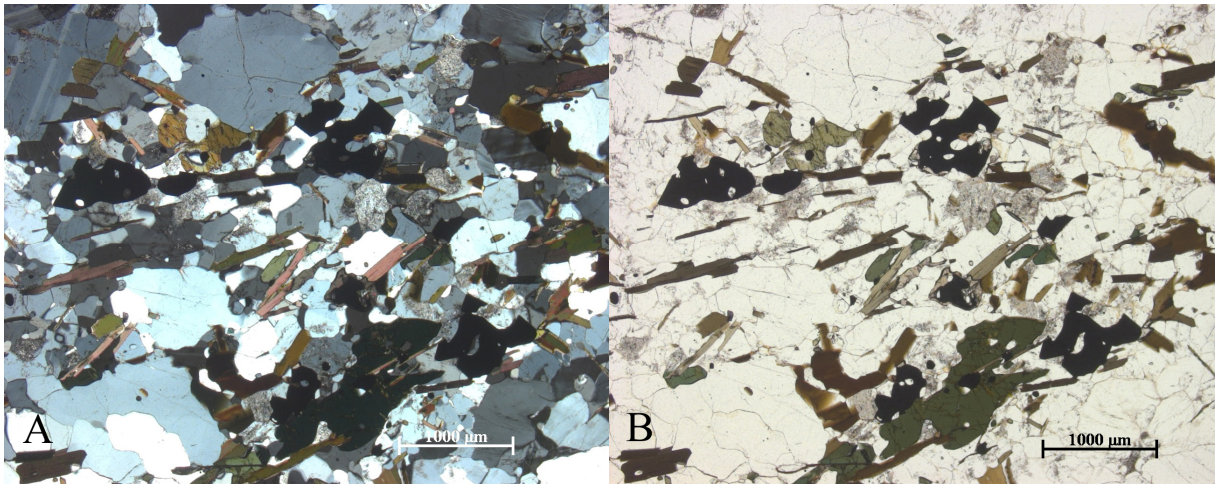

Figure 35. Photomicrographs of the granitic augen gneiss at Skäpparp, under crossed polars (A) and in plane light (B). **A)** Micro-domain with dark minerals in the augen gneiss, illustrating the granoblastic to smoothly irregular grain shapes. **B)** The same micro-domain as in (A). Hornblende is pleochroic in olive green hues, biotite is pleochroic brown, opaque mineral are black. Note the small anhedral grains of titanite (brownish, high relief) that preferentially associate with opaque minerals.

clase is uneven-grained and antiperthitic. Biotite, hornblende, opaque minerals, and anhedral titanite occur in fine-grained aggregates together with quartz and feldspars (Fig. 35B). Accessory minerals are apatite, zircon and altered allanite.

Charnockitised augen granite

Charnockitised augen granite was sampled in a road cut at Rosenberg (SNG: 6298656/1310720). The charnockitisation occurs in a c. 5 metres wide zone next to a metabasic rock (probably a metadolerite). The rock has a distinct augen texture similar to the granite at Skäpparp, but the rock is greenish grey in colour. Elongated augen and aggregates of dark minerals define a stretching lineation (L=95/22). The rock is recrystallised with

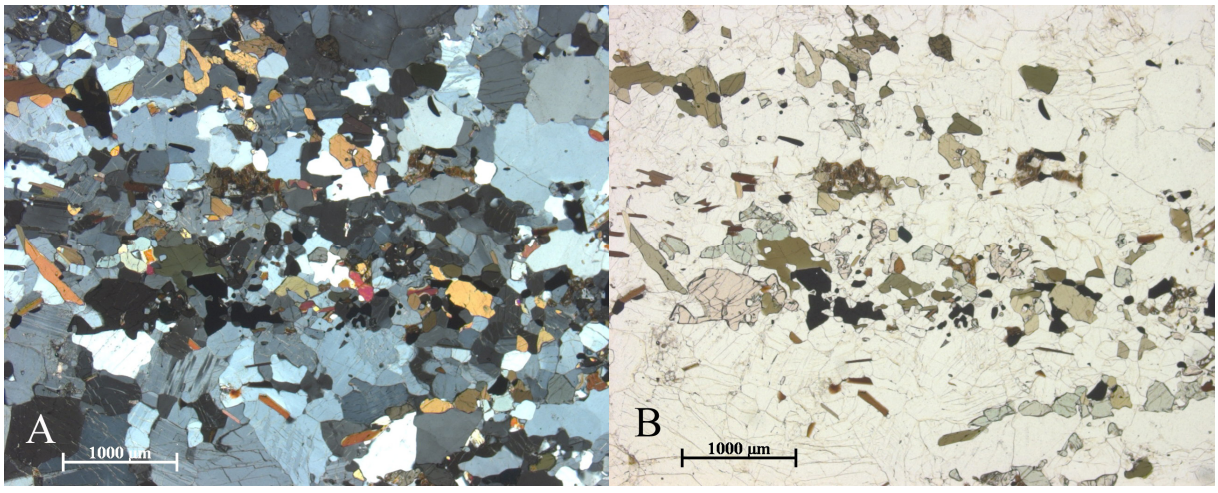

Figure 36. Photomicrographs of the charnockitised augen gneiss at Rosenberg, under crossed polars (A) and in plane light (B). **A)** Micro-domain with dark minerals, illustrating the granoblastic to smoothly irregular grain shapes. **B)** The same micro-domain as in (A) showing the dark minerals. Together with feldspars and quartz, the mineral assemblage consists of hornblende (pleochroic in olive green hues), clinopyroxene (light green, high relief), garnet (anhedral and light reddish, high relief), orthopyroxene (altered, fibrous masses), opaque minerals (black), and biotite (pleochroic brown).

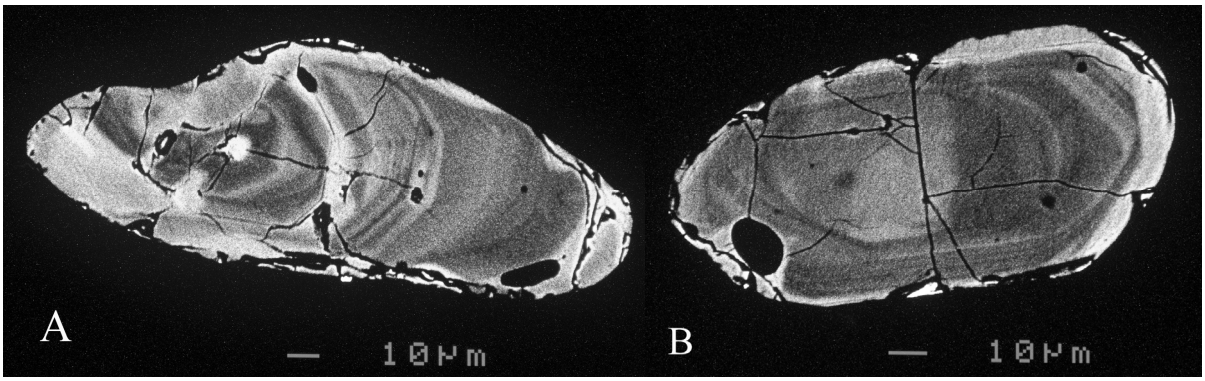

Figure 37. BSE-images of zircon in the augen gneiss at Skäpparp. The crystals are oscillatory zoned, partly resorbed, protolith zircon, with thin BSE-light rims. Very bright spots are remnants of gold coating.**A)** Anhedral grain. **B)** Subprismatic grain with rounded terminations.

granoblastic to smoothly irregular grain boundaries (Fig. 36A). The K-feldspar augen domains consist of fine-grained and granoblastic to irregularly shaped microperthitic K-feldspar. Myrmekite occurs locally. Plagioclase is antiperthitic and occurs in fine-grained aggregates. Quartz grains are uneven in size and have irregular grain shapes. Dark minerals include hornblende, anhedral garnet, opaque minerals, clinopyroxene, and orthopyroxene (partly altered). The dark minerals form fine-grained aggregates together with feldspars and quartz (Fig. 36B). The minerals form a high-pressure granulite facies assemblage that is similar to the assemblages of mafic rocks in the area. Accessory minerals are apatite and zircon.

9.2 Zircon analysis: electron microscopy and analytical results

Zircon crystals in *granitic augen gneiss* have rounded subprismatic outlines, some with pronounced anhedral (resorbed) shapes (Fig. 37A). BSE-images show that the zircons have an igneous character, with oscillatory zoning. Many crystals, however, have a BSE-light rim, up to 30 µm wide (Fig. 37B), commonly with a diffuse or transitional boundary.

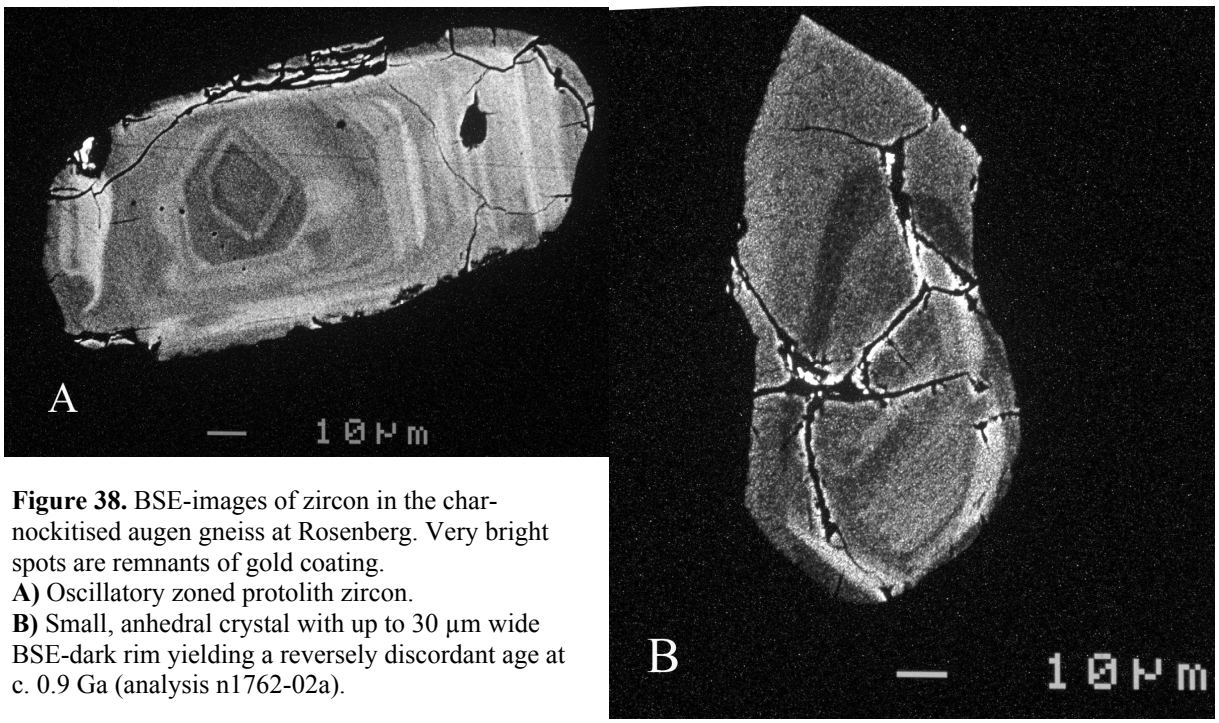

Figure 38. BSE-images of zircon in the charnockitised augen gneiss at Rosenberg. Very bright spots are remnants of gold coating.
A) Oscillatory zoned protolith zircon.
B) Small, anhedral crystal with up to 30 µm wide BSE-dark rim yielding a reversely discordant age at c. 0.9 Ga (analysis n1762-02a).

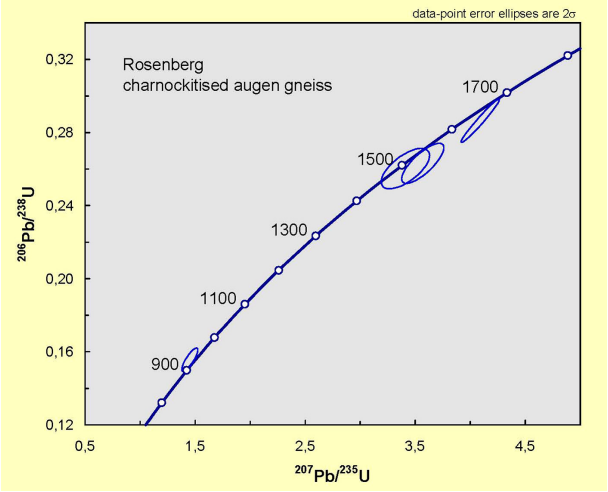

Figure 39. Concordia diagram with analyses of zircon, targeted at BSE-dark domains, in charnockitised augen gneiss at Rosenberg. Error ellipses are plotted at 2σ level.

Zircon crystals in the *charnockitic augen gneiss* are similar to those in the granitic variety in the respect that igneous zircon with oscillatory zoning dominates (Fig. 38A). BSE-dark rims, up to 25 µm wide, occur in the zircon from the charnockitic rock (Fig. 38B). Four analyses were targeted at BSE-dark rims. Three of them yielded Th/U ratios >0.3 and represent igneous domains, most likely mixed with components of secondary zircon (cf. Fig. 39). One analysis with low Th/U ratio (0.01) represents a pure metamorphic domain (Fig. 38B). The age is reversely discordant at c. 0.9 Ga and reflects metamorphism during the Sveconorwegian orogeny.

9.3 Summary and interpretation

The textures and mineral assemblage in the charnockitic augen gneiss at Rosenberg confirm that it is a truly charnockitised variety of the granitic augen gneiss in the area. In the charnockitic augen gneiss, secondary zircon has developed in small amounts only and forms thin BSE-dark rims. The single analysis of secondary zircon has low U content (192 ppm) and a low Th/U ratio (0.01), values that are characteristic of metamorphic zircon. The obtained age at c. 0.9 Ga suggests that the charnockitisation at Rosenberg took place during Sveconorwegian high-pressure granulite facies metamorphism, possibly concomitant with mafic magmatism..

Another true charnockitisation zone occurs in migmatitic gneiss at Söndrum, immediatetely west of Halmstad. There the charnockitisation has been dated at 1.40 Ga (U-Pb zircon analysis, Rimsa et. al 2004) and is clearly associated with fluid infiltration (Harlov et al. in press). It is likely that charnockitisation in the southwest Eastern Segment took place during two separate events, at c. 1.40 Ga and at c. 0.95 Ga. The older event was roughly coeval with 1.40-1.38 Ga intrusions of granite and quartz-monzonite (c.f. Hubbard 1975, Andersson 2002 and references therein). The younger event was associated with regional Sveconorwegian metamorphism in the high-pressure granulite and upper amphibolite facies (c.f. Johansson et al. 1991, Wang & Lindh 1996, Möller 1998, Johansson et al. 2001).

10. Marås: Charnockite-looking syenitoid

10.1 Field relations and petrography

Regional context

Charnockite and charnockite-like rocks are relatively common in southwestern parts of the Eastern Segment. One locality of charnockite-looking rock has been found at a relatively northeastern position, at Marås, 4 kilometres north of Hyltebruk (Fig. 2).

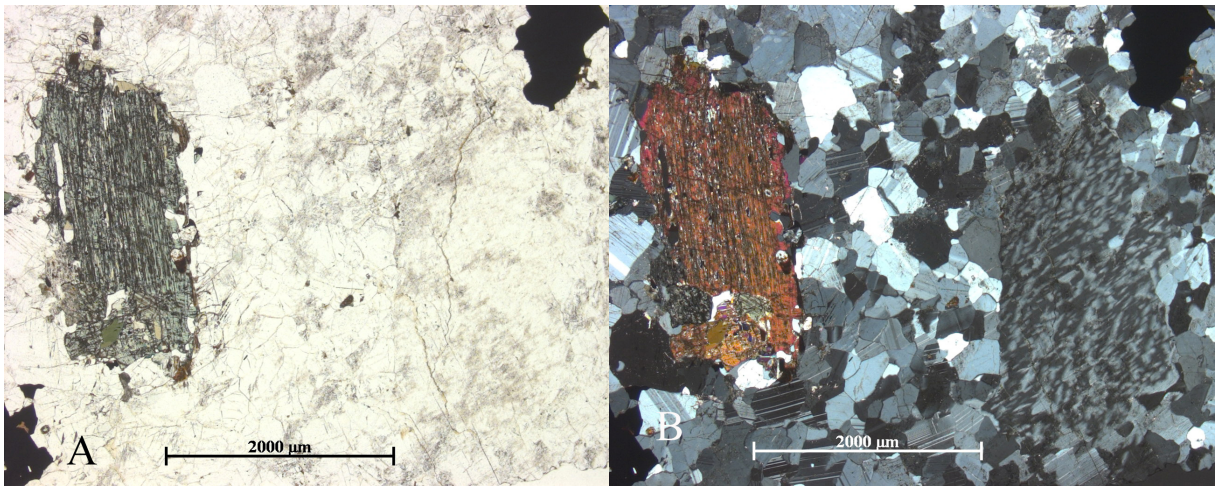

Figure 40. Photomicrographs of the charnockite-looking metasyenitoid at Marås, **(A)** in plane light and **(B)** with crossed polars. Large grains are clinopyroxene (light green) with orthopyroxene lamellae (altered, brown), perthitic K-feldspar (right part of the picture), and opaque mineral (upper right) The matrix is dominated by plagioclase (probably albite) and lesser amounts of perthitic K-feldspar and quartz, with granoblastic to smoothly irregular grain shapes.

Locality

The charnockite-looking rock occurs in outcrops on a large hill in Marås nature reserve (SNG: 6326606/1344130). Surrounding bedrock is composed of gneiss of granitic, quartz syenitic and quartz monzonitic compositions that originally have been coarse-grained or K-feldspar porphyritic (c.f. augen gneiss in the Steninge area, Fig. 34). Protolith zircon from reddish, quartz syenitic gneiss in the area has been dated at 1.68 Ga (Andersson et al. in press). The charnockite-looking rock at Marås is yellowish to greenish grey with an originally medium-grained texture that is largely recrystallised and fine-grained. It has a linear fabric (80/20) defined by elongated (0.5-2 mm thick and 0.5-3 cm long) grey quartz domains and aggregates of dark minerals, the latter including mm-sized grains of dark-green clinopyroxene. Up to 5 mm large remnants of grey K-feldspar occur. Geochemical analysis reveals that the rock is relatively low in SiO_2 (66 wt-%), rich in alkalis (6 % K_2O, 4.5 % Na_2O) and low in CaO (1.6 %) which classifies the rock as a syenitoid gneiss. A thin section shows that clinopyroxene, perthitic K-feldspar and opaque minerals occur as larger grains (1-3 mm, Figs. 40A, B). Quartz occurs as 1-2 mm wide ribbons and lenses. Clinopyroxene grains have fine exsolution lamellae of orthopyroxene, which suggests that they are remnants of primary igneous pyroxene. The fine-grained matrix is granoblastic and dominated by plagioclase (likely albite), with lesser amounts of perthitic K-feldspar and quartz. Small grains of hornblende, biotite, apatite, and garnet occur in the dark mineral aggregates.

10.2 Zircon analysis: electron microscopy

Zircon occurs as 50-150 µm large, rounded grains and short-prismatic crystals with rounded terminations (Figs. 41A, B) and as fragments of broken larger grains (Figs. 41 C, D). In BSE-images the crystals are dark with light bands (Figs. 41A, C, D). BSE-light, distinct rims, up to 50 µm wide, are common (Fig. 41A, B). The bright rims are either late igneous or secondary zircon. Analysis is needed for an interpretation of these rims.

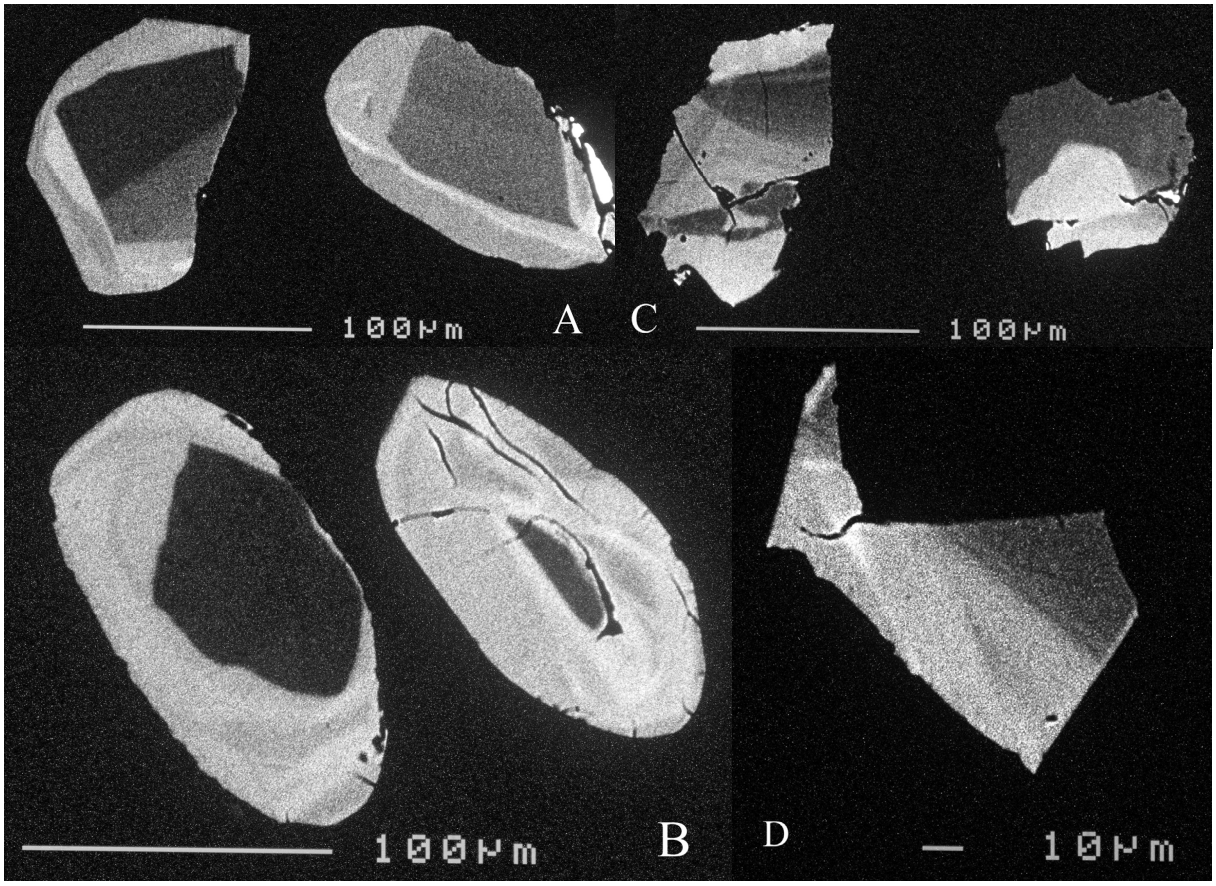

Figure 41. BSE-images of zircon in the charnockite-looking metasyenitoid at Marås. **A, B)** Rounded BSE-dark crystals with bright rims. **C, D)** Fragments of large, BSE-dark grains with lighter bands.

10.3 Summary and interpretation

The charnockitic appearance of the gneiss at Marås is primarily a result of its syenitoid composition. Both orthoclase and pyroxene are most likely remnants of primary igneous minerals. The sharp-edged fragments of large zircon grains are similar to 1.68 Ga protolith zircon in nearby reddish, quartz syenitic gneiss (Andersson et al. in press). The charnockite-looking rock at Marås thus represents a variety of the same 1.68 Ga old syenitoid.

Ackowledgements

Fredrik Hellström, Inger Lundqvist and Hugo Wikman are thanked for suggesting investigation of the localities at Högabjär, Spannarp and Kullaskog. Inger Lundqvist, Sam Sukotjo and Hugo Wikman are warmly thanked for sharing their knowledge during field trips in southwest Sweden. Thanks go to Ulf Söderlund for skilful zircon separation, to Bodil Kajrup for preparation of the ion probe mounts and to Lev Ilyinski for assistance during ion probe analysis. Martin Whitehouse is thanked for reducing the analytical data and Ildiko Antal for providing the magnetic anomaly map used in figures 2, 3, 8 and 13. Leif Johansson is thanked for critical reading of parts of the manuscript.

References

Åhäll, K.-I., Samuelsson, L. & Persson, P.-O., 1997: Geochronology and structural setting of the 1.38 Ga Torpa granite; implications for charnockite formation in SW Sweden. *GFF 119*, 37-43.

Andersson, J., 2001: *Sveconorwegian orogenesis in the southwestern Baltic Shield. Zircon geochronology and tectonothermal setting of orthogneisses in SW Sweden.* Doctoral Thesis. Lund University. 28pp.

Andersson, J., Eliasson, T., Möller, C., Lundqvist, I., Bergström, U. & Lundqvist.L., in press: TIB affinity and a parautochthonous setting of high-grade orthogneisses in the southern Eastern Segment of the Sveconorwegian Province. *Abstract. 27th Nordic Geological Winter Meeting. Bulletin of the Geological Society of Finland*.

Andersson, J., Möller, C. & Johansson, L., 2002: Zircon geochronology of migmatite gneisses along the Mylonite Zone (S Sweden): a major Sveconorwegian terrane boundary in the Baltic shield. *Precambrian Research 114*, 121-147.

Andersson, J., Söderlund, U., Cornell, D., Johansson, L. & Möller, C., 1999: Sveconorwegian (-Grenvillian) deformation, metamorphism and leucosome formation in SW Sweden, SW Baltic shield: constraints from a Mesoproterozoic granite intrusion. *Precambrian Research 98*, 151-171.

Austin Hegardt, E., Cornell, D., Claesson, L., Simakov, S., Stein. H & Hannah, J., 2005: Eclogites in the central part of the Sveconorwegian Eastern Segment of the Baltic Shield: Support for an extensive eclogite terrane. *GFF 127*, 221-232.

Bingen, B., Austrheim, H. & Whitehouse, M., 2001: Ilmenite as a source for zirconium during high-grade metamorphism? Textural evidence from the Caledonides of Western Norway and implications for zircon geochronology. *Journal of Petrology 42*, 355-375.

Bingen, B., Skår, Ø., Marker, M., Sigmond, E.M.O.,Nordgulen, Ø., Ragnhildstveit, J., Mansfeld, J., Tucker, R. D. & Liégeois, J.-P., 2005: Timing of continental building in the Sveconorwegian orogen, SW Scandinavia. *Norwegian Journal of Geology 85*, 87-116.

Cherniak, D.J. & Watson, E.B. 2003: Diffusion in zircon. *In* J.M. Hanchar. & P.W.O Hoskin (eds): *Zircon*. *Reviews in Mineralogy and Geochemistry 53*, 113-143.

Christoffel, C.A., Connelly, J.N. & Åhäll, K.-I., 1999: Timing and characterization of recurrent pre-Sveconorwegian metamorphism and deformation in the Varberg-Halmstad region of SW Sweden. *Precambrian Research 98*, 173-195.

Connelly, J.N., Berglund, J. & Larson, S.Å., 1996: Thermotectonic evolution of the Eastern Segment of SW Sweden; tectonic constraints from U-Pb geochronology. *In* T.S. Brewer (ed): *Precambrian Crustal Evolution in the North Atlantic Region. Geological Society Special Publication 112*, 297-313.

Cornell, D.H., Armstrong, R., Schersten, A. & Åberg, A, 1997: The CANUTE model for dating polyphase zircons by ion-probe. *EUG 9:th meeting Strasbourg. Abstr. Suppl. 1, Terra Nova, 9*, 451.

Fraser, G., Ellis, D. & Eggins, S., 1997: Zirconium abundance in granulite facies minerals, with implications for zircon geochronology in high-grade rocks. *Geology 25*, 607-610.

Harlov. D.E., Johansson, L., van der Kerkhof, A. & Förster, H.-J., in press: The role of advective fluid flow and diffusion during localised, solid-state dehydration: Söndrum Stenhuggeriet, Halmstad, SW Sweden. *Journal of Petrology.*

Hoskin, P.W.O. & Black, L.P., 2000: Metamorphic zircon formation by solid-state recrystallization of protolith igneous zircon. *Journal of Metamorphic Geology 18*, 423-439.

Hoskin, P.W.O. & Schaltegger, U., 2003: The composition of zircon and igneous and metamorphic petrogenesis. *In* J.M. Hanchar. & P.W.O Hoskin (eds): *Zircon*. *Reviews in Mineralogy and Geochemistry 53*, 27-62.

Hubbard, F.H., 1975: The Precambrian crystalline complex of south-western Sweden; the geology and petrogenetic development of the Varberg region. *Geologiska Föreningens i Stockholm Förhandlingar 97*, 223-236.

Johansson, L., 1998: Charnockitisation and polyphase metamorphism in the Eastern Segment of the southwest Swedish Gneiss Region. *Abstract. The 23rd Nordic Geological Winter Meeting in Aarhus, Denmark*, 142.

Johansson, L. & Johansson, Å., 1990: Isotope geochemistry and age relationships of mafic intrusions along the Protogine Zone, southern Sweden. *Precambrian Research 48*, 375-414.

Johansson, L., Lindh, A. & Möller, C., 1991: Late Sveconorwegian (Grenville) high-pressure granulite facies metamorphism in southwest Sweden. *Journal of Metamorphic Geology 9*, 283-292.

Johansson, L., Möller, C., Lundqvist, L. & Sukotjo, S., in press: Late Sveconorwegian syntectonic migmatite formation along the eastern margin of the Eastern Segment, southwest Sweden. *Abstract. 27th Nordic Geological Winter Meeting. Bulletin of the Geological Society of Finland.*

Johansson, L., Möller, C. & Söderlund, U., 2001: Geochronology of eclogite facies metamorphism in the Sveconorwegian province of SW Sweden. *Precambrian Research 106*, 261-275.

Larsson, W. 1956: Berggrundskarta till bladet Halmstad. *Sveriges geologiska undersökning Aa 198*.

Lee, J.K.W., Williams, I.S., Ellis, D.J., 1997: Pb, U and Th diffusion in natural zircon. *Nature 390: 6656*, 159-161.

Ludwig, K.R., 2003: Isoplot 3.00. A geochronological toolkit for Microsoft Excel. *Berkeley Geochronology Center Special Publication No. 4*, 70 pp.

Lundqvist, I., in press: Beskrivning till berggrundskartan 5B Varberg NO. *Sveriges Geologiska Undersökning.*

Lundqvist, L. 1996: *1.4 Ga mafic-felsic magmatism in the southern Sweden; a study of the Axamo Dyke Swarm and a related anorthosite-gabbro intrusion.* Thesis for Licentiate Degree A 11. Earth Science Centre, Göteborg, Sweden.

Moeller, A., O-Brien, P.J., Kennedy, A. & Kroener, A., 2002: Polyphase zircon in ultrahigh-temperature granulites (Rogaland, SW Norway); constraints for Pb diffusion in zircon. *Journal of Metamorphic Geology 20*, 727-740.

Möller, C., 1998: Decompressed eclogites in the Sveconorwegian (-Grenvillian) orogen of SW Sweden: petrology and tectonic implications. *Journal of Metamorphic Geology 16*, 641-656.

Möller, C., 1999: Sapphirine in SW Sweden: a record of Sveconorwegian (-Grenvillian) late-orogenic tectonic exhumation. *Journal of Metamorphic Geology 17*, 127-141.

Möller, C. & Söderlund, U., 1997: Age constraints on the regional deformation within the Eastern Segment, S. Sweden: Late Sveconorwegian granite dyke intrusion and metamorphic – deformational relations. *GFF 119*, 1-12.

Rimsa, A, Whitehouse, M.J. & Johansson, L., 2004: Modification of zircon morphology and geochemistry during metamorphism – a case study from Söndrum, SW Sweden. *Abstract, The 26:th Nordic Geological Winter Meeting. GFF 126*, 34.

Söderlund, P., Söderlund, U., Möller, C., Gorbaschev, R. & Rodhe, A., 2004: Petrology and ion microprobe U-Pb chronology applied to a metabasic intrusion in southern sweden: A study on zircon formation during metamorphism and deformation. *Tectonics 23*, 1-16.

Söderlund, U., 1996: Conventional U-Pb dating versus single-grain Pb evaporation dating of complex zircons from a pegmatite in the high-grade gneisses of southwestern Sweden. *Lithos 38*, 93-105.

Söderlund, U., Isachsen, C., Bylund, G., Heaman. L.M., Patchett, P.J., Vervoort, J. & Andersson, U.B., 2005: U-Pb baddeleyite ages and Hf, Nd isotope chemistry constraining repeated mafic magmatism in the Fennoscandian Shield from 1.6 to 0.9 Ga. *Contributions to Mineralogy and Petrology 150*, 174-194.

Söderlund, U., Möller, C., Andersson, J., Johansson, L. & Whitehouse, M., 2002: Zircon geochronology in polymetamorphic gneisses in the Sveconorwegian orogen, SW Sweden: ion microprobe evidence for 1.46-1.42 and 0.98-0.96 Ga reworking. *Precambrian Research 113*, 193-225.

Stephens, M.B., Wahlgren, C.-H., Weijermars, R. & Cruden, A.R., 1996: Left-lateral transpressive deformation and its tectonic implications, Sveconorwegian Orogen, Baltic Shield, southwestern Sweden. *Precambrian Research 79*, 261-279.

Wahlgren, C.-H., Cruden, A.R. & Stephens, M.B., 1994: Kinematics of a major fan-like structure in the eastern part of the Sveconorwegian Orogen, Baltic Shield, south-central Sweden. *Precambrian Research 70*, 67-91.

Wang, X.-D., 1996: *Metamorphism and Geochronology of the High Pressure Granulite and Upper Amphibolite Facies Rocks from the Southwest Swedish Granulite Region*. Ph.D. Thesis, Lund University, Lund, Sweden.

Wang, X.-D. & Lindh, A., 1996: Temperature-pressure investigation of the southern part of the Southwest Swedish Granulite Region. *European Journal of Mineralogy 8*, 51-67.

Watson, E.B., 1996: Dissolution, growth and survival of zircons during crustal fusion: kinetic principles, geological models and implications for isotopic inheritance. *Transactions of the Royal Society of Edinburgh: Earth Sciences 87*, 43-56.

Whitehouse, M.J., Claesson, S., Sunde, T. & Vestin, J., 1997: Ionmicroprobe U-Pb zircon geochronology and correlation of Archean gneisses from the Lewisian Complex of Gruinard Bay, north-west Scotland. *Geochimica Cosmochimica Acta* 61, 4429-4438.

Whitehouse, M.J., Kamber, B.S. & Moorbath, S., 1999: Age significance of U-Th-Pb zircon data from early Archean rocks of west Greenland - a reassessment based on combined ionmicroprobe and imaging studies. *Chemical Geology 160*, 210-224.

Wikman, H., 2000: Beskrivning till berggrundskartorna 5E Växjö NO och NV. *Sveriges geologiska undersökning Af 201 & 216,* 108 pp.

Appendix

U-Pb-Th zircon analyses

Comments to the data

±s denotes errors given at 1σ level

a) Italics denote discordant data not used for age calculation, unless explicitly stated in the text.

b) Abbreviations: CL = cathodoluminescence, BSE = backscatter electron, zon = zoning, osc = oscillatory, sect = sector, hom = homogeneous, comp = composite, D = dark, B = bright.

c) % of common ^{206}Pb in measured ^{206}Pb, estimated from ^{204}Pb assuming a present day Stacey and Kramers (1975) model for terrestrial Pb-isotope composition.

d) Age discordance at closest approach of error ellipse to concordia (2σ level).

SIMS U-Pb-Th data from Oxanäset

Sample[a]/ spot #	Structural class[b] (from CL and BSE)	Pb (ppm)	U (ppm)	Th/U measured	$^{206}Pb/^{204}Pb$ measured	$f^{206}Pb$[c] %	$^{207}Pb/^{206}Pb$	±s %	$^{206}Pb/^{238}U$	±s %	$^{207}Pb/^{206}U$ age (Ma)	±s	$^{206}Pb/^{238}U$ age (Ma)	±s	Disc.[d] %
Strongly foliated gneiss mesosome (OX-1, n1755)															
OX-1/n1755-01a	osc. zon core CLB	24	61	0.86	20738	0.09	0.1035	1.10	0.2950	1.13	1688	20	1666	17	
OX-1/n1755-02a	osc. and sect. zon core CLB	23	57	0.85	7805	0.24	0.1020	1.21	0.2964	1.09	1661	22	1673	16	
OX-1/n1755-03a	osc. zon core CLB	28	70	0.94	26754	<0.07	0.1021	1.02	0.2936	1.10	1662	19	1660	16	
OX-1/n1755-04a	osc. zon core CLB	24	61	0.76	19676	0.10	0.1036	1.67	0.2994	1.10	1690	30	1688	16	
OX-1/n1755-05a	osc. zon core CLB	26	66	0.77	15243	0.12	0.1014	1.08	0.2988	1.17	1650	20	1686	17	
OX-1/n1755-06a	osc. zon core CLB	42	105	0.80	31406	0.06	0.1031	1.06	0.2985	1.09	1680	20	1684	16	
OX-1/n1755-08a	diffuse osc. zon core CLB	24	62	0.82	4678	0.40	0.1040	1.63	0.2950	1.09	1696	30	1666	16	
OX-1/n1755-07a	diffuse osc. zon core CLB	*28*	*70*	*0.84*	*8518*	*0.22*	*0.0990*	*1.21*	*0.3031*	*1.13*	*1606*	*22*	*1707*	*17*	*0.5*
OX-1/n1755-09a	diffuse osc. zon core CLB	24	63	0.84	>1000000	0.00	0.1004	1.25	0.2855	1.10	1632	23	1619	16	
Veined gneiss with pre-kinematic leucosome (OX-2, n1753)															
Ox-2/n1753-01a	unzon core CLD/BSEB	409	1543	0.03	380342	0.00	0.08861	0.32	0.24160	1.09	1396	6	1395	14	
Ox2/n1753-02a	unzon core CLD/BSEB	*502*	*2774*	*0.00*	*364006*	*0.01*	*0.07143*	*0.32*	*0.16886*	*1.18*	*970*	*7*	*1006*	*11*	*0.7*
OX-2/n1753-03a	osc. and sect. zon	22	55	0.75	29927	<0.06	0.1035	0.97	0.2995	1.10	1688	18	1689	16	
Ox-2/n1753-04a	diffuse zon CLD/BSEB	266	1240	0.02	301506	0.01	0.08075	0.98	0.19768	2.16	1215	19	1163	23	
OX-2/n1753-05a	unzon hom CLD/BSEB	362	847	1.06	309668	0.01	0.1042	0.44	0.3041	1.10	1700	8	1711	17	
OX-2/n1753-06a	irregular zon core CLD/BSEB	*654*	*1562*	*0.77*	*259664*	*0.01*	*0.1030*	*0.22*	*0.3154*	*1.11*	*1679*	*4*	*1767*	*17*	*3.4*
OX-2/n1753-07a	irregular zon core CLD/BSEB	*675*	*1694*	*0.69*	*319542*	*0.01*	*0.1021*	*0.24*	*0.3054*	*1.11*	*1663*	*4*	*1718*	*17*	*1.2*
OX-2/n1753-08a	irregular zon core CLD/BSEB	206	514	0.95	47762	0.04	0.1019	0.95	0.2892	1.10	1659	17	1637	16	
Ox2/n1753-09a	comp. unzon rim CLD/BSEB	*198*	*760*	*0.02*	*27737*	*0.07*	*0.09056*	*0.51*	*0.23748*	*1.09*	1437	10	1374	14	*-1.5*

SIMS U-Pb-Th data from Oxanäset, continued

Sample[a]/ spot #	Structural class[b] (from CL and BSE)	Pb (ppm)	U (ppm)	Th/U[c] measured	$^{206}Pb/^{204}Pb$ measured	$f^{206}Pb^{c}$ %	$^{207}Pb/^{206}Pb$	±s %	$^{206}Pb/^{238}U$	±s %	$^{207}Pb/^{206}U$ age (Ma)	±s	$^{206}Pb/^{238}U$ age (Ma)	±s	Disc.[d] %
Intensely veined gneiss with syn- to post-kinematic leucosome (OX-3, n1754)															
Ox-3/n1754-01a	unzon hom rim CLD/BSEB	332	1861	0.01	203424	0.01	0.07151	0.34	0.16608	1.09	972	7	990	10	
Ox-3/n1754-03a	rim-core contact	262	1347	0.01	66620	0.03	0.07512	0.62	0.18027	1.10	1072	12	1068	11	
Ox-3/n1754-03b	unzon hom rim CLD/BSEB	340	1993	0.01	9054	0.21	0.07112	0.63	0.15874	1.28	961	13	950	11	
Ox-3/n1754-04a	unzon hom rim CLD/BSEB	349	1942	0.01	213152	0.01	0.07170	0.36	0.16731	1.09	977	7	997	10	
Ox-3/n1754-05a	unzon/relict osc zon rim CLD/BSEB	332	1875	0.02	13255	0.14	0.07157	0.34	0.16429	1.18	974	7	981	11	
Ox-3/n1754-06a	unzon/relict osc zon rim CLD/BSEB	286	1598	0.01	90437	0.02	0.07136	0.35	0.16633	1.16	968	7	992	11	
Ox-3/n1754-07a	unzon hom rim CLD/BSEB	*415*	*2270*	*0.00*	*26115*	*0.07*	*0.07116*	*0.30*	*0.17027*	*1.14*	*962*	*6*	*1014*	*11*	*2.7*
OX-3/n1754-08a	diffuse osc. zon core CLB/BSED	32	75	1.00	20519	0.09	0.1032	0.91	0.3008	1.18	1682	17	1695	18	
Ox-3/n1754-09a	unzon hom core CLD/BSEB	244	1394	0.01	89750	0.02	0.07130	0.32	0.16260	1.09	966	6	971	10	
OX-3/n1754-10a	diffuse osc. zon core CLB/BSED	28	73	0.82	32976	<0.06	0.0999	0.89	0.2808	1.13	1622	17	1595	16	
OX-3/n1754-11a	diffuse osc. zon core CLB/BSED	24	60	0.86	12132	0.15	0.1019	1.04	0.2982	1.10	1659	19	1683	16	
OX-3/n1754-12a	diffuse osc. zon core CLB/BSED	26	64	0.79	10049	0.19	0.1019	0.99	0.2962	1.09	1658	18	1672	16	
Ox-3/n1754-13a	unzon hom core CLD/BSEB	772	4412	0.02	7293	0.26	0.07173	0.36	0.16238	1.10	978	7	970	10	
Ox-3/n1754-14a	unzon core CLD/BSEB	*384*	*2049*	*0.01*	*58604*	*0.03*	*0.07096*	*0.60*	*0.17451*	*1.13*	*956*	*12*	*1037*	*11*	*4.3*
Ox-3/n1754-15a	unzon core CLD/BSEB	343	1867	0.02	121918	0.02	0.07220	0.28	0.17058	1.18	992	6	1015	11	
Ox-3/n1754-16a	hom unzon rim domain CLD/BSEB	230	1284	0.01	5687	0.33	0.07218	1.03	0.16615	1.10	991	21	991	10	
Ox-3/n1754-17a	unzon hom rim CLD/BSEB	436	2442	0.01	129709	0.01	0.07145	0.38	0.16625	1.13	970	8	991	10	
Ox-3/n1754-18a	unzon hom rim CLD/BSEB	245	1417	0.01	158737	0.01	0.07219	0.50	0.16104	1.17	991	10	963	10	
Ox-3/n1754-19a	unzon/relict osc zon rim CLD/BSEB	363	1464	0.07	127231	0.01	0.08438	1.10	0.22333	1.19	1301	21	1299	14	

SIMS U-Pb-Th data from Gransjön and Kullaskog

Sample[a]/ spot #	Structural class[b] (from CL and BSE)	Pb (ppm)	U (ppm)	Th/U measured	$^{206}Pb/^{204}Pb$ measured	$f^{206}Pb^{c}$ %	$^{207}Pb/^{206}Pb$	±s %	$^{206}Pb/^{238}U$	±s %	$^{207}Pb/^{206}U$ age (Ma)	±s	$^{206}Pb/^{238}U$ age (Ma)	±s	Conc[d] %
Leucosome in grey gneiss (Gransjön, n1760)															
n1760-01c	igneous	14	38	0.75	40533	<0.0	0.1035	1.08	0.2876	1.68	1688	20	1629	24	
n1760-05a	igneous	18	46	0.83	13013	0.14	0.1013	1.46	0.2828	1.69	1647	27	1606	24	
n1760-07a	igneous	88	204	1.15	43497	0.04	0.1033	0.46	0.2981	1.69	1685	8	1682	25	
n1760-06a	*igneous*	*44*	*123*	*0.96*	*24550*	*0.08*	*0.0975*	*0.80*	*0.2555*	*1.68*	*1576*	*15*	*1467*	*22*	*-2.7*
n1760-02a	secondary BS-bright	119	440	0.05	104096	0.02	0.0903	1.11	0.2453	1.72	1431	21	1414	22	
n1760-04a	secondary BS-bright	94	350	0.04	69275	0.03	0.0907	0.54	0.2444	1.68	1440	10	1410	21	
n1760-09a	secondary BS-bright	101	371	0.04	88290	0.02	0.0909	0.44	0.2479	1.69	1446	8	1428	22	
n1760-10a	secondary BS-bright	140	542	0.03	74501	0.03	0.0883	0.34	0.2363	1.75	1388	7	1367	22	
n1760-08a	secondary BS-bright	59	233	0.04	12038	0.16	0.0889	0.66	0.2313	1.68	1402	13	1341	20	0.0
Migmatitic gneiss (Kull, n1758)															
n1758-01a	igneous core	87	208	0.86	5943	0.31	0.1082	0.83	0.3113	1.12	1769	15	1747	17	
n1758-02a	igneous core	123	275	1.02	80234	0.02	0.1079	0.64	0.3226	1.25	1764	12	1803	20	
n1758-09a@1	igneous core	67	158	0.87	392272	0.00	0.1093	0.81	0.3135	1.09	1787	15	1758	17	
n1758-03a	*inner secondary rim*	*302*	*957*	*0.03*	*5924*	*0.32*	*0.1034*	*0.36*	*0.2842*	*1.09*	*1687*	*7*	*1613*	*16*	*-2.3*
n1758-04a	*inner secondary rim*	*271*	*733*	*0.27*	*27566*	*0.07*	*0.1038*	*0.66*	*0.3157*	*1.11*	*1694*	*12*	*1769*	*17*	*1.1*
n1758-07a@1	*inner secondary rim*	*407*	*1191*	*0.03*	*35621*	*0.05*	*0.1032*	*0.34*	*0.3076*	*1.11*	*1682*	*6*	*1729*	*17*	*0.3*
n1758-05a@1	outer secondary rim	375	1390	0.00	34106	0.05	0.0890	0.32	0.2476	1.11	1405	6	1426	14	
n1758-06a@1	outer secondary rim	430	1589	0.00	33050	0.06	0.0898	0.32	0.2483	1.10	1421	6	1430	14	
n1758-10a@1	outer secondary rim	389	1414	0.02	10964	0.17	0.0896	0.32	0.2522	1.11	1416	6	1450	14	
n1758-08a@1	*outer secondary rim*	*360*	*1297*	*0.01*	*6409*	*0.29*	*0.0887*	*0.46*	*0.2550*	*1.13*	*1397*	*9*	*1464*	*15*	*2.0*

SIMS U-Pb-Th data from Högabjär

Sample[a]/ spot #	Structural class[b] (from CL and BSE)	Pb (ppm)	U (ppm)	Th/U measured	$^{206}Pb/^{204}Pb$ measured	$f^{206}Pb^{c}$ %	$^{207}Pb/^{206}Pb$	±s %	$^{206}Pb/^{238}U$	±s %	$^{207}Pb/^{206}U$ age (Ma)	±s	$^{206}Pb/^{238}U$ age (Ma)	±s	Conc[d] %
Gneiss mesosome (HB1, n1759)															
n1759-01a	*igneous domain*	*139*	*283*	*0.91*	*18395*	*0.1*	*0.1026*	*0.55*	*0.3580*	*1.23*	*1672*	*10*	*1973*	*21*	*16.8*
n1759-03a	*igneous domain*	*80*	*209*	*0.58*	*15454*	*0.12*	*0.1010*	*0.83*	*0.3045*	*1.09*	*1642*	*15*	*1713*	*16*	*0.3*
n1759-04a	*igneous domain*	*105*	*273*	*0.56*	*5971*	*0.31*	*0.1014*	*0.65*	*0.3080*	*1.09*	*1650*	*12*	*1731*	*17*	*1.6*
n1759-05a	igneous domain	89	242	0.48	28369	0.07	0.1040	0.62	0.2958	1.09	1696	11	1670	16	
n1759-06a	igneous domain	54	153	0.45	21793	0.09	0.1006	0.86	0.2886	1.11	1635	16	1634	16	
n1759-07a	igneous domain	113	284	0.87	28758	0.07	0.1034	0.58	0.2938	1.09	1687	11	1660	16	
n1759-08a	igneous, BS-dark	219	639	0.21	10032	0.19	0.1004	0.42	0.2937	1.11	1632	8	1660	16	
n1759-09a	igneous domain	34	91	0.64	12896	0.15	0.1037	1.06	0.2965	1.19	1691	19	1674	18	
n1759-10a	igneous domain	59	149	0.76	72731	<0.0	0.1015	0.78	0.3007	1.10	1652	14	1695	16	
n1759-11a	igneous domain	53	139	0.57	47094	< 0.0	0.1054	0.78	0.3015	1.12	1721	14	1699	17	
n1759-12a	igneous domain	100	224	1.51	29500	0.06	0.1041	0.65	0.2950	1.09	1698	12	1666	16	
n1759-02a	mixed domains	117	363	0.38	7748	0.24	0.0928	1.47	0.2708	1.11	1484	28	1545	15	
Leucosome (HB2, n1757)															
n1757-03a	igneous domain	26	69	0.71	4817	0.39	0.0995	1.17	0.2898	1.12	1615	22	1640	16	
n1757-06a	igneous domain	20	52	0.51	9107	0.21	0.1045	1.46	0.3076	1.10	1706	27	1729	17	
n1757-09a	igneous domain	40	110	0.54	5580	0.34	0.1011	1.24	0.2935	1.09	1645	23	1659	16	
n1757-10a	igneous domain	73	201	0.72	18971	0.10	0.1013	0.97	0.2775	1.10	1647	18	1579	15	
n1757-12a	igneous domain	45	112	0.89	40679	0.05	0.1025	0.91	0.2979	1.09	1671	17	1681	16	
n1757-15a	igneous domain	16	39	0.82	20093	0.09	0.1065	1.36	0.3009	1.11	1741	25	1696	17	
n1757-24a	igneous domain	62	148	1.15	27455	0.07	0.1041	0.76	0.2930	1.10	1699	14	1657	16	
n1757-23a	BS-bright domain	460	1361	0.09	70733	0.03	0.1014	0.51	0.3002	1.10	1650	9	1692	16	

SIMS U-Pb-Th data from Högabjär, continued

Sample[a]/ spot #	Structural class[b] (from CL and BSE)	Pb (ppm)	U (ppm)	Th/U measured	$^{206}Pb/^{204}Pb$ measured	$f^{206}Pb^{c}$ %	$^{207}Pb/^{206}Pb$	±s %	$^{206}Pb/^{238}U$	±s %	$^{207}Pb/^{206}U$ age (Ma)	±s	$^{206}Pb/^{238}U$ age (Ma)	±s	Conc[d] %
Leucosome (HB2, n1757), continued															
n1757-08b	mixed domains	49	172	0.26	32578	0.06	0.0975	3.15	0.2466	6.14	1577	58	1421	79	
n1757-27a	oscillatory	85	258	0.48	5350	0.35	0.0972	1.15	0.2688	1.55	1572	21	1535	21	
n1757-01a	*BS-light rim*	*528*	*1841*	*0.03*	*83147*	*0.02*	*0.0907*	*0.64*	*0.2606*	*1.15*	*1440*	*12*	*1493*	*15*	*0.0*
n1757-18aa	*BS-bright sec domain*	*571*	*1959*	*0.05*	*266841*	*0.01*	*0.0918*	*0.47*	*0.2641*	*1.09*	*1463*	*9*	*1511*	*15*	*0.3*
n1757-02a	BS-dark part of core	242	836	0.17	2342	0.8	0.0895	0.52	0.2527	1.09	1416	10	1453	14	
n1757-04a	BS-light rim	467	1654	0.13	46351	0.04	0.0898	0.54	0.2502	1.09	1421	10	1440	14	
n1757-05a	BS-light rim	540	1871	0.06	410155	0.00	0.0922	0.52	0.2602	1.09	1471	10	1491	15	
n1757-07a	BS-light rim	306	1084	0.05	>100000(	0.00	0.0895	0.72	0.2557	1.09	1414	14	1468	14	
n1757-08a	BS-light rim	522	1843	0.03	417113	0.00	0.0927	0.93	0.2571	1.11	1482	18	1475	15	
n1757-11a	BS-light rim	447	1541	0.05	109353	0.02	0.0922	0.57	0.2619	1.09	1471	11	1500	15	
n1757-13a	BS-light xst	447	1588	0.11	309937	0.01	0.0903	0.27	0.2505	1.11	1431	5	1441	14	
n1757-13b	BS-light xst	232	835	0.11	38173	0.05	0.0898	0.42	0.2479	1.11	1422	8	1427	14	
n1757-14a	BS-light rim	562	1980	0.04	143560	0.01	0.0918	0.34	0.2577	1.09	1462	7	1478	14	
n1757-16a	BS-light domain	451	1592	0.04	102327	0.02	0.0916	0.54	0.2562	1.09	1459	10	1470	14	
n1757-17a	BS-light rim	642	2279	0.03	112775	0.02	0.0914	0.44	0.2561	1.12	1455	8	1470	15	
n1757-19a	BS-light domain	642	2268	0.02	145998	0.01	0.0922	0.69	0.2575	1.09	1471	13	1477	14	
n1757-20a	BS-light domain	783	2777	0.03	140803	0.01	0.0897	1.81	0.2570	1.10	1420	34	1474	14	
n1757-21a	BS-light rim	312	1094	0.03	221332	0.01	0.0924	1.09	0.2584	1.13	1475	21	1482	15	
n1757-22a	BS-light domain	685	2390	0.07	461651	0.00	0.0916	0.64	0.2575	1.09	1458	12	1477	14	
n1757-25a	BS-light rim	485	1733	0.06	194358	0.01	0.0899	0.47	0.2530	1.09	1423	9	1454	14	
n1757-26a	BS-light domain	536	1880	0.04	183421	0.01	0.0919	0.59	0.2583	1.09	1465	11	1481	14	

SIMS U-Pb-Th data from Högabjär, continued

Sample[a]/ spot #	Structural class[b] (from CL and BSE)	Pb (ppm)	U (ppm)	Th/U measured	$^{206}Pb/^{204}Pb$ measured	$f^{206}Pb^{c}$ %	$^{207}Pb/^{206}Pb$	±s %	$^{206}Pb/^{238}U$	±s %	$^{207}Pb/^{206}U$ age (Ma)	±s	$^{206}Pb/^{238}U$ age (Ma)	±s	Conc[d] %
Folded granitic dyke (HB3, n1756)															
n1756-01a	BS-light inner domain	368	1328	0.07	226401	0.01	0.0893	0.41	0.2497	1.10	1411	8	1437	14	
n1756-03a	BS-light rim	269	933	0.17	37367	0.05	0.0899	0.48	0.2533	1.11	1424	9	1455	15	
n1756-04a	BS-light domain	402	1414	0.14	178011	0.01	0.0908	0.32	0.2506	1.09	1442	6	1441	14	
n1756-05a	BS-dark core	203	651	0.45	13444	0.14	0.0908	1.23	0.2547	1.24	1443	23	1463	16	
n1756-07a	BS-light domain	334	1192	0.05	38532	0.05	0.0915	0.46	0.2533	1.09	1457	9	1455	14	
n1756-08a	BS-light xst	300	1072	0.17	41589	0.04	0.0899	0.32	0.2436	1.17	1424	6	1406	15	
n1756-11a	BS-light domain	386	1260	0.41	211008	0.01	0.0905	0.73	0.2546	1.09	1436	14	1462	14	
n1756-12a	BS-light rim	565	2012	0.08	89752	0.02	0.0907	0.33	0.2527	1.09	1441	6	1452	14	
n1756-02a	CL-light oscillatory	86	287	0.34	73816	0.03	0.0916	0.65	0.2498	1.25	1459	12	1438	16	
n1756-02b	CL-light oscillatory	71	238	0.29	37914	0.05	0.0932	0.69	0.2552	1.09	1491	13	1465	14	
n1756-06a	CL-light oscillatory	70	236	0.26	106821	0.02	0.0921	0.61	0.2558	1.12	1469	12	1468	15	
n1756-06b	CL-light oscillatory	86	287	0.29	38874	0.05	0.0931	0.65	0.2554	1.12	1491	12	1467	15	
n1756-09a	CL-light oscillatory	44	157	0.32	25735	0.07	0.0885	0.91	0.2385	1.09	1393	17	1379	14	
n1756-09b	CL-light oscillatory	66	231	0.36	3267	0.57	0.0877	0.91	0.2408	1.11	1377	17	1391	14	
n1756-10a	CL-light oscillatory	110	365	0.52	13704	0.14	0.0895	0.67	0.2434	1.11	1414	13	1404	14	

SIMS U-Pb-Th data from Spannarp and Rosenberg

Sample[a]/ spot #	Structural class[b] (from CL and BSE)	Pb (ppm)	U (ppm)	Th/U measured	$^{206}Pb/^{204}Pb$ measured	$f^{206}Pb$[c] %	$^{207}Pb/^{206}Pb$	±s %	$^{206}Pb/^{238}U$	±s %	$^{207}Pb/^{206}U$ age (Ma)	±s	$^{206}Pb/^{238}U$ age (Ma)	±s	Conc[d] %
Charnockite-looking metasyenitoid (Spannarp, n1761)															
n1761-01a	igneous domain	51	130	0.76	46283	0.04	0.1038	0.61	0.2939	1.81	1693	11	1661	26	
n1761-02a	igneous domain	53	135	0.76	47859	0.04	0.1018	0.92	0.2941	1.80	1657	17	1662	26	
Charnockitised augen granite (Rosenberg, n1762)															
n1762-01a	BS-dark rim	43	133	0.41	3307	0.57	0.0984	1.38	0.2631	1.70	1593	26	1506	23	
n1762-02a	*BS-dark rim*	*32*	*192*	*0.01*	*3277*	*0.57*	*0.0677*	*1.12*	*0.1557*	*1.69*	*858*	*23*	*933*	*15*	*0.3*
n1762-03a	BS-dark rim	47	149	0.36	1284	1.46	0.0951	1.98	0.2603	1.73	1529	37	1491	23	
n1762-04a	*BS-dark domain*	*139*	*402*	*0.37*	*11609*	*0.16*	*0.1036*	*0.38*	*0.2864*	*1.69*	*1689*	*7*	*1624*	*24*	*-0.7*